DISTANCE PROPERTIES OF UNCODED AND CODED CONTINUOUS PHASE FREQUENCY SHIFT KEYED SIGNALS

RANJITH LIYANAPATHIRANA

DISTANCE PROPERTIES OF UNCODED AND CODED CONTINUOUS PHASE FREQUENCY SHIFT KEYED SIGNALS

By

© Ranjith Liyanapathirana, B.Sc.Eng.(Hons.)

A thesis submitted to the School of Graduate

Studies in partial fulfillment of the

requirements for the degree of

Master of Engineering

Faculty of Engineering and Applied Science

Memorial University of Newfoundland

March 1987

St. John's Newfoundland Canada

ISBN 0-315-39472-2

ABSTRACT

This thesis examines the distance properties of uncoded and trellis coded M-ary continuous phase frequency shift keyed (CPFSK) signals, when the receiver consists of a phase detector followed by a trellis decoder. Closed-form expressions for the minimum Euclidean distance of uncoded M-ary CPFSK signals are presented. These expressions yield exact values of minimum Euclidean distance for all rational valued modulation indices. An M-state trellis is shown to achieve almost all performance gain that is guaranteed by the memory of the modulation process of CPFSK signals when $M > 2$.

The minimum distance results for uncoded CPFSK signals show that phase detection and trellis decoding yields larger minimum distances than correlation demodulation and trellis decoding for small modulation indices ($h \leq 1/M$). The minimum distance results for trellis coded CPFSK signals also indicate that phase detection yields larger minimum distances than correlation detection for small h.

A computer search for the optimal codes of quaternary and octal CPFSK signals with phase detection and trellis decoding is carried out. For all constraint lengths and $h \leq 1/M$ these codes are identical to the optimal codes found in the literature for correlation detection. It is also observed that trellis decoding of uncoded and coded CPFSK signals is transparent to the carrier phase ambiguities of the regenerated reference tones of the coherent demodulator. Considering the distance properties and the relative ease of implementation, it is concluded that phase detection and trellis decoding of M-ary CPFSK signals is superior to correlation-detection of the same for $h \leq 1/M$.

ACKNOWLEDGEMENTS

I gratefully acknowledge my indebtedness to Dr. N. Ekanayake for his invaluable guidance and supervision during the course of my studies. I am particularly thankful to Dr. John Quaicoe for his advice and guidance in preparing this thesis.

I am most grateful to Dr. F.A. Aldrich, the Dean of Graduate Studies, Dr. G.R. Peters, the Dean of Engineering, Dr. T.R. Chari, the Associate Dean of Engineering, and the Faculty of Engineering Memorial University of Newfoundland, for the financial support in the form of a Graduate Fellowship and Teaching Assistantships which made this work possible.

I am indebted to the many colleagues who have been helpful in carrying out this research and preparation of the manuscript. Rohan Cooray, Havindra Caldera, and Manora Caldera have been particularly helpful.

Thanks are also due to the Operations Staff at the Computing Services, for their promptness in releasing plots and print jobs.

Finally, I express my special appreciation to all my family members for their continuing encouragement and affection.

Table of Contents

List of Tables

List of Figures

SYMBOLS

AWGN	Additive white Gaussian noise
a_n	n^{th} data symbol
CPFSK	Continuous phase frequency shift keying
CPM	Continuous phase modulation
d^2_{min}	Squared minimum Euclidean distance
$x(t)$	Baseband data signal
E_b	Bit energy
E_s	Symbol energy
FSK	Frequency shift keying
f_c	Nominal carrier frequency
h	Modulation index
ISI	Inter-symbol interference
M	Order of the signaling scheme
MED	Minimum Euclidean distance
MLSE	Maximum likelihood sequence estimation
MSK	Minimum shift keying
$N_0/2$	Double sided power spectral density of noise
p	Numerator of the modulation index
$P[\epsilon]$	Symbol error probability
PSK	Phase shift keying
q	Denominator of the modulation index

$r(t)$	Received signal
RF	Radio frequency
SNR	Signal-to-noise ratio
$s(t)$	Transmitted CPFSK signal
T	Symbol interval
T_b	Bit interval
t	Time
$\theta(t)$	Phase of CPFSK signal
ω_c	Nominal angular frequency of the carrier
ω_d	Frequency deviation

Chapter 1

INTRODUCTION

1.1. Digital modulation techniques

Communication systems are used to convey information from one point to another. Telephony, telegraphy, AM/FM radio, TV and land mobile radio are some examples of these systems. To transmit information over a channel, efficiently and reliably, many operations have to be usually performed on the input messages. Modulation is one of the most important, the others being source-coding, multiplexing, frequency spreading, multiple access and synchronization. Modulation involves the systematic alteration of one or more parameter of a carrier wave, such as amplitude or phase, in accordance with a message. It is also characterized by a frequency translation to a new higher band of frequencies to match the transmission medium. Information is retrieved at the receiver by means of the complementary operation of demodulation.

There are two types of modulation, analog and digital. In analog modulation the modulated parameter of the carrier wave varies in direct proportion to the message signal. In digital modulation the message is first transformed to a sequence of pulses and then used to modulate a sinusoidal carrier. Two well known techniques of digital modulation are phase shift keying

(PSK) and frequency shift keying (FSK). Digital modulation schemes use far more bandwidth than their analog counterparts.

The recent trend has been towards digital modulation techniques. This is partly due to the rapid advances in digital technology (very large scale integration, computers etc.) and partly due to the advantages these systems offer, such as, capacity to transmit any kind of baseband signals and the ability to regenerate the signal thereby minimizing the effects of noise and interference. Though classical digital modulation techniques such as PSK and FSK are still extensively being used, many new techniques have been analyzed and implemented recently. Today it is common practice to transmit analog information by means of digital techniques.

In many communication situations the available transmitter power and the RF bandwidth are limited. These two are the primary communication resources. A general system design objective would be to use these two resources as efficiently as possible. Modulation techniques used in communication systems vary in their ability to transmit information, while maintaining an acceptable grade of service. Some are more power efficient while the others are more bandwidth efficient. A particular choice depends on the classification of the channel. For example, telephone circuits with approximately 3 kHz bandwidth are band-limited channels, while space communication links are power-limited channels. In power-limited channels, coding schemes would be generally used to efficiently utilize the available power at the expense of bandwidth, while in band-limited channels spectrally efficient techniques would be used [4, 12]. Also, there

are other attributes affecting this choice. For instance, in satellite communication systems, where often nonlinear amplifiers are used, techniques which perform well over nonlinear channels should be employed; whereas, in land mobile radio, techniques which are bandwidth efficient as well as suitable for multipath channels are advantageous.

1.2. Literature review

In recent years, power and bandwidth efficient modulation schemes have been the subject of extensive research. Introducing memory into the modulation process has been shown to give signals with good bandwidth efficiency. One way to introduce memory is to have continuity in the phase of the modulated signal. The class of digital modulation schemes often referred to as continuous phase modulation (CPM) has this property. Also CPM schemes are of narrowband with low spectral sidelobes. They use constant amplitude sinusoidal signals and therefore are suitable for nonlinear channels [1, 2, 4, 5].

The transmitted CPM signal can be viewed as either a frequency modulated signal or a phase modulated signal. The symbol pulse shape affects the instantaneous frequency or the phase of the signal. By choosing different symbol pulse shapes it is possible to obtain a variety of CPM schemes (see [5], [22], and the references therein). All these schemes fall into one of two classes of 'full response' CPM and 'partial response' CPM. In 'full response' CPM schemes the symbol pulses do not overlap with adjacent symbols. But in 'partial response' CPM schemes the symbol pulses are allowed to overlap with adjacent symbols.

Continuous phase frequency shift keying (CPFSK) [4, 8, 18] belongs to the full response class of CPM schemes. In CPFSK signals, the phase in any symbol interval depends upon the previous data symbols due to the dependency generated by the continuous nature of the phase [4]. A detailed discussion on distance properties, relative performances and spectral characteristics of CPFSK signals as functions of modulation index, pulse shape, alphabet size, and receiver complexity are found in [4] and [22].

Power efficiency of CPFSK schemes can be improved while preserving the attractive spectral characteristics by combining with convolutional codes [14, 17, 20] or more generally with trellis codes. Research on combined channel coding and modulation schemes is reported in [14, 15, 16, 20, 24]. Out of these schemes, the channel coding scheme due to Ungerboeck [24] achieves remarkable coding gains for band-limited channels and these codes and variants thereof have received much attention. Pizzi and Wilson [20] consider rate 1/2 convolutional coding of quaternary CPM and present optimal codes for quaternary CPFSK signals, and two partial response schemes. Similar but more detailed work including higher rate convolutional codes can be found in [14-16].

There are three well known symbol-by-symbol detection schemes available for the detection of CPFSK signals: synchronous detection, noncoherent detection, and limiter-discriminator detection. The performance of the above detection schemes are almost 3 dB inferior to coherent PSK. Multiple bit detection or sequence detection of CPFSK is discussed in several papers. In [8] de Buda has discussed coherent detection of MSK using a two-bit observation interval.

Forney [11] has discussed the use of the Viterbi algorithm for detection of coherent MSK. Coherent detection and noncoherent detection of binary CPFSK with arbitrary modulation indices and arbitrary observation intervals are found in [18]. In [21] Schonhoff extends the above results for the M-ary case (see also [3]).

In a recent paper Ekanayake [9] has shown that M-ary CPFSK signals can be detected by either differentially coherent detection or coherent detection followed by differential decoding. Both the methods are straight forward adaptations of the well known detection techniques for PSK. Several noncoherent detection schemes for CPM have been investigated in [23]. It has been shown that the performance of symbol-by-symbol detectors can be improved by using a trellis decoder with Viterbi decoding. For example, a conventional limiter-discriminator detector when followed by a trellis decoder improves in performance [23].

1.3. M-ary continuous phase frequency shift keying and trellis coding

The CPFSK signal is mathematically given by

$$s(t) = \sqrt{2E_s/T}\cos(2\pi f_c t + \phi(t) + \phi_0) \qquad (1.1)$$

where the information is contained in the excess phase function

$$\phi(t) = \pi h \sum_{n \to -\infty}^{\infty} a_n q(t - nT) \qquad (1.2)$$

with

$$q(t) = \int_{-\infty}^{t} g(\tau)d\tau \qquad (1.3)$$

Here $g(t)$ is a rectangular pulse of unit amplitude over the time interval $0 \le t \le T$. f_c is the nominal carrier frequency and h is the modulation index. a_n denotes discrete data. In each symbol interval, a_n assumes one of the values of the

set $\{\pm1, \pm3, \pm5, \ldots, \pm(M-1)\}$ with equal probability. ϕ_0 is an arbitrary constant phase shift. E_s is the energy per data symbol and T is the symbol duration.

The phase change during any symbol interval is $\pi a_n h$. For continuity of the phase at bit transition times, $\phi(t)$ should satisfy

$$\phi[(n+1)T] - \phi(nT) = \pi a_n h. \qquad (1.4)$$

The phase of the CPFSK signal forms a tree structure. The phase tree or the phase trajectories of quaternary CPFSK is shown in Fig. 1.1 . This tree structure can be simplified to form a finite state trellis for rational value modulation indices. This is discussed in the next chapter.

The continuous nature of the phase adds memory into the CPFSK scheme [11]. Referring to a point such as P in Fig. 1.1 , the part of the phase tree between this point and the origin represents forty different possible data symbol sequences. That is, if the phase of the signal at $t = 4T$ is known as $2\pi h$; then, assuming that the phase at $t = 0$ is zero, only one of forty different sequences could have been transmitted. Sequence detection techniques can use this memory to detect the transmitted sequence.

1.3.1. Detection of M-ary CPFSK signals

As mentioned before, CPFSK signals can be detected either by sequence detection techniques or by symbol-by-symbol detection schemes. This thesis considers a sequence detection technique, namely, phase detection and trellis decoding. This detection technique is compared with the well known correlation

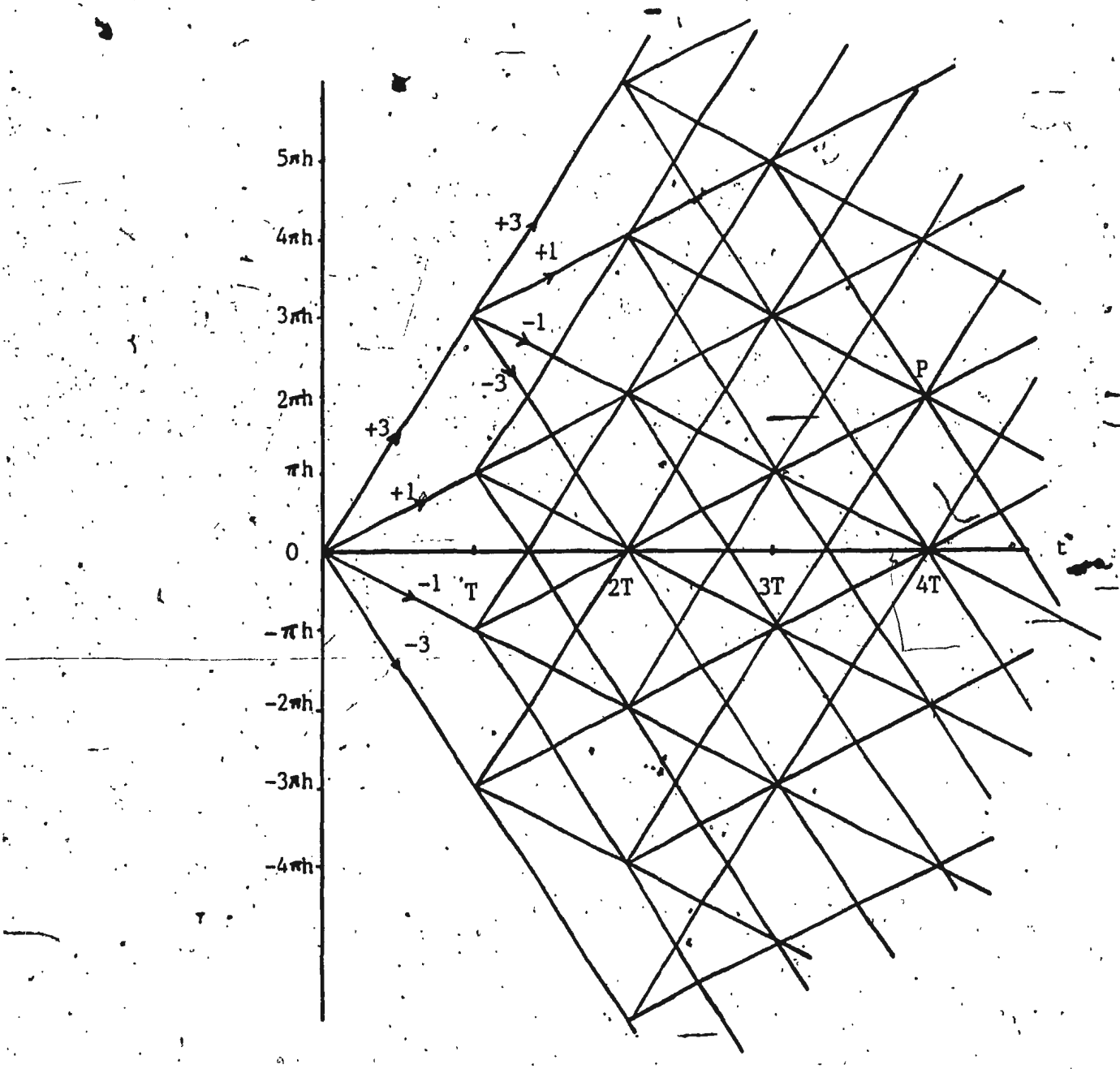

Figure 1.1: Phase tree of quaternary CPFSK.

detection and trellis decoding technique for CPFSK signals. Both are coherent detection techniques and rely on the ability of the receiver to generate a reference carrier in exact phase coherence with the incoming signal.

The correlation receiver for coherent reception of CPFSK signals is shown in Fig. 1.2 . It consists of two parts. The detector or the demodulator part is formed by a bank of correlators supplied with a corresponding set of coherent reference signals $s_1(t), s_2(t), \ldots, s_{L}(t)$. In general, to decode an M-ary CPFSK signal, qM such reference signals are needed, where q is the denominator of the modulation index h. The information of the signal is contained in the correlator outputs and these are used to calculate the Euclidean distance between different branches in the trellis. Distances between the branches are known as the *metrics*. The second part of the receiver, namely the trellis decoder, uses these metrics for the Viterbi algorithm, which finds the sequence of symbols most likely to have been transmitted.

The receiver for M-ary CPFSK studied in this thesis is shown in Fig. 1.3 . It basically consists of a coherent phase detector followed by a trellis decoder. The CPFSK signal is treated as a PSK signal and its phase is measured at the end of each signaling interval. In this method, the received signal is demodulated by multiplying with two coherent carriers in quadrature. The resulting inphase and quadrature waveforms are low pass filtered and sampled synchronously with the transmitter. The phase is computed from the inphase and quadrature samples. The trellis decoder then uses this information to decode the most likely transmitted sequence using the Viterbi algorithm. The distance measure for this receiver is given in Sec.2.4.2.

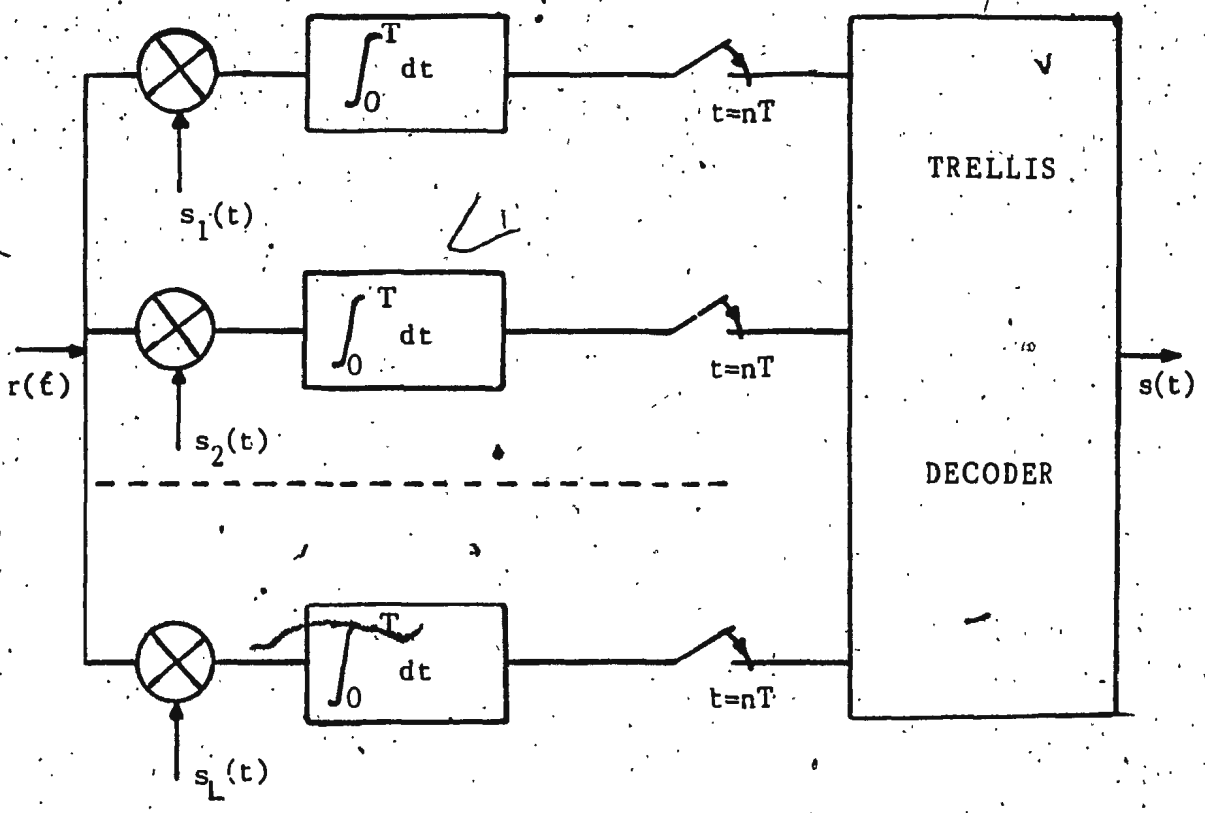

Figure 1.2: Correlation detection and trellis decoding.

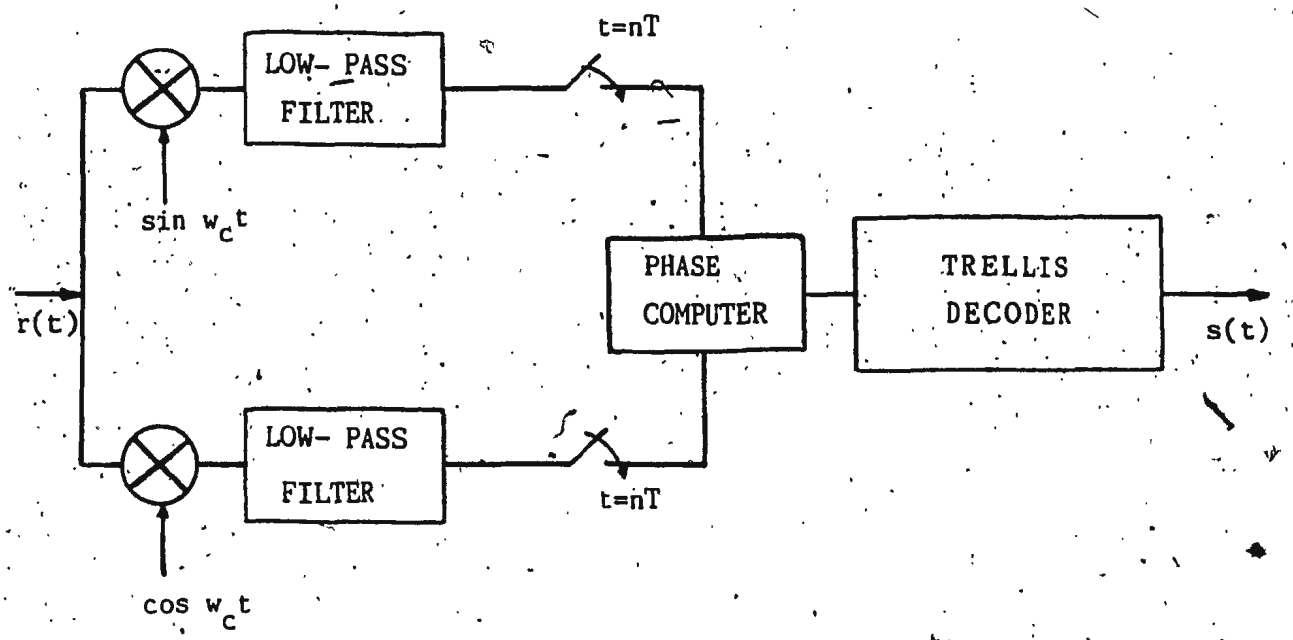

Figure 1.3: Phase detection and trellis decoding.

1.3.2. Minimum Euclidean distance and probability of error

Consider an M-ary signal set consisting of M finite energy signals $\{s_i(t), i = 1, 2, ..., M\}$. One waveform from the set of M waveforms is transmitted every T seconds depending on the incoming message and possibly on the waveforms transmitted in preceding time intervals. The well known geometric interpretation of signals [26] permits representation of the above signals as linear combinations of N orthonormal basis functions where $N \leq M$. This can be seen as an N-dimensional coordinate representation of a signal set and is known as the *signal space*.

The distance between two signal points in the signal space is the same as the Euclidean distance between those two points. The minimum Euclidean distance (MED) between the signal points in a signal constellation is important as it influences the probability of error of a modulation scheme. For signal reception in additive white Gaussian noise channels the probability of error is dominated by the minimum Euclidean distance at high SNR [26].

For M-ary CPFSK signals the squared Euclidean distance between any two signals $s_n(t)$ and $s'_n(t)$ is defined by

$$d^2(s_n, s'_n) = \int_{nT}^{(n+1)T} [s_n(t) - s'_n(t)]^2 dt \qquad (1.5)$$

where

$$s_n(t) = \sqrt{2E_s/T} \cos(\omega_c t + \pi h a_n t/T + \theta_n) \; ; \; nT \leq t \leq (n+1)T \qquad (1.6)$$

and

$$s'_n(t) = \sqrt{2E_s/T} \cos(\omega_c t + \pi h a'_n t/T + \theta'_n) \; ; \; nT \leq t \leq (n+1)T. \qquad (1.7)$$

θ_n and θ'_n are the phase angles of the two signals $s_n(t)$ and $s'_n(t)$ at $t = nT$.

From (1.5) we have

$$d^2(s_n, s'_n) = \int_{nT}^{(n+1)T} s^2{}_n(t)dt + \int_{nT}^{(n+1)T} s'^2{}_n(t)dt - \int_{nT}^{(n+1)T} 2s_n(t)s'_n(t)dt$$

$$= 2E_s - 2\int_{nT}^{(n+1)T} s_n(t)s'_n(t)dt \qquad (1.8)$$

Substituting for $s_n(t)$ and $s'_n(t)$ from (1.6) and (1.7) respectively in (1.8)

$$d^2(s_n, s'_n) = 2E_s - 2\int_{nT}^{(n+1)T} \sqrt{2E_s/T}\cos(\omega_c t + \pi h a_n t/T + \theta_n)$$
$$\sqrt{2E_s/T}\cos(\omega_c t + \pi h a'_n t/T + \theta'_n)dt$$

$$= 2E_s - (2E_s/T)\int_{nT}^{(n+1)T} \{\cos[\pi h(a_n - a'_n)t/T + \theta_n - \theta'_n] +$$
$$\cos[2\omega_c t + \pi h(a_n + a'_n)t/T + \theta_n + \theta'_n]\}dt$$

Assuming $\omega_c \gg 2\pi/T$,

$$d^2(s_n, s'_n) = 2E_s - (2E_s/T)\int_{nT}^{(n+1)T} \cos[\pi h(a_n - a'_n)t/T + \theta_n - \theta'_n]\,dt + e$$

where $e \to 0$ as $\omega_c \to \infty$

$$d^2(s_n, s'_n) = 2E_s\{1 - \frac{\sin[\pi h(a_n - a'_n)/2]}{\pi h(a_n - a'_n)/2}\cos[\pi h(a_n - a'_n)/2 + \theta_n - \theta'_n]\} + e$$

$$d^2(s_n, s'_n) \approx 2E_s\{1 - \mathrm{sinc}[h(a_n - a'_n)/2]\cos[\pi h(a_n - a'_n)/2 + \theta_n - \theta'_n]\} \qquad (1.9)$$

The overall probability of error of a signal set is given by [26],

$$P[\epsilon] = \sum_{i=0}^{M-1} P[\epsilon|s_i(t)]\,P[s_i(t)] \qquad (1.10)$$

where $P[s_i(t)]$ denotes the *apriori* probability that the signal $s_i(t)$ is transmitted and $P[\epsilon|s_i(t)]$ denotes the conditional probability of error given the signal $s_i(t)$ is transmitted. If the signals are equiprobable, that is $P[s_i(t)] = 1/M$ for all $i = 0, 1, \ldots, M-1$ then (1.10) reduces to

$$P[\epsilon] = \frac{1}{M}\sum_{i=0}^{M-1} P[\epsilon|s_i(t)] \qquad (1.11)$$

$P[\epsilon]$ is lower bound by [26],

$$P[\epsilon] \geq Q(d^2_{min}/2N_0) \tag{1.12}$$

while it is upper bound by [26],

$$P[\epsilon] \leq (M-1)\, Q(d^2_{min}/2N_0) \tag{1.13}$$

where $Q(x) = \frac{1}{\sqrt{2\pi}}\int_x^\infty e^{-y^2/2}dy$ [7] and d^2_{min} is the minimum distance of the signal set. This bound is asymptotically tight for small error probabilities [26].

(1.12) and (1.13) indicate that the probability of error for any signal set is asymptotically dependent on the minimum distance between the signals in the set. Also, the minimum distance is a function of symbol energy E_s. Thus $P[\epsilon]$ can be reduced by increasing E_s. However, this is not always a feasible solution because in most communication situations the average power at the transmitter is limited. Therefore we have to resort to other methods such as coding to improve the error performance.

1.3.3. Trellis codes combined with CPFSK signals

A trellis encoder can be considered as a linear finite-state sequential circuit. Generally a trellis code produces $(m+l)$ coded bits from m current information bits and ν preceding bits. The encoder has 2^ν finite states and the code rate is $m/(m+l)$. The encoded bits require $2^{(m+l)}$ channel signals for transmission.

Trellis coding can be implemented by using a convolutional code as follows. The incoming bits are encoded by a $r = m/(m+1)$ binary convolutional code and the resulting coded bits are mapped on to a channel signal set. Since convolutional codes form a subset of trellis codes this process of encoding a binary data stream as a sequence of channel signals is generally known as trellis coding.

Consider an uncoded system that transmits binary data at a rate of nR bit/s, where n is the number of bits per symbol and $R = 1/T$ is the symbol rate. To transmit n bit/symbol 2^n discrete signals are needed. (In the signal space representation of this signal set, there will be 2^n symbol points.) The channel is assumed Gaussian. As stated before, the error performance of such a system, depends upon the minimum Euclidean distance between the symbol points in the signal space.

For a given average power the minimum Euclidean distance decreases with increasing n, that means, an increase in the bit rate degrades the error performance of the communication system. Improved performance within the constraint of average power limitation can be achieved by coding. Either algebraic type block coding or probabilistic type trellis coding can be chosen for implementation in a communication system [24]. In both block coding and trellis coding redundancy is added to the system, thereby enhancing the ability to detect and/or correct errors. However, the effective information rate per transmission bandwidth is reduced [24]. The increase in the minimum Euclidean distance achieved as a result of coding is referred to as the coding gain.

The encoder/modulator of a trellis coded CPFSK scheme is shown in Fig. 1.4. The input bit sequence is converted to a k-bit parallel sequence; then, the serial to parallel converter generates a k-bit output every kT_b seconds, where T_b is the bit duration. The symbol time $T = kT_b$. This k-bit sequence is fed to a (n, k, m) trellis encoder which produces an n-bit output coded sequence. m is the memory of the encoder. The encoded n bits require $M = 2^n$ discrete channel

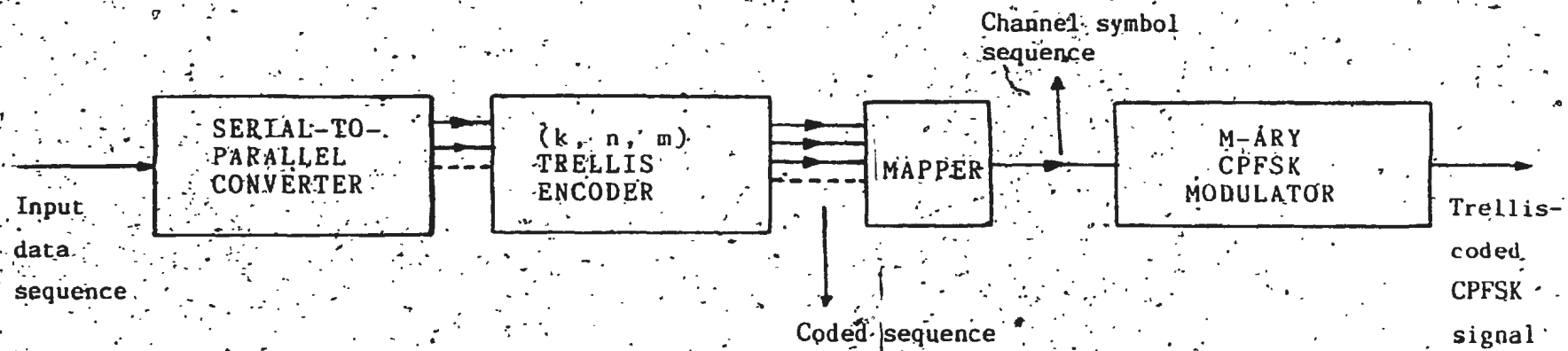

Figure 1.4: Encoder/modulator for trellis coded CPFSK scheme [20].

signals for transmission and therefore are mapped onto an M-ary CPFSK signal set.

As a result of trellis coding, an expanded channel signal set is needed for transmission, for example, where a $(2, 1, m)$ code is used to code the data sequence, the number of possible combinations of output bits is four; then, a quaternary CPFSK scheme is required. If instead a $(3, 2, m)$ or a $(3, 1, m)$ code is used for coding, the number of distinct signaling waveforms required is $M = 2^3 = 8$ and octal CPFSK scheme could satisfy this requirement. By enhancing the memory of CPFSK signals further by trellis coding, better energy efficiency can be expected in addition to the good spectral properties. Detection schemes for M-ary CPFSK signals previously considered can be used to detect trellis coded CPFSK signals as well.

The performance of trellis coded CPFSK schemes, like most other modulation schemes, is commonly evaluated by calculating the symbol error probability. Although in most cases it is not possible to calculate the exact symbol error probability, various performance bounds have been established. For large SNR the symbol error probability is asymptotically determined by the minimum Euclidean distance [26]. Also for CPFSK signaling schemes the minimum Euclidean distance has been shown to be a good performance measure [14].

1.4. Scope of the thesis

The minimum Euclidean distances of CPFSK signals have been calculated in the literature, based on the assumption that the receiver consists of a correlation detector followed by a trellis decoder [4, 15]. A comparison of minimum distances of M-ary CPFSK signals with modulation index $1/M$ with minimum distances of PSK signals is shown in Table 1. Clearly M-ary PSK signals have larger minimum distances than the corresponding CPFSK signals for modulation index $1/M$, even though multiple bit detection is used in the latter case.

As explained in Sec.1.3.1, to coherently decode an M-ary CPFSK signal with modulation index $h\ (= p/q)$ the correlation receiver needs qM correlators. In most cases, however, the number of correlators can be reduced below qM, depending on the value of the modulation index; but, the complexity of the correlation receiver is still too much for implementation, except for small M and q values. On the other hand by treating the CPFSK signal as a PSK signal, and measuring the phase at symbol transition instants it is possible to achieve a larger minimum distance than that achieved by correlation detection. Thus a phase detector which makes its decisions solely by observing the phase can outperform the more complex correlation detection and trellis decoding. Research reported in this thesis is motivated by the above observation. The remaining chapters are organized as follows.

In Chapter 2, uncoded CPFSK signals are considered in detail. Minimum distance values of uncoded M-ary CPFSK signals have been calculated by several

Table 1: Comparison of minimum Euclidean distances of PSK and M-ary CPFSK with modulation index 1/M.

M	$d^2_{min}/2E_b$ M-ary PSK	$d^2_{min}/2E_b$ M-ary CPFSK with h=1/M
2	2.000	2.000
4	2.000	1.454
8	0.879	0.598
16	0.305	0.204

investigators. These calculations are based on various trellis-search algorithms [4, 17]. We derive closed-form expressions for the minimum Euclidean distance of uncoded M-ary CPFSK signals. The distances obtained for the correlation receiver are compared with those obtained for a phase detector. Next it is shown that an M-state trellis is sufficient to achieve almost all performance gain guaranteed by the memory of the modulation process of CPFSK signals when $M > 2$. We also make the observation that trellis decoding of uncoded CPFSK signals is transparent to the carrier phase ambiguities of the regenerated reference tones at the receiver.

In Chapter 3, the minimum Euclidean distances for trellis coded quaternary CPFSK signals and octal CPFSK signals are evaluated, when the receiver consists of a phase detector followed by a trellis decoder. The minimum distances obtained are compared with previously reported results for a correlation receiver. We also search for good codes in the small h region for combined channel coding and CPFSK modulation. Finally it is shown that trellis decoding of coded CPFSK signals is transparent to phase ambiguities of the regenerated reference tones of the coherent demodulator.

The implications of the results are discussed in Chapter 4 and conclusions made thereof. The thesis is concluded after a brief discussion of future work pertaining to this research.

Chapter 2

DISTANCE PROPERTIES OF UNCODED CPFSK SIGNALS

2.1. Introduction

In this chapter it is shown how continuous phase frequency shift keyed (CPFSK) signals with rational value modulation index h ($h = p/q$, where p and q are relatively prime numbers), can be represented by a finite-state trellis whose states have a one-to-one relationship to the phase of the CPFSK signal. Next it is shown that trellis decoding is transparent to q-fold phase ambiguities of the regenerated reference tones of the coherent demodulator. Then, closed-form expressions are presented for the minimum Euclidean distance (MED) of uncoded M-ary CPFSK signals. These expressions yield exact values of the MED for all rational valued modulation indices. A coherent phase detector followed by a trellis decoder is shown to out-perform the more complex correlation detection and trellis decoding of uncoded CPFSK signals in the small h region ($h \leq 1/M$). After presenting extensive numerical results, it is also shown that the optimum modulation index for correlation detection of M-ary CPFSK signals can be approximated by $(M-1)/M$, without an appreciable reduction in the largest minimum distance that is achieved. The optimum modulation index for phase detection of M-ary CPFSK signals is shown to be $1/M$.

2.2. Trellis representation of CPFSK signals

The M-ary CPFSK signaling waveform can be mathematically expressed as

$$s(t) = \sqrt{2E_s/T}\cos(\omega_c t + \omega_d \int_0^t x(t)\,dt + \phi_0) \qquad (2.1)$$

with the frequency deviation ω_d given by

$$\omega_d = \pi h/T \qquad (2.2)$$

where h is the modulation index. $x(t)$ is the baseband data sequence used to modulate the carrier of nominal angular frequency ω_c. E_s is the symbol energy and T is the symbol duration. ϕ_0 is the phase of the carrier at $t = 0$ or the phase accumulated over the period $-\infty < t < 0$. For coherent systems ϕ_0 can be set equal to zero without any loss of generality. The baseband data signal $x(t)$ is represented as,

$$x(t) = \sum_n a_n\, g(t - nT) \qquad (2.3)$$

where $\{a_n\}=\{...,a_{-1}, a_0, a_1,...\}$ is the data sequence. a_n can take on any value of the M-ary set $\{\pm 1, \pm 3, \ldots, \pm(M-1)\}$ with equal probability. $g(t)$ is a rectangular pulse given by

$$g(t) = \begin{cases} 1/T, & 0 \le t \le T \\ 0, & \text{otherwise} \end{cases} \qquad (2.4)$$

2.2.1. Trellis representation of MSK signals

Binary CPFSK signaling with modulation index $h = 1/2$ is considered first. This is also referred to as minimum shift keying (MSK). The following trellis description can be found in [11] and is presented here for the completeness of this discussion.

There are two tones transmitted in the instance of MSK, -1 corresponding

to the angular frequency $(\omega_c - \pi/2T)$ and $+1$ corresponding to $(\omega_c + \pi/2T)$. Assume that the lowest tone of the MSK signal goes through an integer multiple of cycles during one signaling interval [11]. Then

$$(\omega_c - \pi/2T)T = 2n\pi = 0 \qquad \text{(modulo } 2\pi) \qquad (2.5)$$

This assumption simplifies the phase trellis, but does not alter the spectral characteristics and the distance properties of the phase trellis. For the higher frequency tone

$$(\omega_c + \pi/2T)T = \pi \qquad \text{(modulo } 2\pi) \qquad (2.6)$$

Recalling that ϕ_0 in (2.2) can be set equal to zero without any loss of generality, when $+1$ is transmitted,

$$s_{+1}(t) = \sqrt{2E_s/T}\cos[(\omega_c + \pi/2T)t + x_n] \qquad (2.7)$$

and when -1 is transmitted

$$s_{-1}(t) = \sqrt{2E_s/T}\cos[(\omega_c - \pi/2T)t + x_n] \qquad (2.8)$$

where

$$x_n = x_{n-1} + n\pi h\,(a_{n-1} - a_n) \qquad (2.9)$$

From $(2.5) - (2.8)$ it can be seen that when $+1$ is transmitted the phase of $s(t)$ advances by π and that -1 does not cause any change in the phase of $s(t)$. Specializing (2.9) for MSK

$$x_n = 0, \pi \qquad \text{(modulo } 2\pi) \qquad (2.10)$$

Therefore for MSK, x_n can take only the two values 0 and π (modulo 2π). The phase trellis of MSK can be drawn using this result and the earlier results that $+1$ causes a phase change of π and -1 causes a phase change of 0. This is shown in Fig. 2.1a . The state diagram of MSK is shown in Fig. 2.1b . $\theta(t)$ in Fig. 2.1a represents the phase of the MSK signal. The phase trellis consists of two states at each level, corresponding to the two possible phase values. These states are

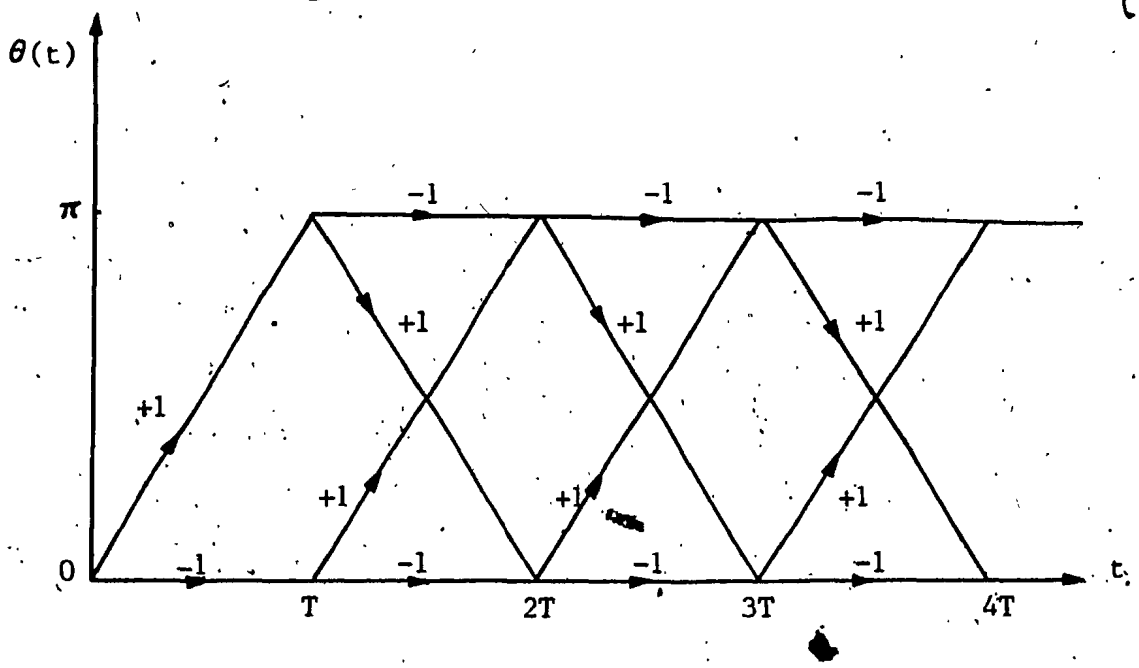

(a)

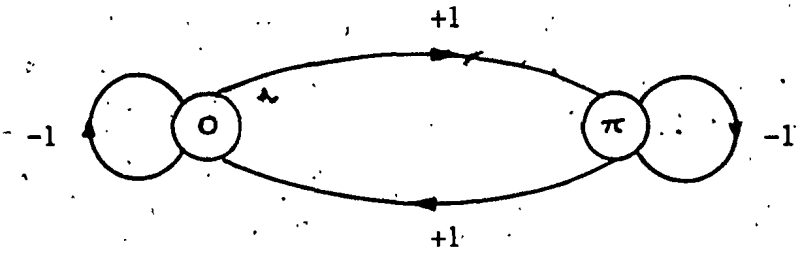

(b)

Figure 2.1: Trellis representation of MSK [11].
(a) Trellis. (b) State diagram.

obtained by a one-to-one mapping of the phase values x_n (modulo 2π). Every state has two branches leaving, each related to $+1$ or -1. A total of four branches connect the states of any two adjacent levels. Four different waveforms are transmitted depending on the MSK modulator state (0 or π) and the input symbol ($+1$ or -1). They are

$$+1: \quad s_1(t) = \sqrt{2E_s/T}\cos(\omega_c t + \pi t/2T + 0) \tag{2.11a}$$

$$+1: \quad s_2(t) = \sqrt{2E_s/T}\cos(\omega_c t + \pi t/2T + \pi) \tag{2.11b}$$

$$-1: \quad s_3(t) = \sqrt{2E_s/T}\cos(\omega_c t - \pi t/2T + 0) \tag{2.11c}$$

$$-1: \quad s_4(t) = \sqrt{2E_s/T}\cos(\omega_c t - \pi t/2T + \pi) \tag{2.11d}$$

In Section 2.3 these waveforms are encountered again with respect to the correlation receiver for MSK, where the correlators are provided with the above four coherent tones.

2.2.2. Trellis representation of quaternary CPFSK signals

For quaternary CPFSK signals, a_n can take on values from the set $\{\pm 1, \pm 3\}$. This example considers signaling with modulation index 1/4. Rewriting (2.9) with $h = 1/4$

$$x_n = x_{n-1} + \frac{n\pi}{4}(a_{n-1} - a_n) \tag{2.12}$$

where $a_n, a_{n-1} = \{\pm 1, \pm 3\}$ for all integral values of n. Then

$$x_n = 0, \pi/2, \pi, 3\pi/2 \quad \text{(modulo } 2\pi) \tag{2.13}$$

Therefore x_n can take only the four values 0, $\pi/2$, π, and $3\pi/2$ for quaternary CPFSK signals with $h = 1/4$.

Four different tones are transmitted in this instance. Quaternary symbols -3, -1, $+1$, and $+3$ correspond to the tones of angular frequency

$(\omega_c - 3\pi/4T)$, $(\omega_c - \pi/4T)$, $(\omega_c + \pi/4T)$ and $(\omega_c + 3\pi/4T)$ respectively. Again it is assumed that the tone with the lowest angular frequency goes through an integer multiple of cycles during one signaling interval. Thus

$$-3: \quad (\omega_c - 3\pi/4T)T = 2n\pi = 0 \qquad \text{(modulo } 2\pi) \qquad (2.14a)$$

$$-1: \quad (\omega_c - \pi/4T)T = \pi/2 \qquad \text{(modulo } 2\pi) \qquad (2.14b)$$

$$+1: \quad (\omega_c + \pi/4T)T = \pi \qquad \text{(modulo } 2\pi) \qquad (2.14c)$$

$$+3: \quad (\omega_c + 3\pi/4T)T = 3\pi/2 \qquad \text{(modulo } 2\pi) \qquad (2.14d)$$

$(2.14a) - (2.14d)$ reveal that the symbols -3, -1, $+1$, and $+3$ are associated with phase changes of 0, $\pi/2$, π and $3\pi/2$ respectively in the phase of $s(t)$, where $s(t)$ is given by

$$s(t) = \sqrt{2E_s/T}\cos(\omega_c t + \pi a_n t/4T + x_n) \qquad (2.15)$$

Using the results of equations (2.13) and (2.14), the phase trellis of quaternary CPFSK for $h = 1/4$ can now be drawn as shown in Fig. 2.2a. The state diagram representation of the same trellis is given in Fig. 2.2b. The above trellis comprises of four states. They are obtained by a one-to-one mapping of the phase values x_n. Every state has four branches leaving, each of which is related to one of -3, -1, $+1$, or $+3$. A total of sixteen branches connect the states of any two adjacent levels of the trellis. Consequently sixteen different waveforms are possible depending on the state of the modulator and the input signal.

In the two examples considered above, the number of states of the trellis at a given level, and the number of branches leaving each state were equal. Next, a

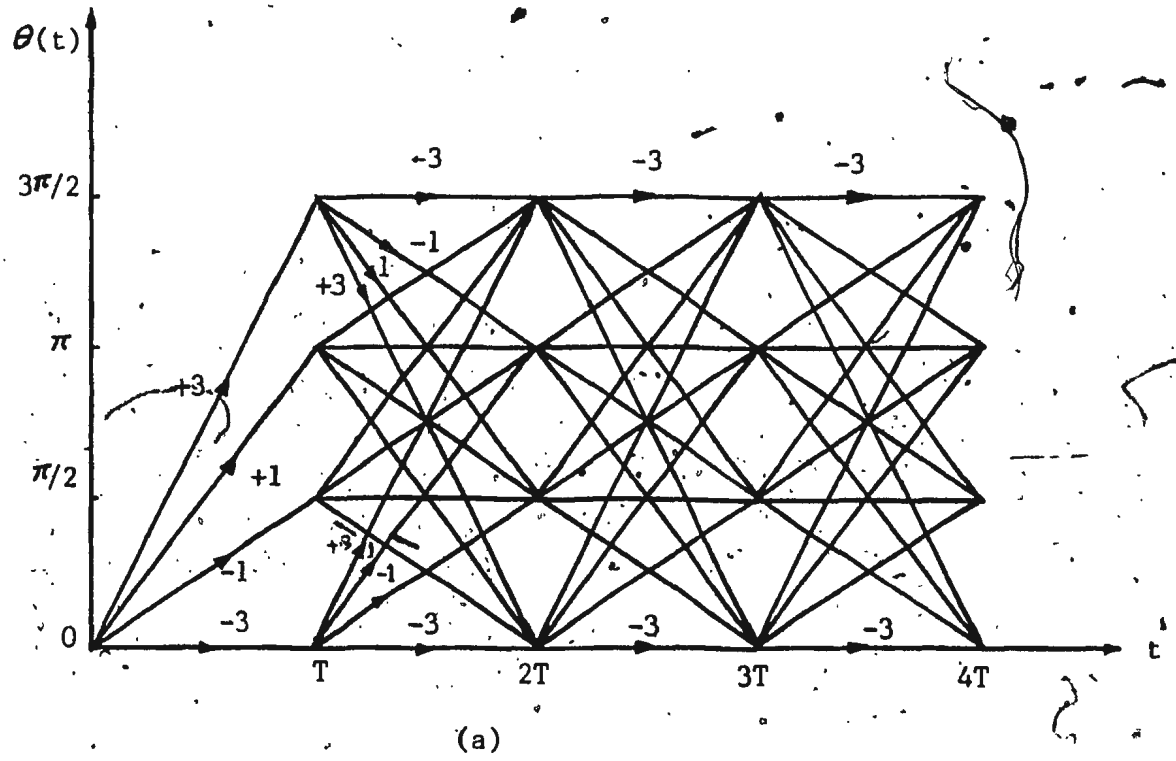

(a)

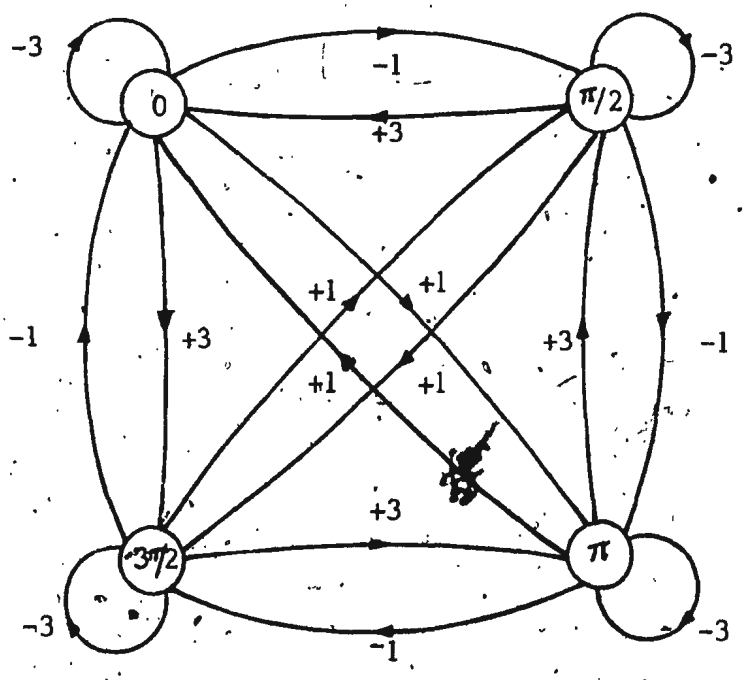

(b)

Figure 2.2: Trellis representation of quaternary CPFSK for h=1/4.
(a) Trellis. (b) State diagram.

case where the number of states of the trellis at a given level is less than the number of branches leaving a state is considered.

Now consider quaternary CPFSK for $h = 1/3$. From (2.9)

$$x_n = x_{n-1} + \frac{n\pi}{3}(a_{n-1} - a_n) \tag{2.16}$$

where a_{n-1}, $a_n = \{\pm 1, \pm 3\}$ for all integral values of n. With arguments similar to those of previous examples, in general

$$x_n = x_{n-1} + \frac{n\pi}{3}(a_{n-1} - a_n) \tag{2.17}$$

$$= 0, 2\pi/3, 4\pi/3 \qquad \text{(modulo } 2\pi) \tag{2.18}$$

Therefore x_n can take only three values, for quaternary CPFSK signals with $h = 1/3$. The quaternary symbols -3, -1, $+1$, and $+3$ correspond to tones of angular frequency $(\omega_c - \pi/T)$, $(\omega_c - \pi/3T)$, $(\omega_c + \pi/3T)$, and $(\omega_c + \pi/T)$ respectively. As before, if the frequency of the lowest tone is fixed such that

$$-3: \quad (\omega_c - \pi/T)T = 2n\pi = 0 \qquad \text{(modulo } 2\pi) \tag{2.19a}$$

then the phase angles accumulated in each signaling interval for the other tones are

$$-1: \quad (\omega_c - \pi/3T)T = 2\pi/3 \qquad \text{(modulo } 2\pi) \tag{2.19b}$$

$$+1: \quad (\omega_c + \pi/3T)T = 4\pi/3 \qquad \text{(modulo } 2\pi) \tag{2.19c}$$

$$+3: \quad (\omega_c + \pi/T)T = 0 \qquad \text{(modulo } 2\pi) \tag{2.19d}$$

With the above results, the trellis of quaternary CPFSK signals for $h = 1/3$ can be drawn as shown in Fig. 2.3a. The state diagram is given in Fig. 2.3b. The number of states in the trellis at each level is less than the number of branches leaving each state. Therefore there are parallel branches between the

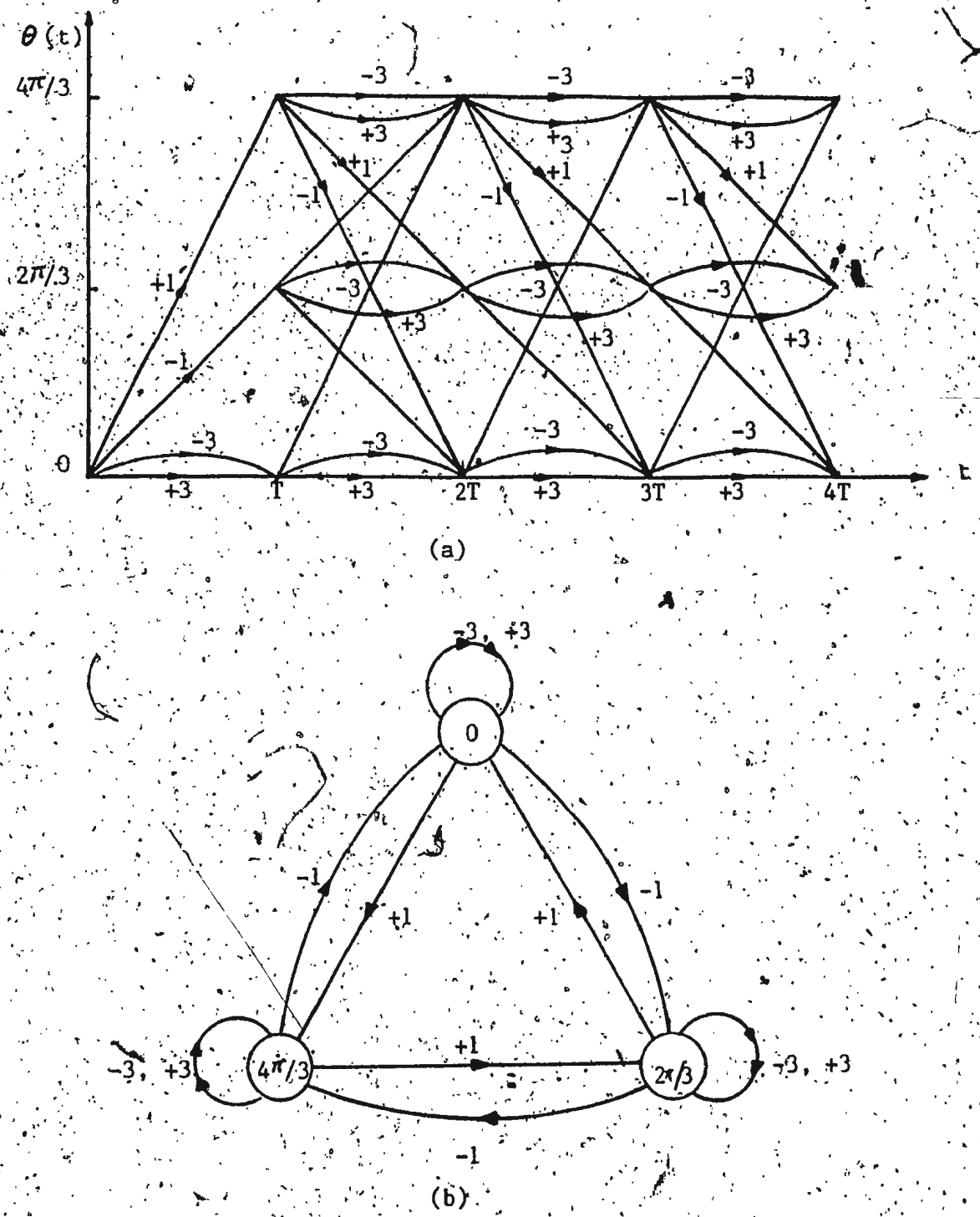

Figure 2.3: Trellis representation of quaternary CPFSK for h=1/3.
(a) Trellis. (b) State diagram.

states of adjacent levels. Moreover, the waveforms associated with the parallel branches are orthogonal. The presence of parallel branches mentioned above, also has implications on the distance properties of the CPFSK modulation scheme. These implications as well as their effect on the distance properties will be discussed in Section 2.4.

2.2.3. Trellis representation of M-ary CPFSK signals

This section considers trellis representation of M-ary CPFSK signals. As stated earlier for M-ary CPFSK signaling, a_n can take on any value from the set $\{\pm 1, \pm 3, \ldots, \pm(M-1)\}$ with equal probability. M distinct tones are transmitted in relation to each of the M symbols in the above set. The lowest tone has an angular frequency of $\{\omega_c - \pi h(M-1)/T\}$. Assuming that this lowest tone goes through an integer multiple of cycles during one signaling interval,

$$-(M-1): \ [\omega_c - (\pi h/T)(M-1)]T = 2n\pi = 0 \quad \text{(modulo } 2\pi) \quad (2.20a)$$

$$-(M-3): \ [\omega_c - (\pi h/T)(M-3)]T = 2\pi h \quad \text{(modulo } 2\pi) \quad (2.20b)$$

.....

$$+(M-1): \ [\omega_c + (\pi h/T)(M-1)]T = 2(M-1)\pi h \quad \text{(modulo } 2\pi) \quad (2.20c)$$

Therefore x_n (modulo 2π) assumes the values of the set given by $X = \{0, \ 2\pi h, \ 4\pi h, \ \ldots, \ 2(M-1)\pi h\}$. x_n is constant over a signaling interval. The value of x_n in the current signaling interval depends upon the value of x_n during the preceding signaling interval and the symbol transmitted during that signaling interval. With the further assumption that h is a rational number such that $h = p/q$, where p and q are relatively prime numbers, coupled with the modulo 2π rendition of the phase, the elements of the set X reduce to q distinct values. This

was clear with quaternary CPFSK signaling for $h = 1/3$, where the modulo 2π reckoning left us with only three states instead of four.

This reduction in the number of states enables the CPFSK signaling waveforms to be described by a q-state trellis, where the q states are obtained by a one-to-one mapping of the phase values x_n. For M-ary signaling, every state has M branches leaving and M branches merging. Each branch is associated with a symbol of the M-ary alphabet. When $q \geq M$ the number of distinct states is greater than the number of branches leaving each state; therefore, no parallel branches exist between the states of adjacent levels. When $q < M$ the number of states at a given level is less than the number of branches leaving each state, which gives rise to parallel paths in the trellis. This was obvious with quaternary CPFSK trellis for $h = 1/3$ ($q = 3$ and $M = 4$; $q < M$) where it was shown that two parallel paths exist for each state. For integer valued modulation indices

$$2\pi h = 4\pi h = \ldots = 2(M-1)\pi h = 0 \quad \text{(modulo } 2\pi\text{)} \qquad (2.21)$$

Therefore the set X has only one element, and the trellis degenerates into a single state trellis. There are M parallel branches between the states.

2.3. Carrier phase ambiguity and trellis decoding of CPFSK signals

To use coherent demodulation techniques with CPFSK signaling, coherent tones need to be locally regenerated at the receiver, in exact phase coherence with the received signal. This can be achieved by several techniques [6], one of which, the M^{th} power method, is examined in the example given below. However, irrespective of the method being used, an ambiguity concerning the true carrier phase always remains unresolved.

One method of carrier recovery entails passing the received signal through a nonlinear circuit such as a $\times M$-multiplier, filtering the output in a narrowband filter, limiting the output of the filter to remove amplitude fluctuations and then frequency dividing to yield a reference at the carrier frequency. For binary CPFSK signals with modulation index 0.5, the above method involves squaring of the signal, narrowband filtering and then frequency dividing by two to recover the tones required for coherent demodulation. This process introduces a 180° phase ambiguity due to the divide-by-two circuit. In general where a phase reference is obtained by a divide-by-N circuit the phase reference is determined only by modulo $2\pi/N$; thus N-fold phase ambiguity may occur [10]. In the following section it is shown that trellis decoding of CPFSK signals is transparent to the phase ambiguity of locally generated reference tones.

As the first example, consider trellis decoding of MSK (binary CPFSK with modulation index 1/2). Trellis representation of MSK was discussed in Section 2.2.1. Recall that in every signaling interval one of four distinct waveforms is transmitted, the actual transmitted waveform being dependent upon the bit in that interval and the bit in the preceding interval. The correlation receiver for MSK is shown in Fig. 2.4 . In every signaling interval the receiver correlates the received signal with the waveforms, and the correlator outputs are used to determine the path-metric for the trellis decoder. The four correlator outputs of the correlation receiver shown in Fig. 2.4 can be treated as the path-metrics for the trellis decoder, and Viterbi algorithm is used to determine the path with the largest metric which is subsequently declared as the decoded path. In general

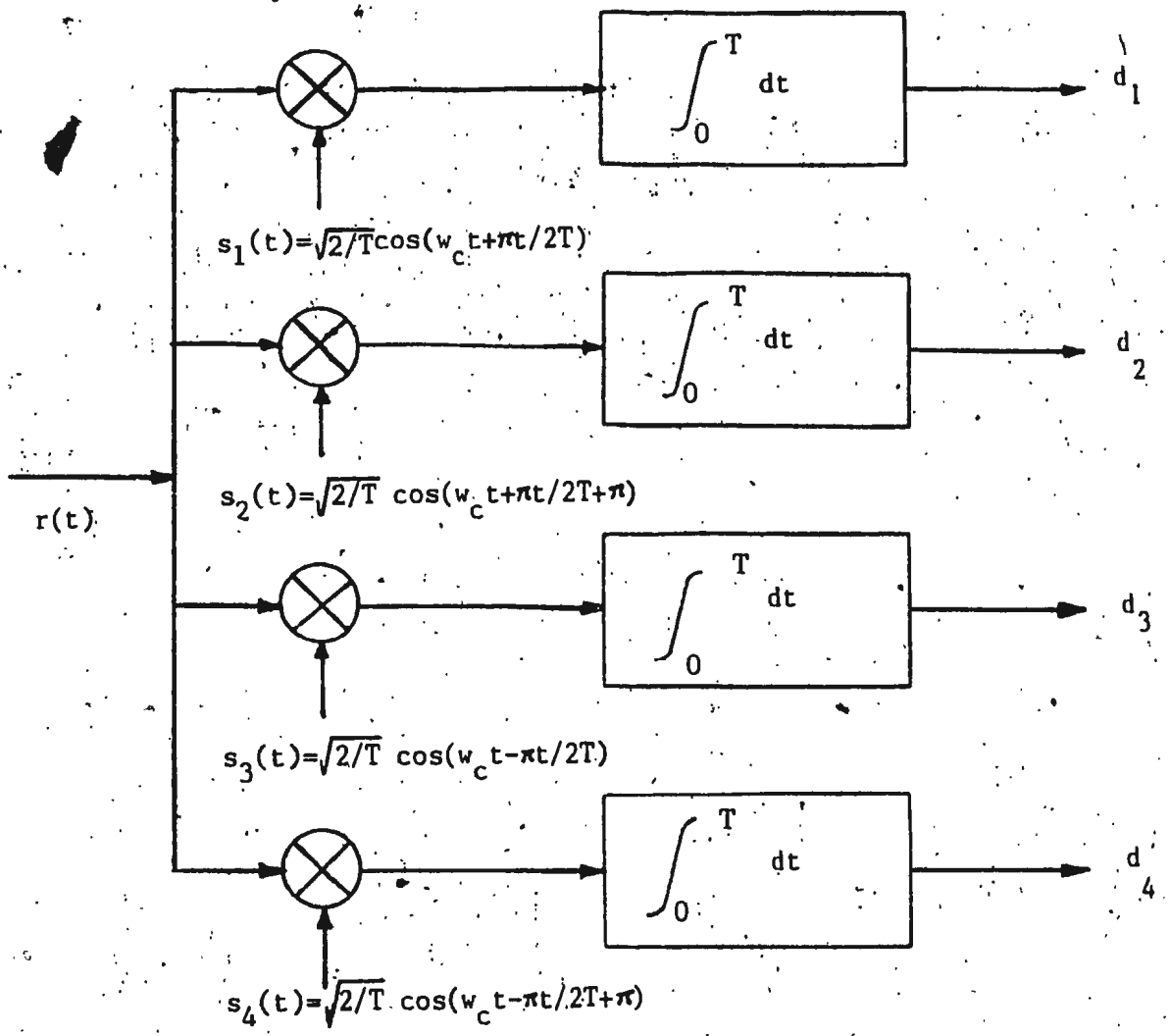

Figure 2.4: Correlation receiver for binary CPFSK signals.

there are qM correlators in the correlation receiver; however, in most cases the number of correlators required can be reduced depending on the value of h.

Consider the data sequence 1, 1, −1, 1, −1, 1, −1, −1. The path of this data sequence through the MSK trellis is shown in Fig. 2.5. The solid line indicates the path selected when the reference tones are in exact phase synchronism with the incoming signal. The assumption that the demodulator starts at '0' state implies the knowledge of the carrier phase. If the receiver were unable to resolve the phase ambiguity and consequently the reference tones are 180° out of phase with the incoming tones, the correlator outputs can be recalculated and the path which yields the largest metric determined. The above data sequence when decoded with a 180° phase ambiguity results in the path, indicated by the dotted line. The new path also decodes the data sequence correctly. The reason for this can be explained by a careful analysis of the trellis itself.

The MSK trellis is symmetrical. If the two states are interchanged by relabeling them such that states 0 and π become π and 0 respectively, the trellis remains unchanged. This relabeling is equivalent to giving a rotational shift to the states by adding 180° to each state. As mentioned in Section 2.2.1, the phase angles of the transmitted signal and the states of the trellis are one-to-one related. Therefore a rotational shift to the trellis can be interpreted as adding 180° to the incoming signals' phase or alternatively, to the reference tones of the correlation receiver. Thus for MSK signaling the trellis is invariant to rotational shifts of 180° and the phase ambiguity of the tones does not affect the process of trellis decoding.

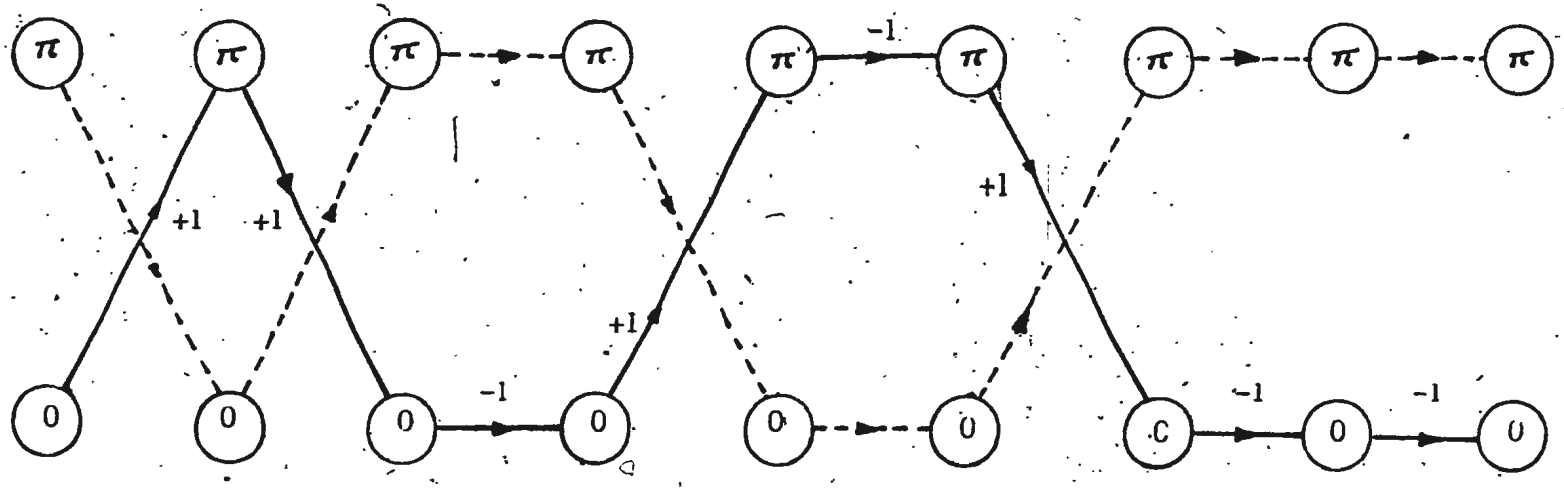

Figure 2.5: Effect due to carrier phase ambiguity of 180° on binary CPFSK for $h=\frac{1}{2}$.

Next, quaternary CPFSK signaling with $h = 1/4$ is considered. The trellis and the state diagram of quaternary CPFSK were given in Fig. 2.2. Any rotational shift of the states by an integer multiple of $\pi/2$ does not change the trellis and the state diagram. This is because the labeling of the branches is rotationally symmetric and the paths merging at a state as well as those leaving a state are unchanged by a rotational shift. Because of the one-to-one relationship between the states and the phase angles of the transmitted signal, a rotational shift of the states by an integer multiple of $\pi/2$ is equivalent to shifting the phase angles of the reference tones by the same amount, all phase angles being reckoned modulo 2π. Therefore it can be concluded that trellis decoding of quaternary CPFSK signals for $h = 1/4$ is transparent to phase ambiguities of $0°$, $90°$, $180°$ and $270°$.

For M-ary CPFSK signals with modulation index $h = p/q$, where p and q are relatively prime integers, as discussed in Section 2.2.3, the trellis reduces to a q-state trellis. Also it is invariant to rotational shifts of integer multiples of $2\pi h$. Again because of the one-to-one mapping between the signal phase angles and the trellis states, it is concluded that trellis decoding of M-ary CPFSK signals is transparent to q-fold ambiguities of the reference tones. The trellis decoder successfully resolves phase ambiguities of $2\pi h$, $4\pi h$, . . . , $2(q-1)\pi h$.

2.4. Closed-form expressions for the minimum Euclidean distance of M-ary CPFSK signals

2.4.1. Correlation detection and trellis decoding

Consider the reception of M-ary CPFSK signals in an AWGN channel using the correlation receiver shown in Fig. 1.2 on page 9. The squared Euclidean distance between any two branches that start at level n and end in level $(n+1)$, illustrated in Fig. 2.6, is evaluated in Section 1.3 as

$$d^2_n = \int_{nT}^{(n+1)T} [s_n(t) - s'_n(t)]^2 dt \tag{2.22}$$

$$= 2E_s\{1 - \text{sinc}\,[h(a_n - a'_n)/2] \cos[\pi h(a_n - a'_n)/2 + \theta_n - \theta'_n]\} \tag{2.23}$$

where θ_n and θ'_n are the phase angles of the two signals $s_n(t)$ and $s'_n(t)$ respectively at $t = nT$. θ_n and θ'_n can also be identified as the values corresponding to the initial states of the two branches $s_n(t)$ and $s'_n(t)$ at level n of the CPFSK trellis. θ_{n+1} and θ'_{n+1} are the terminating states at level $(n+1)$.

The minimum Euclidean distance (MED) is the smallest distance between all possible pairs of signals $s_n(t)$ and $s'_n(t)$ through the trellis. The MED in general depends upon the length of the signal pair and the modulation index. The probability of error is asymptotically dependent upon the MED. Therefore it is needed to calculate this distance to evaluate the error performance of a CPFSK signaling scheme. Some previous approaches to find the minimum Euclidean distance involved employing various trellis-search algorithms to minimize (2.23) for all possible signal paths [4, 17].

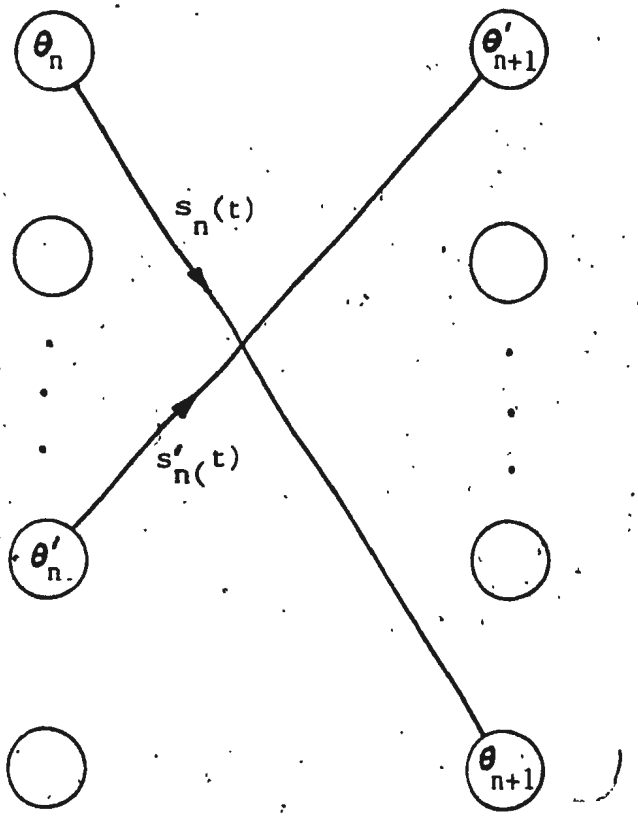

Figure 2.6: Two signal paths of the CPFSK trellis.

Although the algorithms for trellis-search can be implemented on a digital computer, the time and memory requirements makes the algorithmic approach unattractive except for small M and q values. Alternatively, in some cases bounds on the MED have been presented [3, 4].

Focusing on the trellis structure of M-ary CPFSK signals, closed-form expressions are derived for the MED of M-ary CPFSK signals in the following section. The following analysis and the resulting expressions yield exact values of the minimum Euclidean distance. The MED is evaluated for M=2, 4, 8 and 16 using these expressions, as well as using a conventional trellis-search algorithm [17]. Numerical results are presented in Section 2.4.4.

To facilitate evaluation of the MED, the rational valued modulation index ($h = p/q$) is split into two disjoint regions such that $q \geq M$ and $q < M$. In addition all integral values of h will be considered separately. Each case is considered in detail below.

Case (i): $q \geqslant M$

To calculate the minimum Euclidean distance of a given M-ary CPFSK scheme, all possible signal pairs through the trellis have to be considered. When $q \geq M$, as shown in Section 2.2.3 the trellis of CPFSK has no parallel branches. Therefore the pair of paths that produces the MED begins from a common state at a certain level, diverges and traverses through the trellis without encountering any state at the same time. After a finite number of split levels it remerges at another level. For simplicity it is assumed that a split takes place at level zero. In other words the two paths have identical phase trajectories up to level zero.

The above assumption does not cause any loss of generality. This is due to the rotational symmetry of the trellis of CPFSK signals discussed in Section 2.3.

Let the signals transmitted during the first time interval of the split-merge event be $s_0(t)$ and $s_0'(t)$. The symbol a_0 corresponds to $s_0(t)$, a_0' to $s_0'(t)$. The squared distance between these two signals in the first split interval can be obtained by setting $\theta_n = \theta_n'$ in (2.23). Then

$$d^2_0 = 2E_s\{1 - \text{sinc}\,[h(a_0 - a'_0)/2]\cos[\pi h(a_0 - a'_0)/2]\}$$
$$= 2E_s\{1 - \text{sinc}\,[h(a_0 - a'_0)]\} \qquad (2.24)$$

Suppose merging takes place at level $(n+1)$, the squared distance between the last two branches of the split-merge event can be obtained from (2.23) by making use of $\theta_{n+1} = \theta'_{n+1}$. Let this distance be d_n^2. Then

$$d^2_n = 2E_s\{1 - \text{sinc}\,[h(a_n - a'_n)]\} \qquad (2.25)$$

Next concentrating on a split-merge event of length two, which consists of a pair of paths splitting at level zero and merging at level two, for merging of signal paths the modulo 2π phase change along each path should be equal and opposite. Thus the symbols associated with these two paths satisfy the relation

$$a_0 - a'_0 = -(a_1 - a'_1) \qquad (2.26)$$

Defining $\gamma = a_0 - a'_0$, the squared distance between the two paths can be obtained from (2.24) and (2.25) as

$$d^2(0,2) = d^2_0 + d^2_1$$
$$= 4E_s[1 - \text{sinc}\,(\gamma h)] \qquad (2.27)$$

The argument of $d^2(.)$ where shown, denotes the split level and the merging level.

The squared MED of all split-merge events of length two for a given h is obtained by minimizing (2.27) over all possible values of γ as

$$d^2_{min}(0, 2) = \text{Min}_{\gamma}\, 4E_s[1 - \text{sinc}(\gamma h)], \qquad (2.28)$$

where $\gamma \in \{2, 4, \ldots, 2(M-1)\}$. From (2.24) and (2.25) it is seen that $d_0^2 = d_1^2$. Therefore when $d^2(0,2)$ minimizes for any γ, then d^2_0 and d^2_1 also minimize for the same γ.

$$d^2(0, 2) = \text{Min}_{\gamma}\, [d^2_0] + \text{Min}_{\gamma}\, [d^2_1] \qquad (2.29)$$

Next considering a split-merge event of length n, the squared Euclidean distance between the two paths can be written as

$$d^2(0, n+1) = d^2_0 + d^2_1 + \ldots + d^2_n \qquad (2.30)$$

where the split interval distance d^2_0 is given by (2.24) and the merging interval distance d^2_n is given by (2.25). Noting that the Euclidean distance is never negative, it can be observed that for any split-merge event of length n

$$\begin{aligned} d^2(0,n+1) &\geq \text{Min}\,(d^2_0) + d^2_1 + d^2_2 + \ldots \text{Min}\,(d^2_n) \qquad (2.31) \\ &\geq d^2_{min}(0, 2) \end{aligned}$$

Therefore the MED is given by the paths of split-merge event of length two.

The expression for the squared MED is

$$d^2_{min} = \text{Min}_{\gamma}\, \{4E_s[1 - \text{sinc}(\gamma h)]\}, \quad q \geq M, \qquad (2.32)$$

where the minimization is carried out over $\gamma \in [2, 4, \ldots, 2(M-1)]$. In order to evaluate the exact values of d^2_{min} for a given M, comparison among only $(M\text{-}1)$ values is required, thereby greatly simplifying the calculation procedure. For binary CPFSK signals, γ can take only one value; $\gamma = 2$.

$$d^2_{min} = 4E_s[1 - \text{sinc}(2h)], \quad q \geq 2 \tag{2.33}$$

Case (ii): q < M

An example with $q < M$ for quaternary CPFSK, with modulation index $h = 1/3$ was considered in Section 2.2.2. When $q < M$, the number of branches per state exceeds the total number of states at each level of the trellis of CPFSK. Thus there will be parallel branches between the states of adjacent levels. It can be shown easily that the signal waveforms associated with these parallel branches are orthogonal.

Consider one of the parallel paths of the trellis of quaternary CPFSK signals for $h = 1/2$ shown in Fig. 2.7 . The two signal waveforms transmitted between '0' state of one level and 'π' state of the following level are $\sqrt{2E_s/T}\cos(\omega_c t + 3\pi t/2T)$ corresponding to +3 and $\sqrt{2E_s/T}\cos(\omega_c t - \pi t/T)$ corresponding to −1. Clearly, these two waveforms are orthogonal to each other. Signals associated with all other parallel branches are also orthogonal. From the knowledge of geometric representation of signals, it is known that the signal space distance between any two orthogonal signals is $\sqrt{2E_s}$. Therefore the distance between any two parallel paths is also $\sqrt{2E_s}$. This result is important in evaluation of the MED for $q < M$.

It remains to establish the condition under which these parallel branches become the minimum distance paths. Bearing in mind that two consecutive signals do not yield parallel branches [if so, the trellis degenerates to a single state

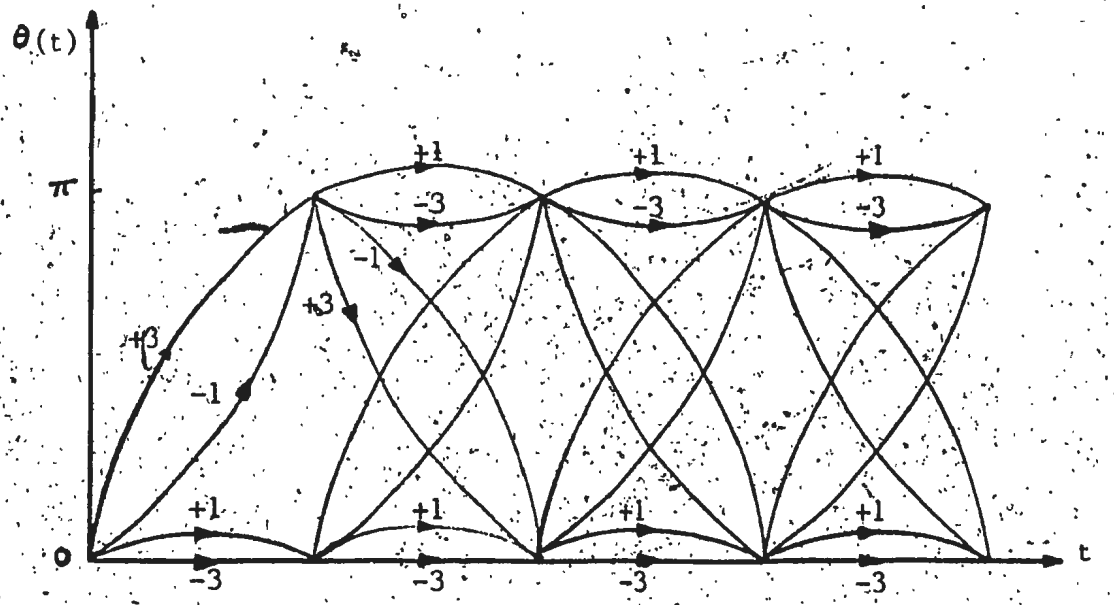

Figure 2.7: Trellis of quaternary CPFSK for h=1/2.

trellis, because $2\pi h = 0$ (modulo 2π), which is considered under Case (iii)], it can observed that the inequality

$$4E_s[1 - \text{sinc}(\gamma h)] \geq 2E_s \tag{2.34}$$

is satisfied if $\gamma h > 0.603355$ approximately. If $2E_s$ is less than the minimum value of $4E_s(1 - \text{sinc}\,\gamma h)$ then the parallel paths yield the MED. The smallest value of γ is two. Therefore it is concluded that if $h > 0.301677$ parallel paths yield the minimum distance. Thus the squared MED of CPFSK signals for $h = p/q$, when $q < M$ is given by

$$d^2_{min} = \begin{cases} 2E_s, & h > 0.301677 \\ 4E_s[1 - \text{sinc}(2h)], & h < 0.301677 \end{cases} \tag{2.35}$$

Case (iii): Integral values of h

For integral values of h, $2\pi h = 0$ (modulo 2π). Correspondingly the trellis degenerates into a single state trellis and there are M parallel branches between adjacent levels. The distance between any two parallel branches is $2E_s$. Therefore the squared MED for integral values of h is $2E_s$.

Combining the results of the above three cases, the squared MED of M-ary CPFSK signaling with $h = p/q$ is

$$d^2_{min} = \begin{cases} 2E_s, & \text{(integer h)} \\ \text{Min}_{\gamma}\,[4E_s(1 - \text{sinc}\,\gamma h)], & q \geq M \\ 4E_s[1 - \text{sinc}(2h)], & h < 0.301677,\ q < M \\ 2E_s, & h > 0.301677,\ q < M \end{cases} \tag{2.36}$$

where, $\gamma = 2, 4, \ldots, 2(M-1)$.

2.4.2. Phase detection and trellis decoding

In deriving the Euclidean distance in (2.23), it was assumed that the receiver is of correlation type. In other words the distance measure as given is valid only for correlation detection and trellis decoding using maximum likelihood sequence estimation.

The coherent phase detector discussed in Section 1.2 for detection of M-ary CPFSK signals is considered below. In this receiver the CPFSK signal is treated as a PSK signal and the trellis decoder has only the phase information of the CPFSK signal obtained at the end of each signaling interval. Consequently the path-metric depends only upon the phase of the transmitted signal at those time instances. Therefore the squared Euclidean distance between any two signals $s_n(t)$ and $s'_n(t)$ in the interval $nt \leq t \leq (n+1)T$ is given by

$$d^2_n = 2E_s|1 - \cos(\theta_n - \theta'_n)| \tag{2.37}$$

In the trellis of CPFSK, θ_n and θ'_n are the values of the terminating states of the two branches corresponding to the signals $s_n(t)$ and $s'_n(t)$ respectively.

To obtain d^2_{min}, (2.37) has to be evaluated for all possible pairs of signals through the trellis. As before a trellis-search algorithm can be used. Following a similar argument to that of correlation detection and trellis decoding, closed-form expressions for d^2_{min} are derived below for phase detection and trellis decoding.

Here again the rational valued modulation index is split into two disjoint regions such that $q \geq M$ and $q < M$. In addition to this all integral values of h will be considered separately.

Case (i): q ⩾ M

There are no parallel paths in the trellis of CPFSK signals when $q \geq M$. Consider a split-merge event of length n, splitting at level zero and merging at level $(n+1)$. The distance between the signals $s_0(t)$ and $s'_0(t)$, assumed to be transmitted during the first split level can be obtained as follows.

We have $\theta_1 = \theta_0 + a_0\pi h$ and $\theta'_1 = \theta'_0 + a'_0\pi h$ where $\theta_0 = \theta'_0$. Substituting in (2.37) yields

$$d^2_0 = 2E_s\{1 - \cos[(a_0 - a'_0)\pi h + \theta_0 - \theta'_n]\}$$
$$= 2E_s[1 - \cos(a_0 - a'_0)\pi h] \qquad (\theta_0 = \theta'_0) \qquad (2.38)$$

If the merging takes place at level $(n+1)$, then the squared distance between the last two branches is zero. That is

$$d^2_n = 0 \qquad (2.39)$$

This is due to $\theta_n = \theta'_n$ in (2.37).

Next consider a split-merge event of length two, consisting of the pair of paths splitting at level zero and merging at level two. The distance contribution by the two merging branches is zero. Therefore the squared distance between the two paths is

$$d^2(0, 2) = d^2_0$$
$$= 2E_s(1 - \cos\gamma\pi h), \qquad (2.40)$$

where, $\gamma = a_0 - a'_0$. γ can take values from the set $\{2, 4, \ldots, 2(M\text{-}1)\}$. For any split-merge event of length n

$$d^2(0, n+1) \geq \text{Min}_{\gamma}\,(d^2_0) + d^2_1 + d^2_2 + \ldots + d^2_{n-1} = 0$$
$$\geq d^2(0, 2)$$
$$= \text{Min}\,(d^2_0) \qquad (2.41)$$

Thus the desired minimum Euclidean distance is

$$d^2_{min} = \text{Min}_{\gamma}\,[2E_s(1 - \cos \gamma\pi h)]\,, \quad q \geq M \qquad (2.42)$$

Case (ii): q < M

When $q < M$ there will be parallel branches between states of the adjacent levels of the CPFSK trellis. The squared Euclidian distance between two parallel branches is

$$d^2 = 4E_s[1 - \cos(\theta_n - \theta'_n)], \text{ where } \theta_n = \theta'_n$$
$$= 0 \qquad (2.43)$$

Since the squared Euclidean distance between any two branches can not be negative, the parallel branches are the minimum distance paths and $d^2_{min} = 0$ for $q < M$.

Case (iii): Integral values of h

For integral values of h, the trellis degenerates into a single state trellis and all the branches are in parallel. This makes the MED equal to zero.

Combining the results for the above three cases, the squared MED of M-ary CPFSK signals with $h = p/q$ for phase detection and trellis decoding can be given as

$$d^2_{min} = \begin{cases} \text{Min}_{\gamma}\,[2E_s(1-\cos\gamma\pi h)], & q \geq M \\ 0, & q < M \text{ and integer } h \end{cases} \tag{2.44}$$

where γ=2, 4, ..., 2(M-1).

2.4.3. Optimum modulation index

For a given M, the value of h that produces the largest MED is the optimum modulation index, h_{opt}. For correlation detection and trellis decoding of M-ary CPFSK signals h_{opt} has been calculated in [4]. h_{opt} for phase detection and trellis decoding of M-ary CPFSK signals is calculated below.

The minimum Euclidean distance for phase detection of M-ary CPFSK signals was given in (2.44). Because γ and h are both positive, for $q \geq M$ the right hand side of (2.44) is minimum when $\cos(\gamma\pi h)$ is maximum. For binary CPFSK signals $\gamma = 2$. Thus the minimum squared Euclidean distance is

$$d^2_{min} = \begin{cases} 2E_s[1-\cos(2\pi h)], & q \geq M \\ 0, & \text{otherwise} \end{cases} \tag{2.45}$$

To obtain h_{opt} [1-cos(2πh)] has to be maximized. This is a periodic function of h with maxima at $2\pi h = m\pi$, for odd integral values of m. For binary CPFSK signaling, (2.45) is maximum when $h_{opt} = m/2$, $m = 1, 3, 5,...$ and $d^2_{min} = 2.000$. Similarly for all other M values $h_{opt} = m/M$, $m = 1, 3, 5,...$ and $d^2_{min} = 2E_s[1-\cos(2\pi/M)]$. Numerical results are presented in the next section.

2.4.4. Numerical results

In order to make proper comparisons with previously reported results, all numerical results are presented according to the following normalization. The squared MED for binary PSK is $2E_b$, where E_b is the energy per bit. E_b is related to energy per symbol E_s by

$$E_s = E_b \log_2 M \tag{2.46}$$

All distances are divided by $2E_b$ to get the normalized distances. Thus for MSK, binary PSK and QPSK (quaternary phase shift keying) d^2_{min} equals 2·000 becomes the reference value. Hereafter all distances will be given as normalized distances.

The values of normalized MED (d^2_{min}) for correlation detection and trellis decoding were computed for M=2, 4, 8, and 16, by using (2.36). Variation of minimum Euclidean distance with the modulation index h is shown in Figs. 2.8 – 2.11 . Numerical values of minimum distances for some h values are given in Table 2.1. Our results are in exact agreement with those of Aulin et.al. [4], for long observation intervals. In [4] the MED is referred to as the normalized squared free Euclidean distance (NSFED). It is noteworthy that the bounds given in [4] are actually the exact values of the MED in our case. Eventhough a trellis search algorithm was used in [4] for the evaluation of the MED, the same could be evaluated with just a few computations. For instance when $q > M$, comparison among only (M-1) values is needed to determine d^2_{min} for M-ary CPFSK signals.

Examining Figs. 2.8 – 2.11 it can be seen that at all points where $q < M$

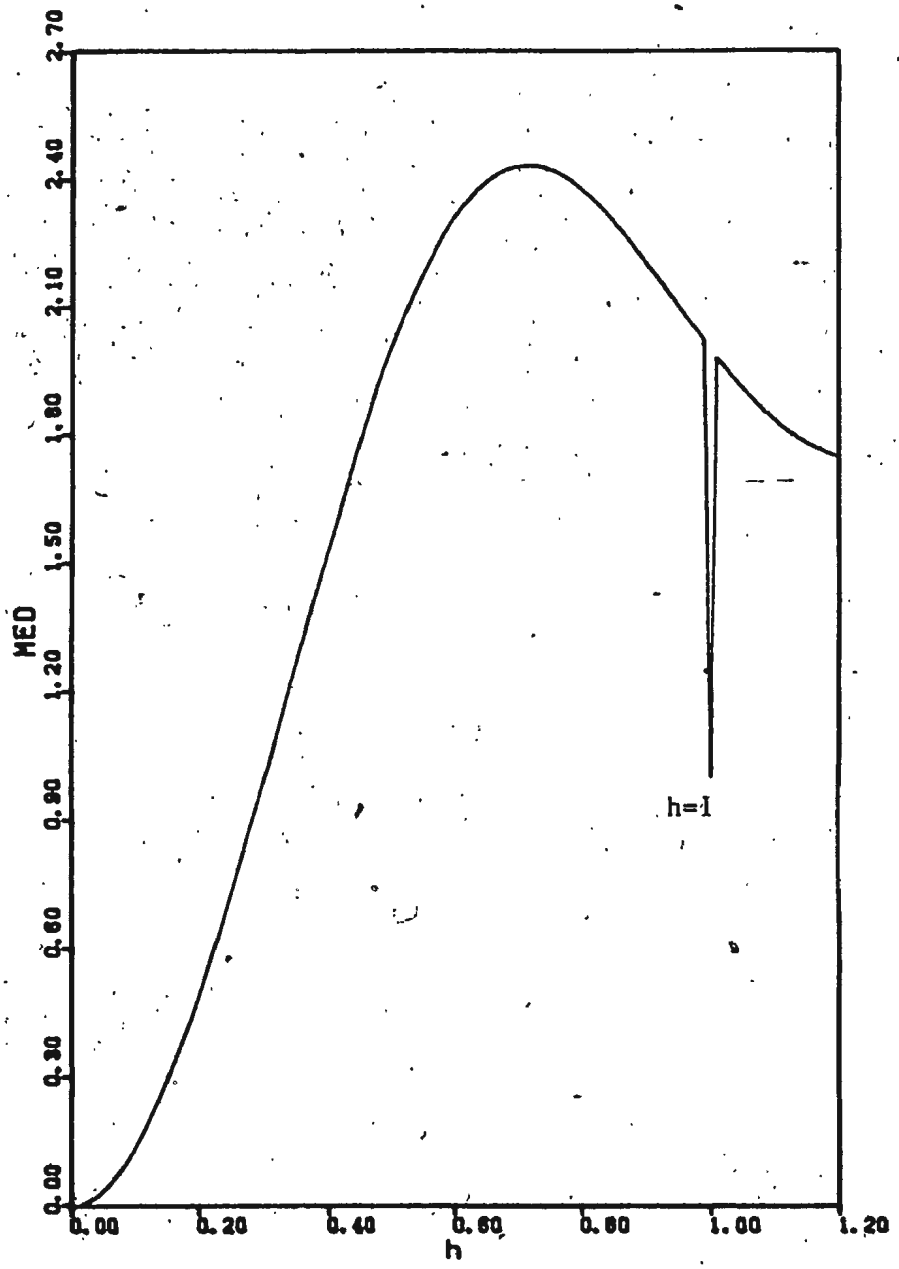

Figure 2.8: Minimum distance versus modulation index for uncoded binary CPFSK; Correlation detection.

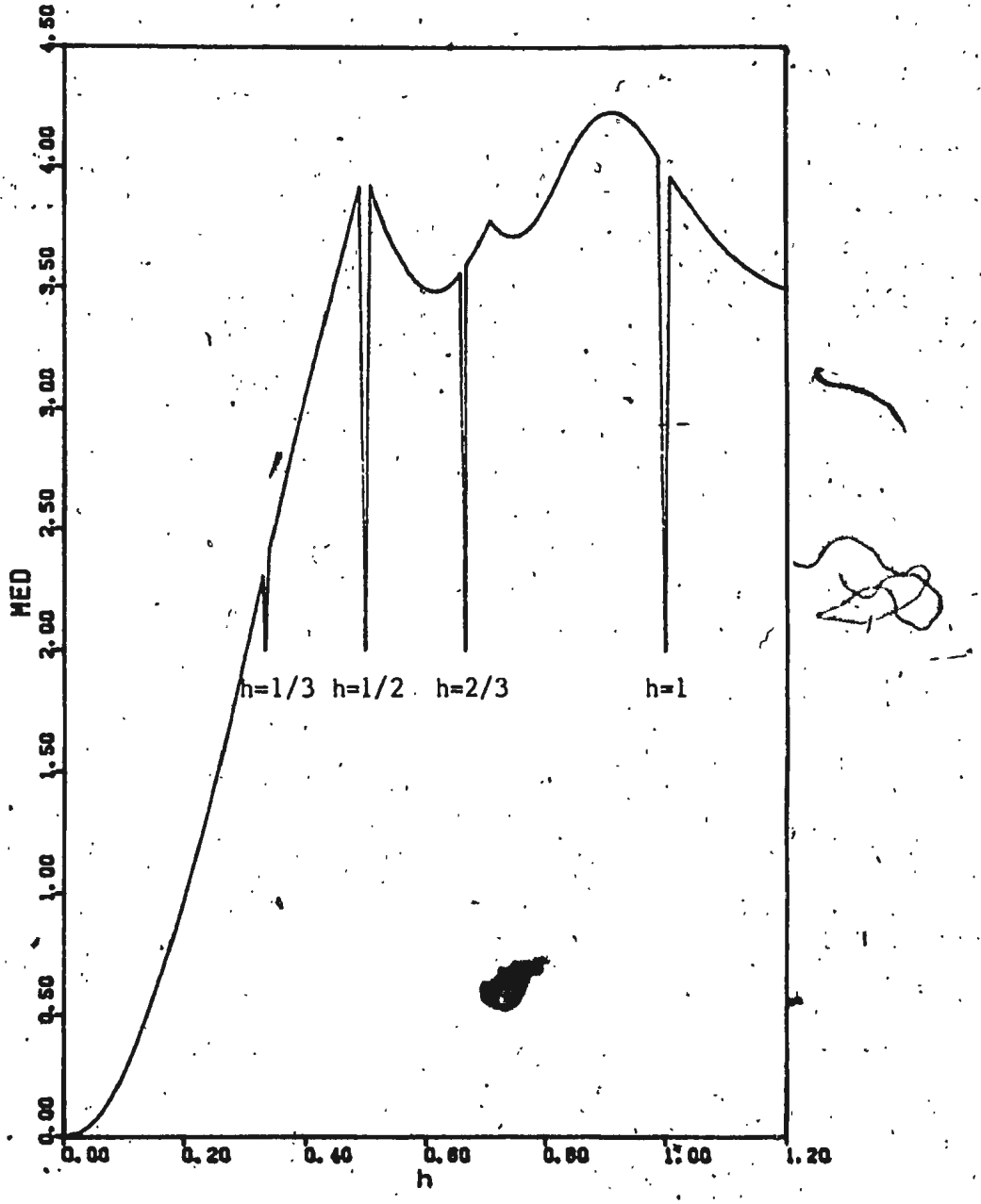

Figure 2.9: Minimum distance versus modulation index for uncoded quaternary CPFSK; Correlation detection.

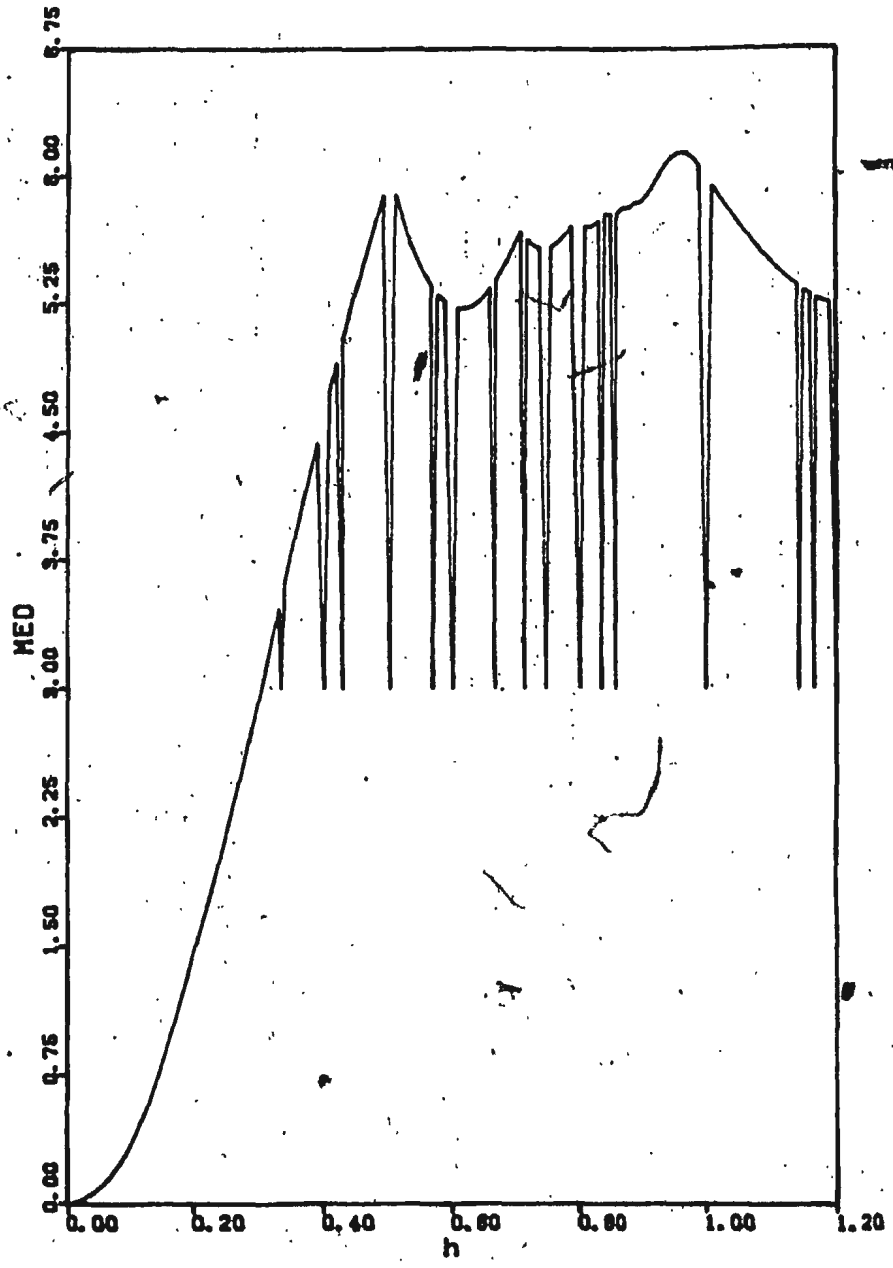

Figure 2.10: Minimum distance versus modulation index for uncoded octal CPFSK; Correlation detection.

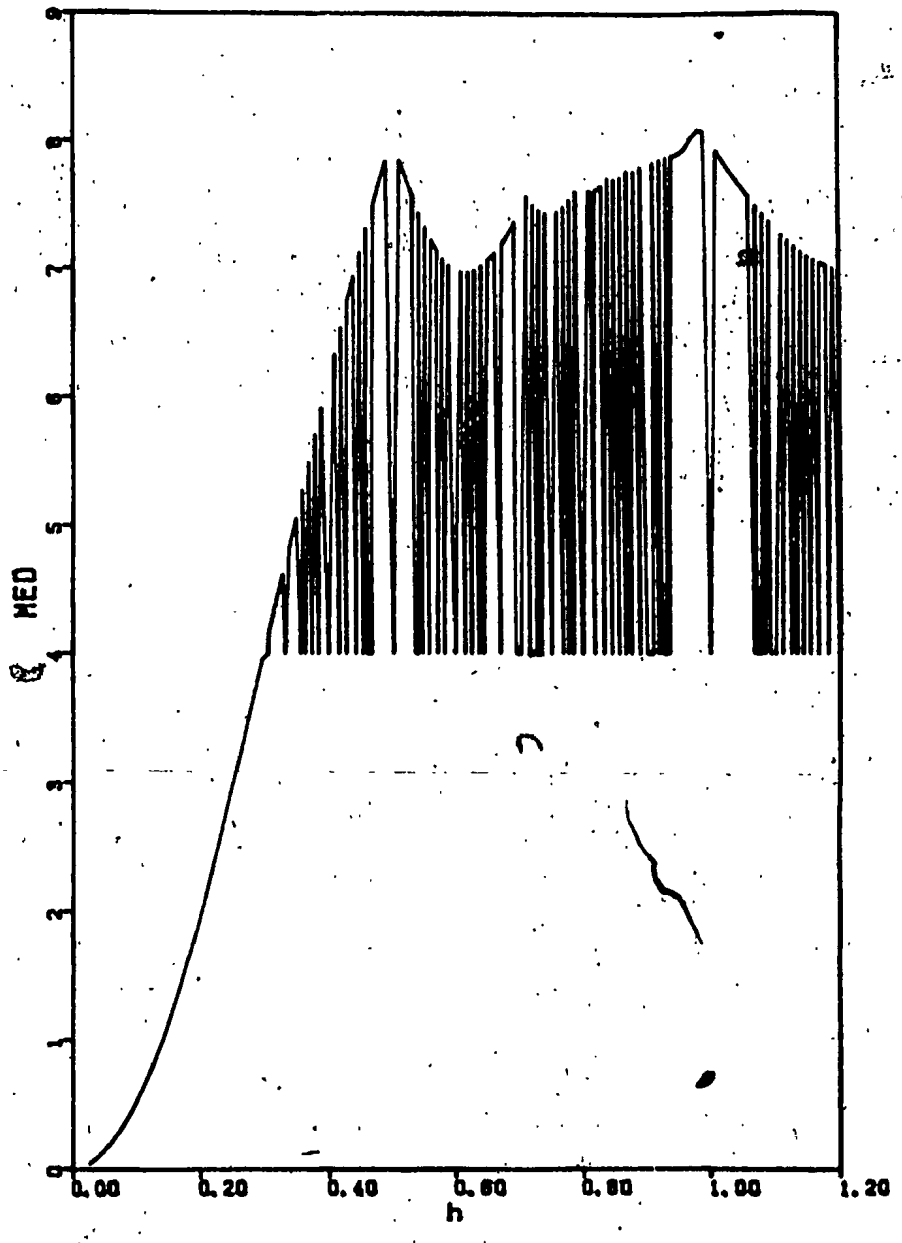

Figure 2.11: Minimum distance versus modulation index for uncoded 16-ary CPFSK; Correlation detection.

Table 2.1: Normalized minimum Euclidean distance for M-ary CPFSK signals; Correlation detection and trellis decoding.

Modulation Index, h	Minimum Euclidean Distance, $d^2_{min}/2E_b$			
	M=2	M=4	M=8	M=16
1/20	0.033	0.065	0.098	0.131
1/10	0.129	0.258	0.387	0.516
1/9	0.159	0.317	0.476	0.634
1/8	0.199	0.399	0.598	0.797
1/7	0.258	0.516	0.774	1.032
3/20	0.283	0.566	0.850	1.133
1/6	0.346	0.692	1.038	1.384
1/5	0.486	0.973	1.459	1.945
1/4	0.727	1.454	2.180	2.907
3/10	0.991	1.982	2.973	3.964
7/20	1.264	2.528	3.793	5.057
2/5	1.532	3.065	3.000	4.000

and $h > 0.301677$ parallel branches become the minimum distance paths and the normalized minimum distance is $2 \log_2 M$. When $q < M$ and $h < 0.301677$ parallel branches do not become the minimum distance path. For all integral values of h there are only parallel branches in the trellis and again $d^2_{min} = 2 \log_2 M$. Another important observation is that minimum distance paths merge in at most two symbol intervals, regardless of the number of states in the trellis. This implies, as in Viterbi decoding of convolutional codes [13, 25], in trellis decoding of CPFSK signals, the decisions on symbols can be made after only a few signaling intervals, thereby reducing the memory requirements of maximum likelihood decoding.

The values of normalized MED for phase detection and trellis decoding were evaluated for M=2, 4, 8, and 16 by using (2.44). Plots of d^2_{min} against h are shown in Figs. 2.12 – 2.15 and the numerical values are given in Table 2.2. Here again the discontinuities of the curves are due to parallel branches of the trellis. For $q < M$ and for all integer h values the MED is zero. This implies that phase detection can not be used at these particular modulation indices.

The values of h for which the largest MED occurs in correlation detection and trellis decoding are tabulated in Table 2.3. When $M = 2$ (binary PSK) the largest MED occurs at $h = 0.715$. The corresponding d^2_{min} is 2.4345. $h_{opt} = 0.715$ can be represented by the rational number 143/200 implying that a 200-state trellis is needed for trellis decoding. Clearly, a receiver with such a large number of states is not practicable. On the other hand, if 0.715 is approximated by 2/3, then only a three-state trellis is required for decoding. The

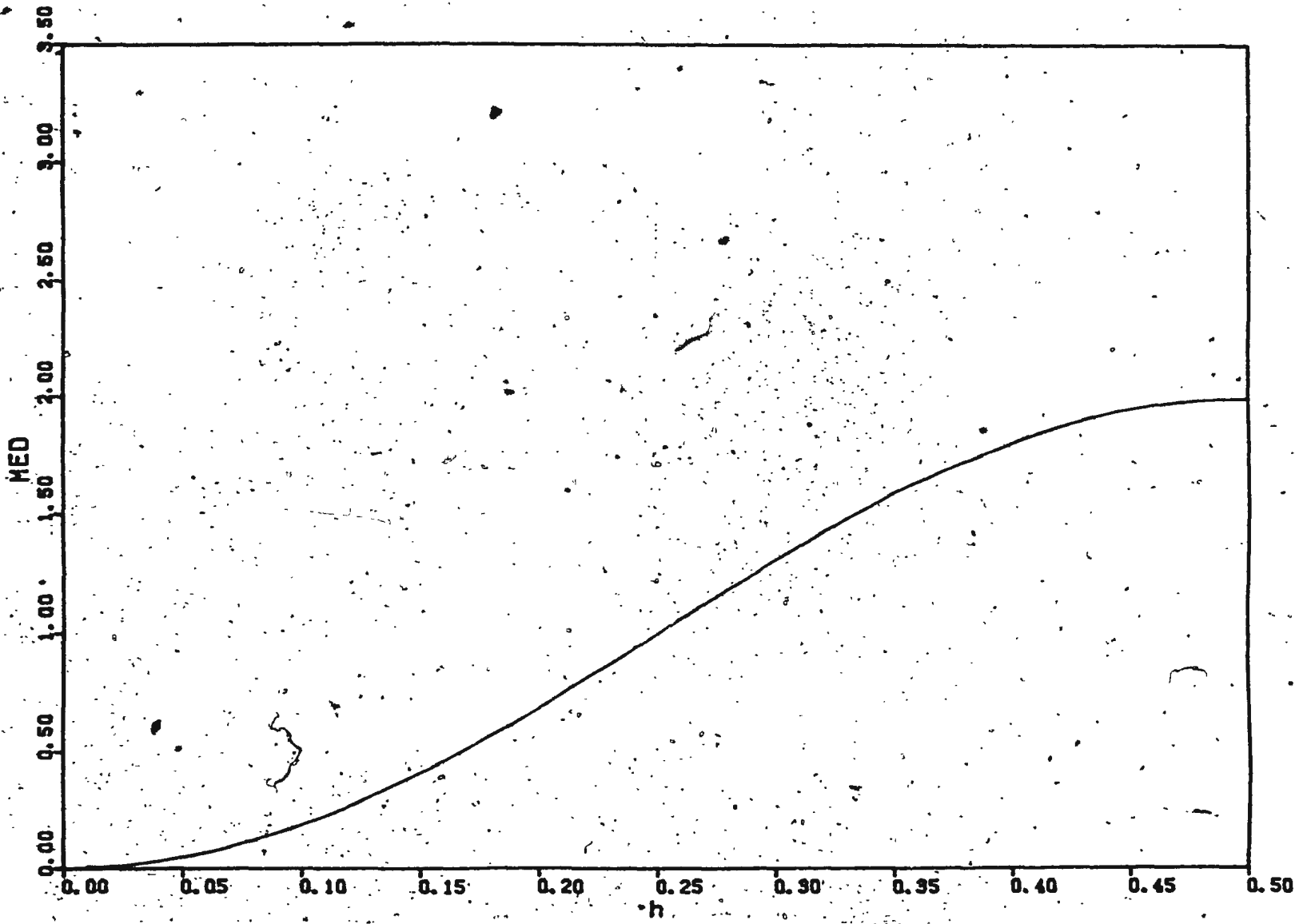

Figure 2.12: Minimum distance versus modulation index for uncoded binary CPFSK; Phase detection.

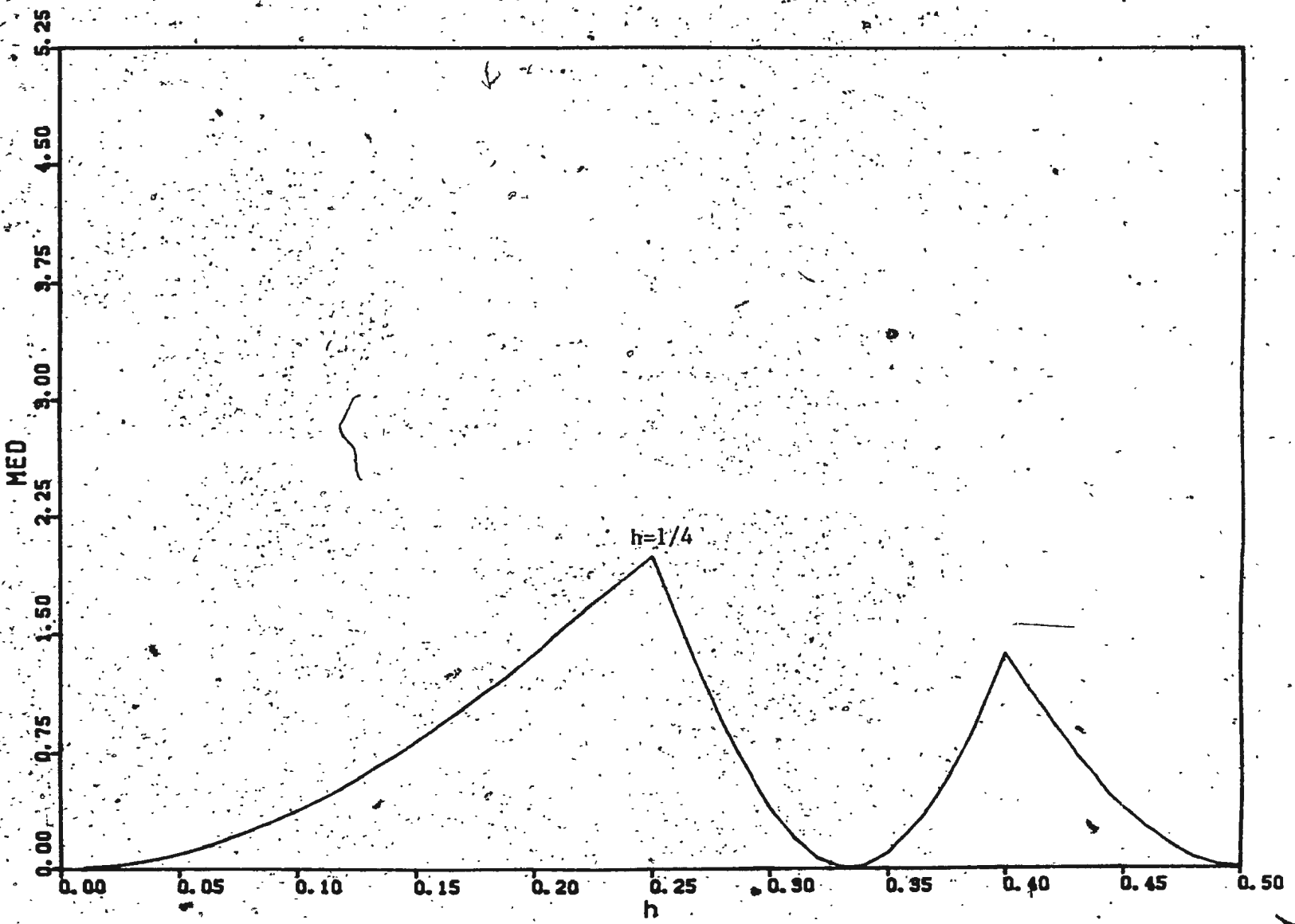

Figure 2.13: Minimum distance versus modulation index for uncoded quaternary CPFSK; Phase detection.

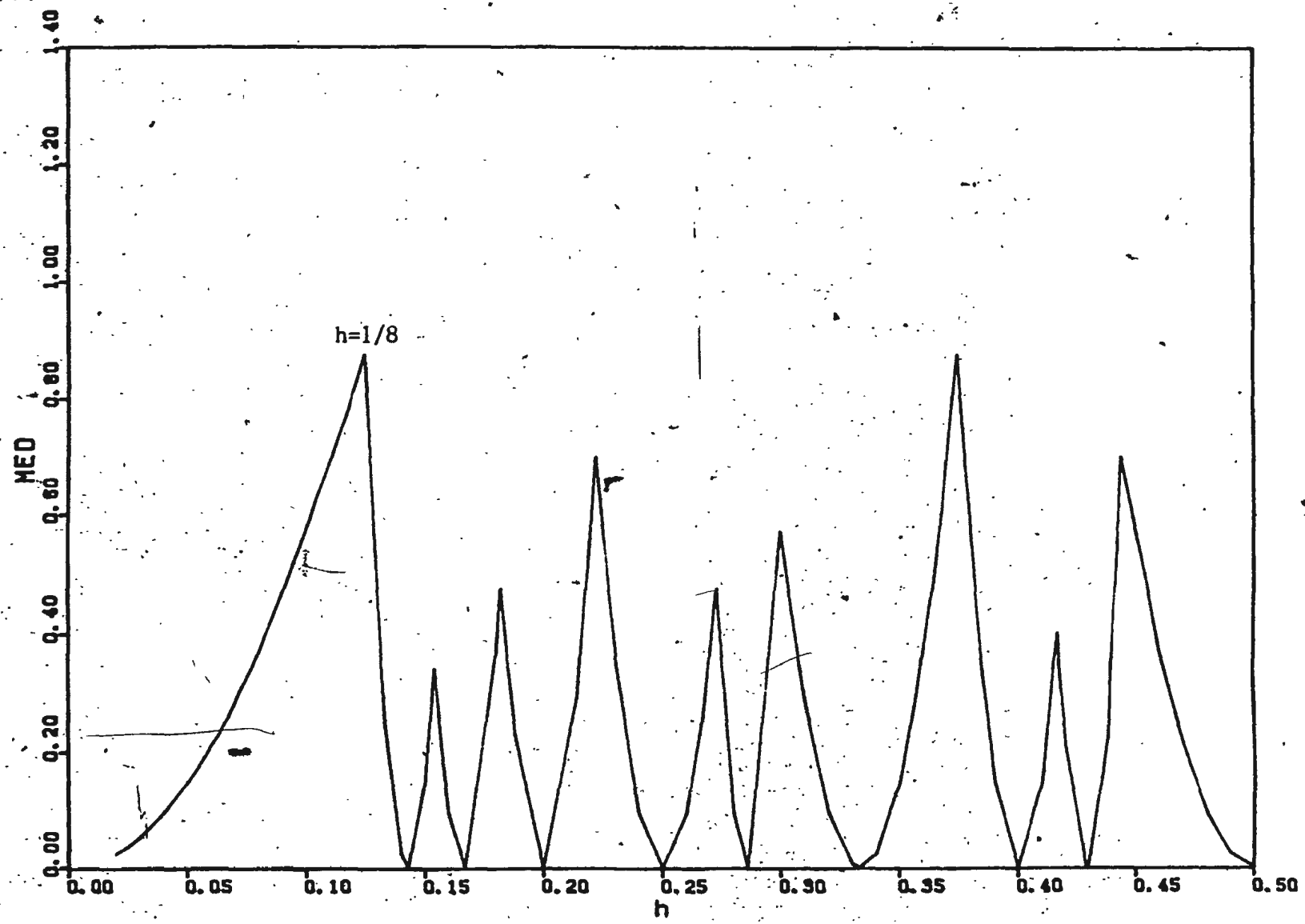

Figure 2.14: Minimum distance versus modulation index for uncoded octal CPFSK; Phase detection.

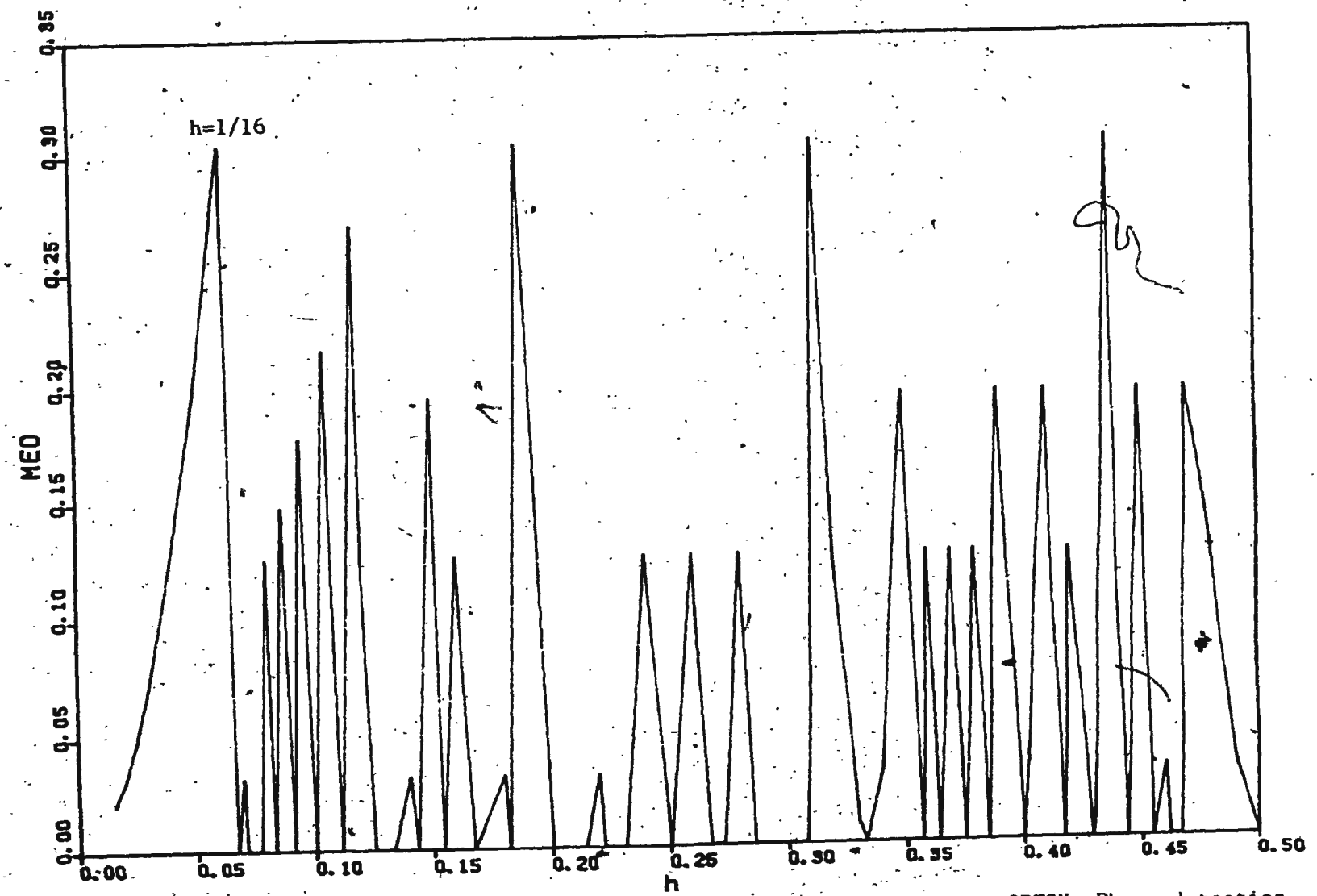

Figure 2.15: Minimum distance versus modulation index for uncoded 16-ary CPFSK; Phase detection.

Table 2.2: Normalized minimum Euclidean distance for M-ary CPFSK signals; Phase detection and trelllis decoding.

Modulation Index, h	Minimum Euclidean distance, $d^2_{min}/2E_b$		
	M=2	M=4	M=8
1/20	0.049	0.098	0.147
1/10	0.191	0.382	0.573
1/9	0.234	0.468	0.702
1/8	0.293	0.586	0.879
1/7	0.377	0.753	0.000
3/20	0.412	0.824	1.237
1/6	0.500	1.000	0.000
1/5	0.691	1.382	0.000
1/4	1.000	2.000	0.000
3/10	1.309	2.618	3.927
7/20	1.588	3.176	4.763
2/5	1.809	3.618	0.000

MED for $h = 2/3$ is 2.413, which is only 0.08% less than the best value. Thus using $h = 2/3$ instead of $h = 0.715$, a three-state trellis decoder can achieve almost all the performance gain that is achievable with a 200-state trellis decoder.

As a second example consider octal CPFSK. From Table 2.3, h_{opt} for octal CPFSK signaling is approximately 0.964 and the corresponding d^2_{min} is 6.1415. 0.964 can be represented by the fractional number 241/250, implying the need for 250 states in the decoder. Approximating 0.964 by 7/8 instead, an eight-state trellis can be used. The MED for $M = 8$, $h = 7/8$ is 5.818. That is a reduction of 5.27% in d^2_{min}. The degradation is somewhat higher in this case; however, when compared with the substantial reduction in decoder complexity, it is insignificant. Similarly for other M values h_{opt} can be approximated by $(M-1)/M$. The results are tabulated in Table 2.4. The number of states required in the decoder is of the order of M for achieving almost all the performance gain that is guaranteed by the memory of the modulation process. This can not be reduced below M, because parallel branches would then occur in the trellis thereby reducing the minimum distance drastically.

Next the optimum modulation index, h_{opt}, is considered for phase detection and trellis decoding of CPFSK signals in the small h region. For all M values h_{opt} equals $1/M$ and these values along with the corresponding MED are given in Table 2.5. Therefore an M state trellis gives the largest possible MED in this case.

Although minimum distances for a wide range of h values were evaluated,

Table 2.3: Optimum modulation index and corresponding minimum Euclidean distance for correlation detection and trellis decoding of M-ary CPFSK signals [4].

M	h_{opt}	$d^2_{min}/2E_b$
2	0.715	2.434
4	0.914	4.232
8	0.964	6.142
16	0.983	8.086
32	0.992	10.052

Table 2.4: Minimum Euclidean distance for correlation detection and trellis decoding of M-ary CPFSK signals with an M-state decoder.

M	h=(M-1)/M	$d^2_{min}/2E_b$	$\left[d^2_{min}/2E_b\right]_{max}$	% difference
2	2/3	2.413	2.434	-0.08
4	3/4	3.717	4.232	-12.16
8	7/8	5.818	6.142	-5.27
16	15/16	7.886	8.086	-2.47
32	31/32	9.930	10.052	-1.21

Table 2.5: Optimum modulation index and corresponding minimum Euclidean distance for phase detection and trellis decoding of M-ary CPFSK signals.

M	h_{opt}	$d^2_{min}/2E_b$
2	1/2	2.000
4	1/4	2.000
8	1/8	0.879
16	1/16	0.304
32	1/32	0.096

the comparisons are restricted to values of d^2_{min} for $h \leq 1/M$, because it is only for these values of h, CPFSK signals become attractive from the point of view of bandwidth occupancy [20]. Figs. 2.16 – 2.19 show comparisons of d^2_{min} for correlation detection and phase detection. Coherent phase detection yields larger minimum distances than correlation detection when $h \leq 1/M$. Table 2.6 lists the relative improvements in dB, relative to MSK, for selected h values.

2.5. Conclusion

In this chapter it was shown that trellis decoding of uncoded CPFSK signals is transparent to the phase ambiguities of the locally generated reference tones of the coherent demodulator. It was also shown that the optimum modulation index (h_{opt}) for correlation detection and trellis decoding of M-ary CPFSK signals can be approximated by $(M-1)/M$ without an appreciable reduction in the largest minimum distance that can be achieved. For phase detection and trellis decoding, the optimum modulation index was $1/M$. Therefore for both correlation detection and phase detection, it is sufficient to consider an M-state trellis in the decoder. Minimum distance values for correlation detection and phase detection were compared. The numerical results indicated that for uncoded CPFSK signals with modulation index $h \leq 1/M$, phase detection and trellis decoding yields minimum distance gains of approximately between 1 and 1.8 dB (calculated with respect to binary PSK distances) over correlation detection and trellis decoding..

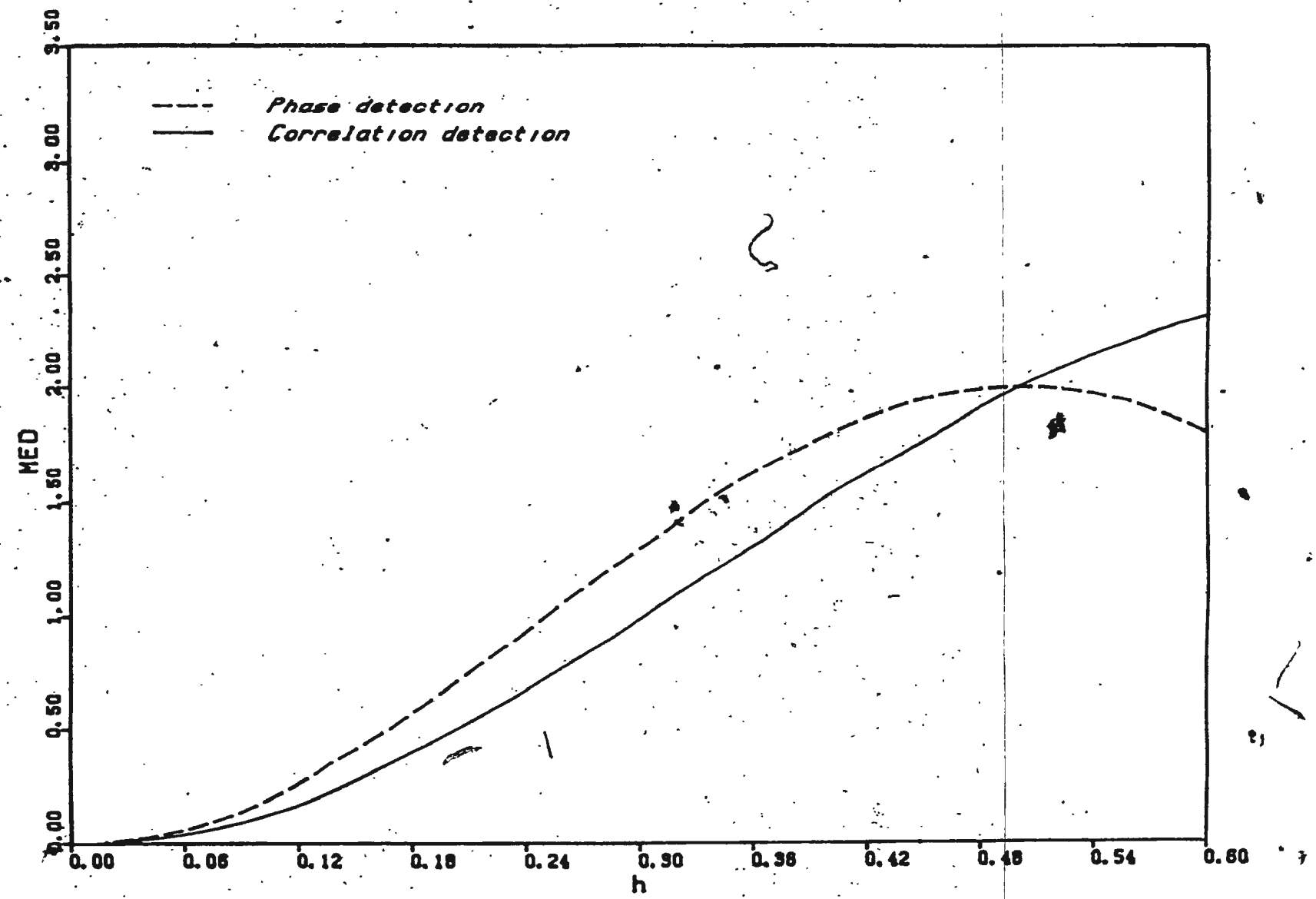

Figure 2.16: Comparison of minimum distance for uncoded binary CPFSK signals.

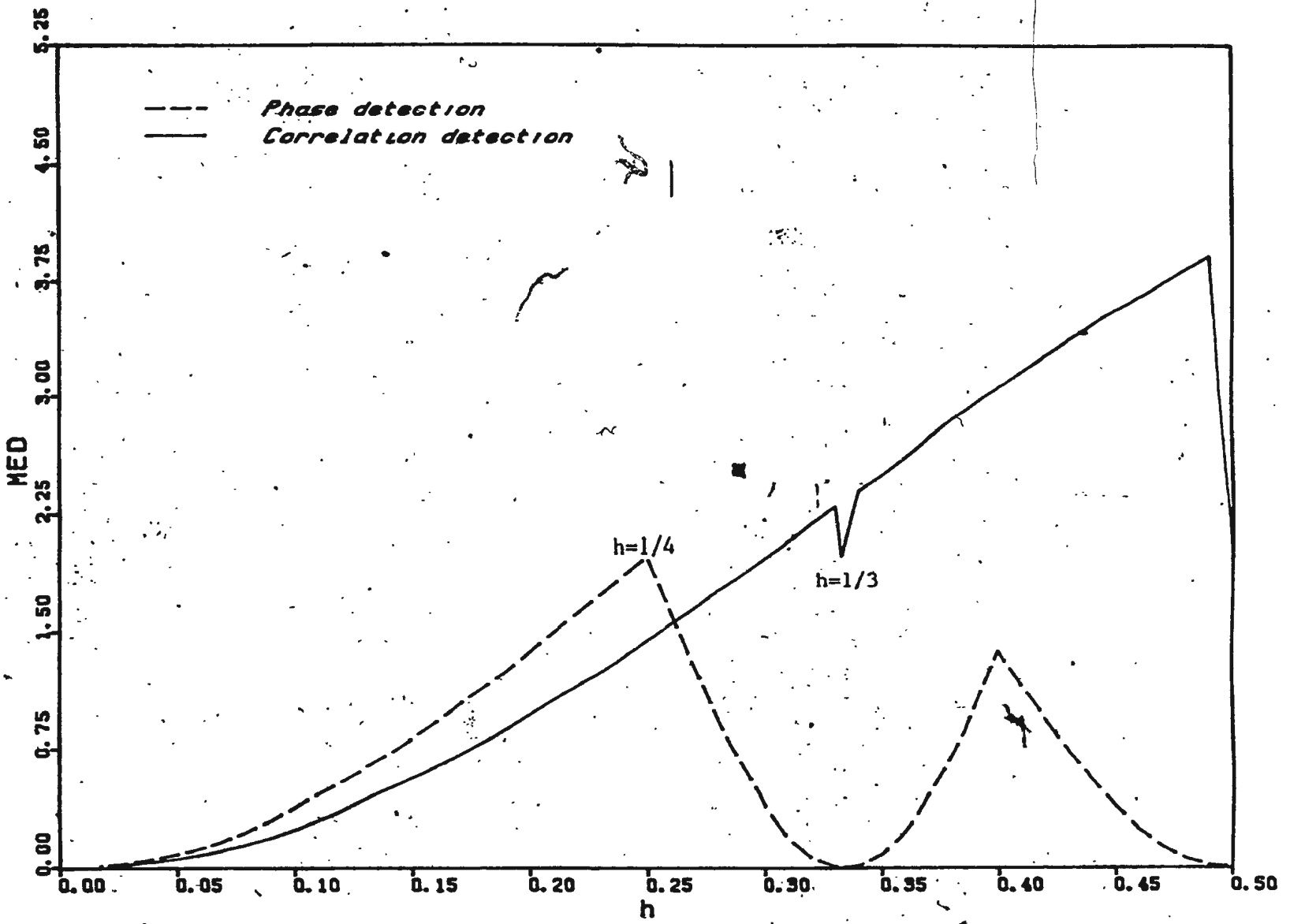

Figure 2.17: Comparison of minimum distance for uncoded quaternary CPFSK signals.

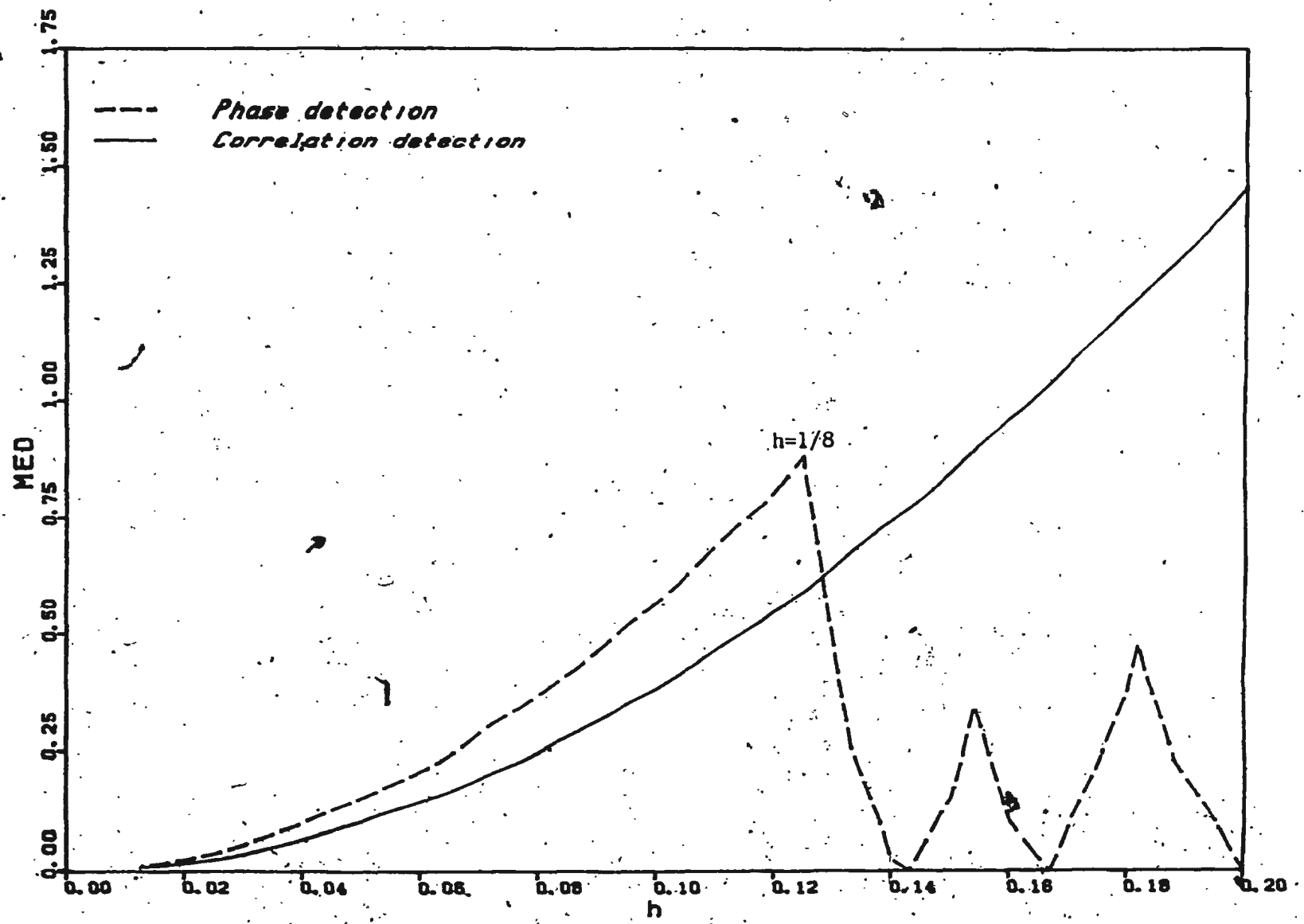

Figure 2.18: Comparison of minimum distance for uncoded octal CPFSK signals.

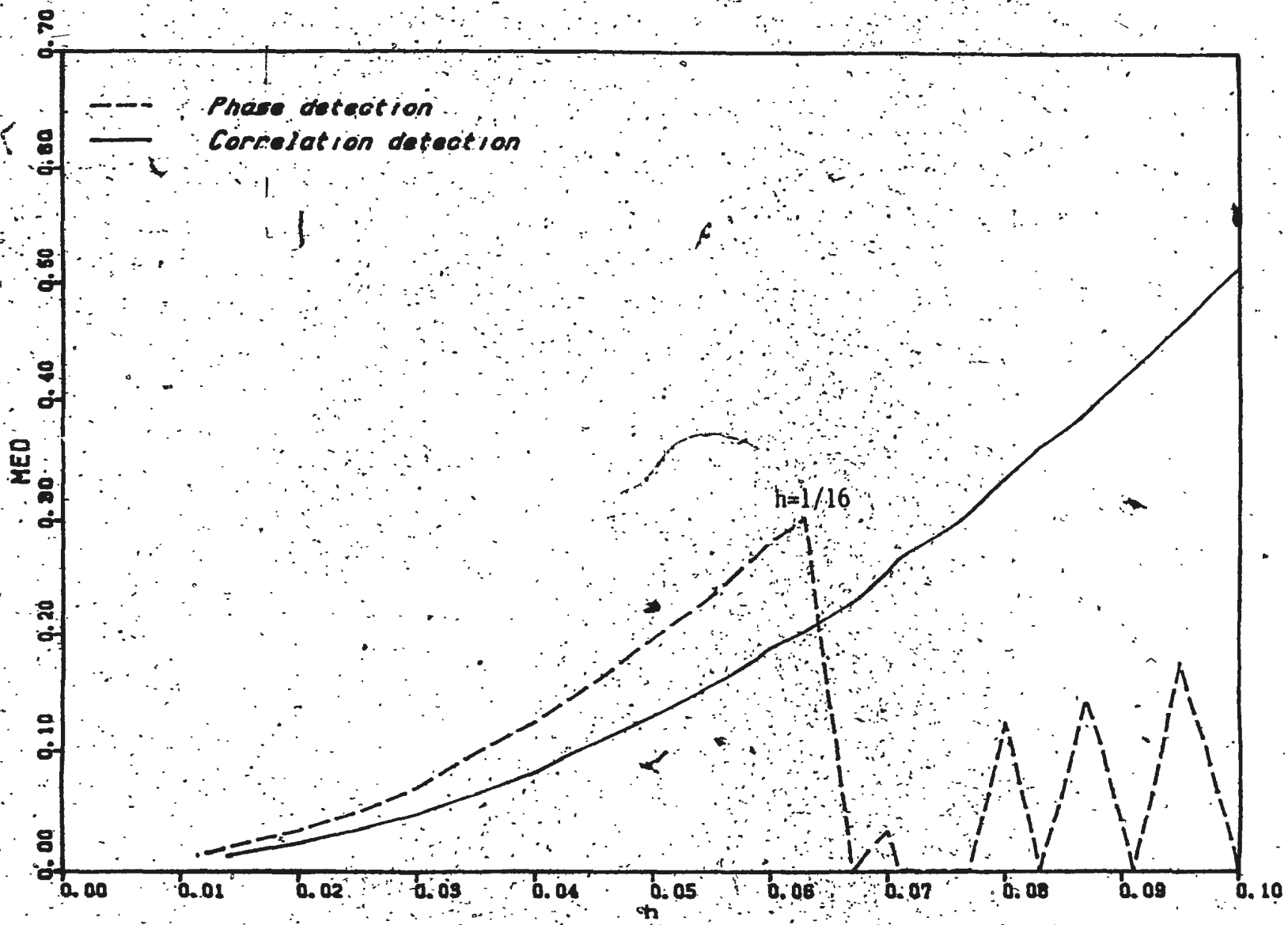

Figure 2.19: Comparison of minimum distance for uncoded 16-ary CPFSK signals.

Table 2.6a: Comparison of minimum distance for correlation detection and phase detection; Binary CPFSK and quaternary CPFSK.

M	Modulation Index, h	Minimum distance (dB)		dB gain
		Correlation detection	Phase detection	
2	1/10	-11.90	-10.20	1.70
	1/8	-10.02	-8.34	1.68
	1/5	-6.14	-4.62	1.52
	1/4	-4.39	-3.01	1.38
	1/3	-2.32	-1.25	1.07
	7/20	-1.99	-1.00	0.99
4	1/10	-8.89	-7.19	1.70
	1/9	-8.00	-6.31	1.69
	1/8	-7.00	-5.33	1.67
	1/6	-4.61	-3.01	1.60
	1/5	-3.13	-1.60	1.53
	2/9	-2.29	-0.83	1.46
	1/4	-1.38	0.00	1.38

Table 2.6b: Comparison of minimum distances for correlation detection and phase detection; Octal CPFSK and 16-ary CPFSK.

M	Modulation Index, h	Minimum distance (dB)		dB gain
		Correlation detection	Phase detection	
8	1/32	-17.21	-15.38	1.83
	1/15	-10.60	-8.88	1.72
	2/25	-9.05	-7.32	1.73
	1/10	-7.13	-5.43	1.70
	1/9	-6.23	-4.55	1.68
	3/25	-5.58	-3.91	1.67
	1/8	-5.24	-3.57	1.67
16	1/32	-15.93	-14.14	1.79
	1/25	-13.77	-12.01	1.76
	3/50	-10.27	-8.52	1.75
	1/16	-9.91	-8.18	1.73

Chapter 3

DISTANCE PROPERTIES OF TRELLIS CODED CPFSK SIGNALS

3.1. Introduction

In this chapter the distance properties of trellis coded quaternary and octal CPFSK signals are studied for small modulation indices ($h \leq 1/M$). A receiver consisting of a phase detector followed by a trellis decoder is considered. The minimum distances of trellis coded CPFSK signals obtained with this receiver are compared with the distances obtained with a correlation receiver. A search is carried out for optimal codes which give large minimum distances when combined with CPFSK signaling. Also it is observed that trellis decoding of coded CPFSK signals is transparent to phase ambiguities of the regenerated reference tones of the coherent demodulator.

3.2. System description and the computer search for optimal codes

The communication system studied in this chapter is shown in Fig. 3.1 . The idea is to reliably transmit a sequence of binary information bits, generated at the rate of $1/T_b$ bit/second, using a suitable channel coding scheme.

The information sequence is encoded by an (n, k, m) trellis encoder. Thus

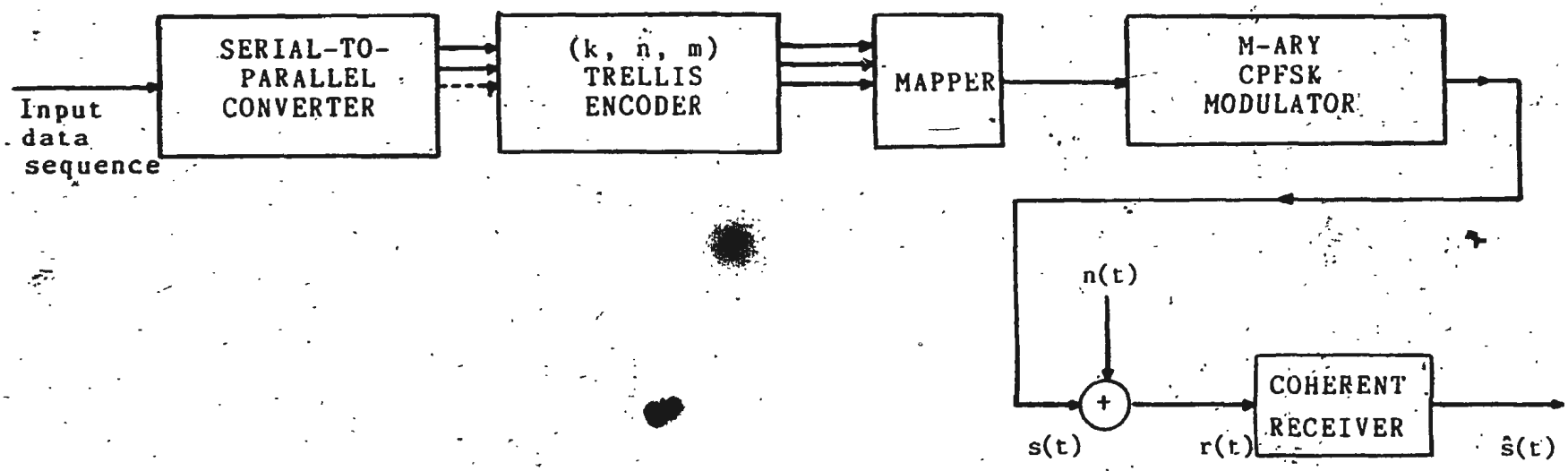

Figure 3.1: General model of trellis-coded CPFSK scheme.

the rate of the code is k/n and the memory length m. The n output coded sequence is mapped on to a M-ary alphabet $\{\pm1,\pm3,\pm5,...\pm(M-1)\}$. The channel symbols a_n are chosen from the above set. M is assumed to be a power of 2, that is $M = 2^n$. Whenever a block of coded binary symbols of $\log_2 M$ bits enters the mapper, one channel symbol is produced according to the mapping function used. In other words the n output bits of the encoder are seen by the mapper as one M-ary symbol. The channel symbol sequence is fed to a CPFSK modulator which generates the transmitted signal.

The communication channel is assumed to be corrupted by additive white Gaussian noise only. The received signal $r(t) = s(t) + n(t)$, where $n(t)$ is a stationary white Gaussian random process with zero mean and double sided power spectral density $N_0/2$. The receiver is assumed to be coherent, and consists of a phase detector followed by a trellis decoder. This receiver was discussed in Chapter 1.

3.2.1. State diagram representation of trellis coded CPFSK signals

By combining the state diagram of the uncoded CPFSK scheme and the state diagram of a trellis code it is possible to obtain a combined state diagram for trellis coded CPFSK signals. This can be illustrated by a simple example.

Consider (2, 1, 1) coding of quaternary CPFSK for $h = 1/4$, the general model of which is given in Fig. 3.2. The information sequence is encoded by a $r = 1/2$ trellis code. The pair of outputs of the binary code can be mapped on to the set $\{\pm1, \pm3\}$ in 24 different ways [20]. Only the natural binary mapping

Table 3.1; Natural binary mapping rule for quaternary CPFSK.

Encoder output	Channel symbol
0 0	-3
0 1	-1
1 0	1
1 1	3

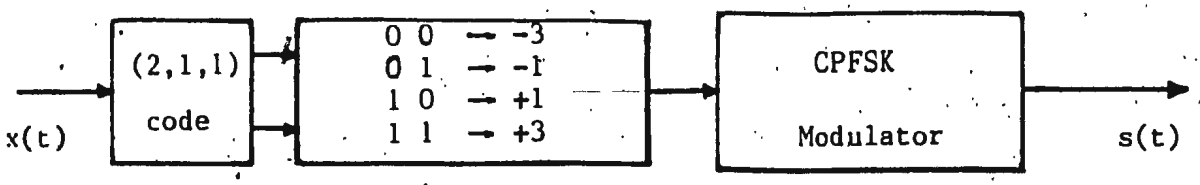

Figure 3.2: (2, 1, 1) trellis coding of quaternary CPFSK.

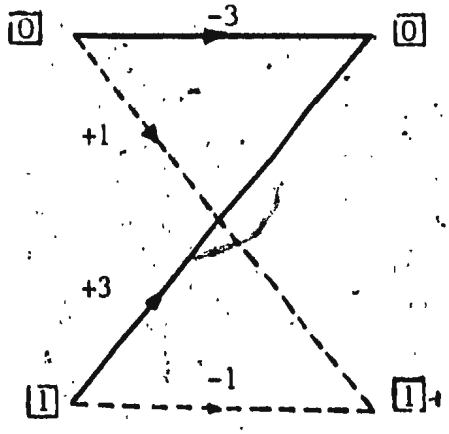

Fig.3.3: Trellis of (2,1,1) code.

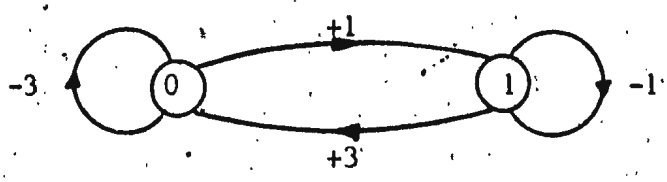

Fig.3.4: State diagram of (2,1,1) code.

rule shown in Table 3.1 is considered. The operation of the encoder is described by the trellis of Fig. 3.3 or the state diagram of Fig. 3.4 , where the transitions are labelled with quaternary channel symbols $a_n \in \{\pm 1, \pm 3\}$. The trellis and the state diagram of the uncoded quaternary CPFSK scheme for $h = 1/4$, from Chapter 2, is reproduced in Fig. 3.5 .

The process of (2, 1, 1) coding of CPFSK gives rise to 8 states. These are the combinations of two states of the trellis code and four states of the CPFSK signal. Each state of the combined state diagram thus consists of two parts: one, corresponding to the phase of the CPFSK signal; and the other, corresponding to the binary state of the code. In the combined state diagram shown in Fig. 3.6 , there are two branches leaving each state. But, in the uncoded quaternary CPFSK there were four branches leaving each state. In other words the connectivity of the CPFSK trellis has been reduced due to coding.

Irrespective of how the trellis of Fig. 3.3 is labelled, that is, whether we follow a binary mapping function or not, the combined state diagram can be drawn, though we have to be careful to avoid catastrophic codes (-in terms of the state diagram, a code is catastrophic if and only if the state diagram contains a loop of zero weight other than the self-loop around the state S_0 [13]). For a given binary code of memory 1, twenty four different trellis labellings are possible. The uncoded CPFSK trellis, for a given M and h, remains unchanged. Therefore altogether 24 different combined state diagrams are present. Twelve of these, however, can be obtained simply by inverting the trellis of the other twelve by interchanging the states 0 and 1. The state diagram is always rotationally symmetrical.

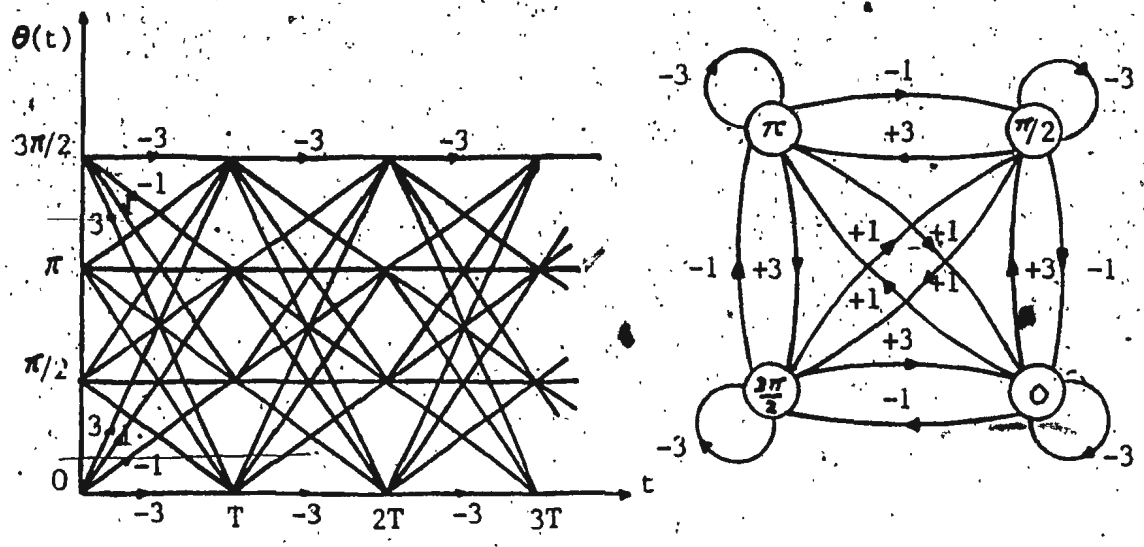

Figure 3.5: Trellis and the state diagram of quaternary CPFSK for h = $\frac{1}{4}$.

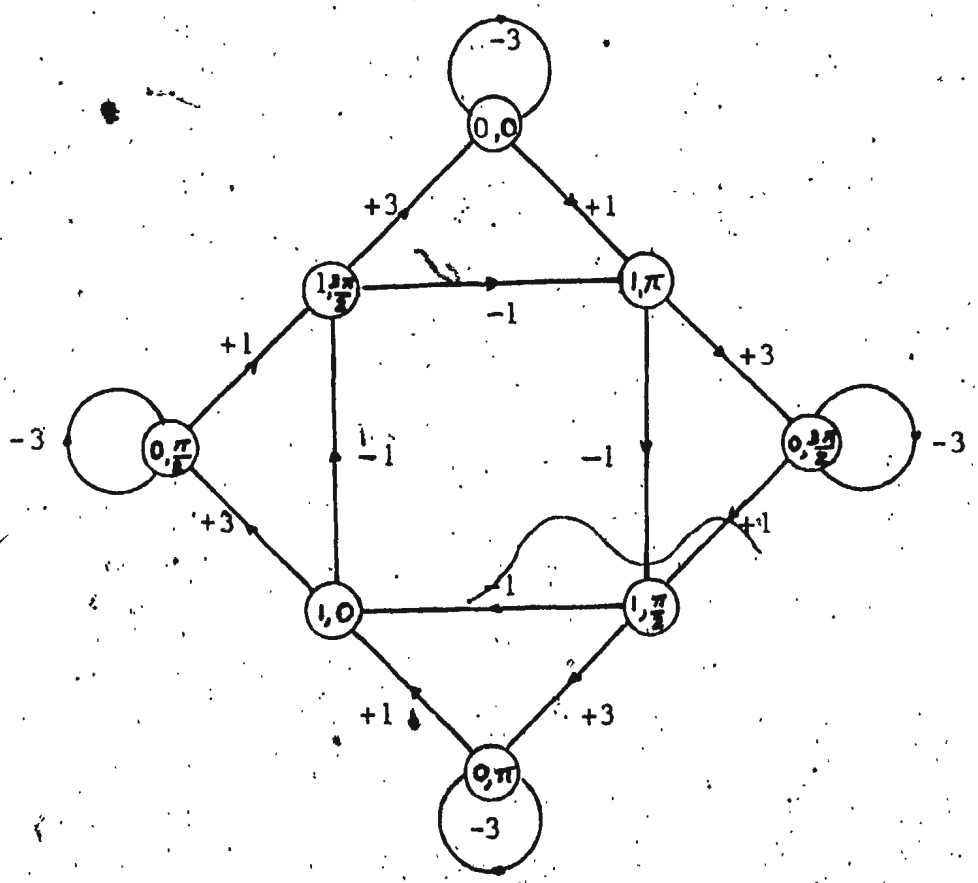

Figure 3.6: Combined state diagram of code of Fig. 3.3 and quaternary CPFSK for h = $\frac{1}{4}$.

Two of the combined state diagrams degenerate into two separate state diagrams, thereby isolating four states from the other four. For (2, 1, 1) coding of quaternary CPFSK this occurs when the two self loops of the trellis are labelled with -3 and $+1$. However, for higher memory codes this is not always true. An example of degeneracy with a (2, 1, 2) code [Fig. 3.7] and quaternary CPFSK with $h = 1/4$ is given in Fig. 3.8 . In this example, the combined state diagram has 16 states and there are two transitions leaving as well as converging at each state. Eight of the states are isolated from the other eight states.

In the M-ary case, the number of states in the combined state diagram depends upon the memory, m, of the code and the denominator of the rational valued modulation index $h = p/q$, where p and q are relatively prime numbers. There are always $q.2^m$ states in the combined state diagram.

In order to evaluate the error performance of the above combined coding and modulation scheme, the Viterbi algorithm needs to be applied to the combined trellis or the combined state diagram to determine the minimum free Euclidean distance on which the probability of error asymptotically depends at high SNR. In this thesis the minimum free Euclidean distance is simply referred to as the minimum Euclidean distance (MED) or the minimum distance. For a given CPFSK scheme optimal codes can be found by varying the trellis labelling to maximize the MED.

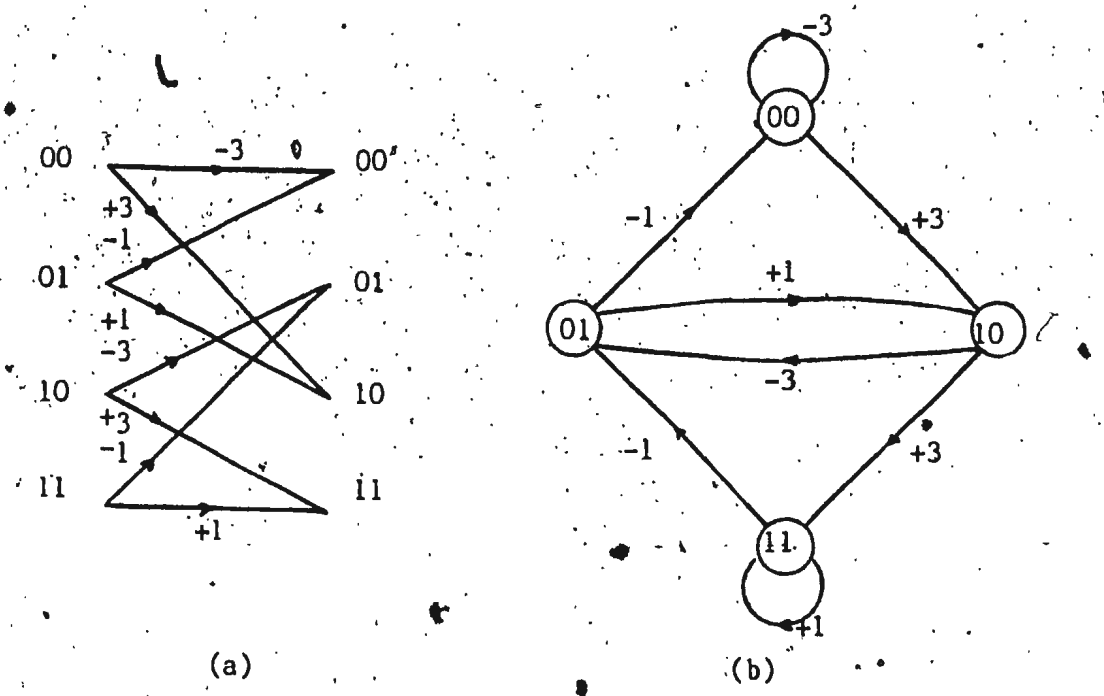

Figure 3.7: Trellis and the state diagram of a (2, 1, 2) code.

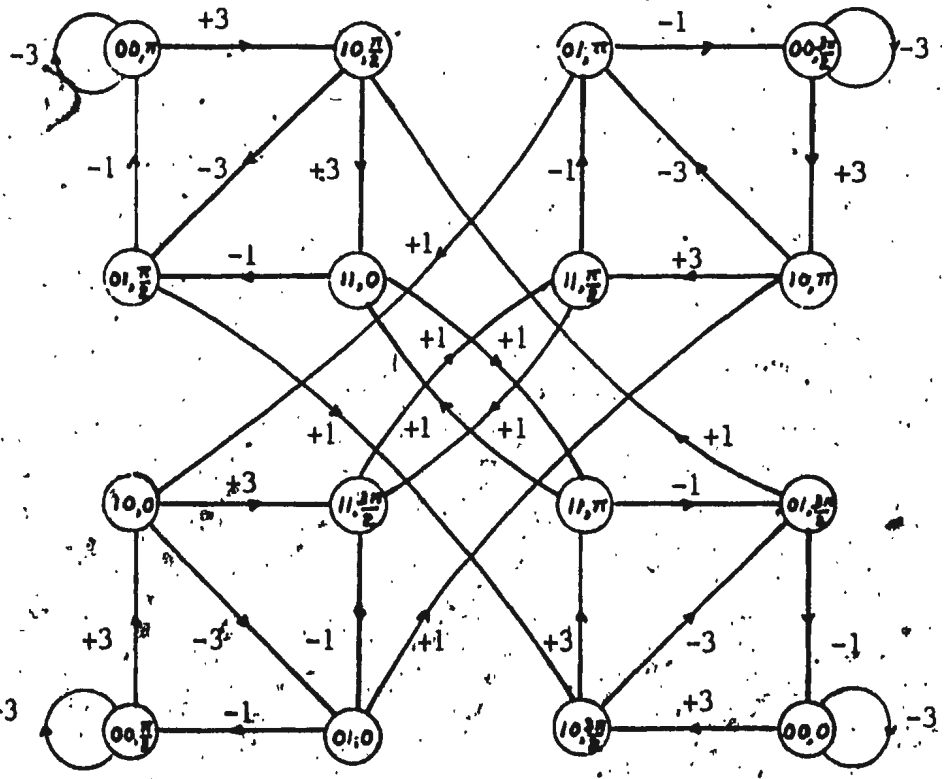

Figure 3.8: Degenerated state diagram of (2, 1, 2) coded quaternary CPFSK for $h = \frac{1}{2}$.

3.2.2. Computer search for optimal codes

A trellis code is optimal at a certain modulation index and for a given CPFSK scheme, if it produces the largest MED when used to code the information sequence. For small q values and codes with small memory, it is possible to identify the minimum distance path and calculate the minimum distance for that path simply by examining the state diagram of the coded system.

Consider the code shown in Fig. 3.9 in combination with quaternary CPFSK for $h = 1/4$ resulting in the combined state diagram of Fig. 3.10 . This code was found by Pizzi and Wilson to be the optimal (2, 1, 2) code for quaternary CPFSK when $h \leq 3/10$ [20]. To find the minimum distance for this scheme, as well as others, all possible pairs of paths through the trellis have to be considered. The minimum distance path-pair begins from a common state, diverges and traverses through the trellis without encountering any state at the same time. After a finite number of split intervals it remerges at another state.

For the state diagram of Fig. 3.10 , the minimum distance path can be found, with some effort. This consists of the channel symbols $a_n = 1, 3, -3, 3, -3, -1$ and $a'_n = -3, -3, 1, -1, 3, 3$. It is shown in Fig. 3.10b . The minimum distance path begins at the state (S_0, π) and ends at the state $(S_3, 3\pi/2)$. The states S_0, S_1, S_2, and S_4 of the trellis code could have been labelled in binary as well.

(2.23) can be used to calculate the minimum distance of the above path-pair for correlation detection. Then

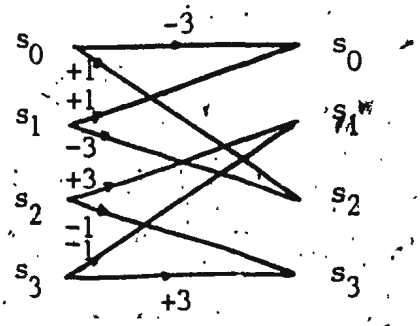

Figure 3.9: Trellis of (2, 1, 2) code.

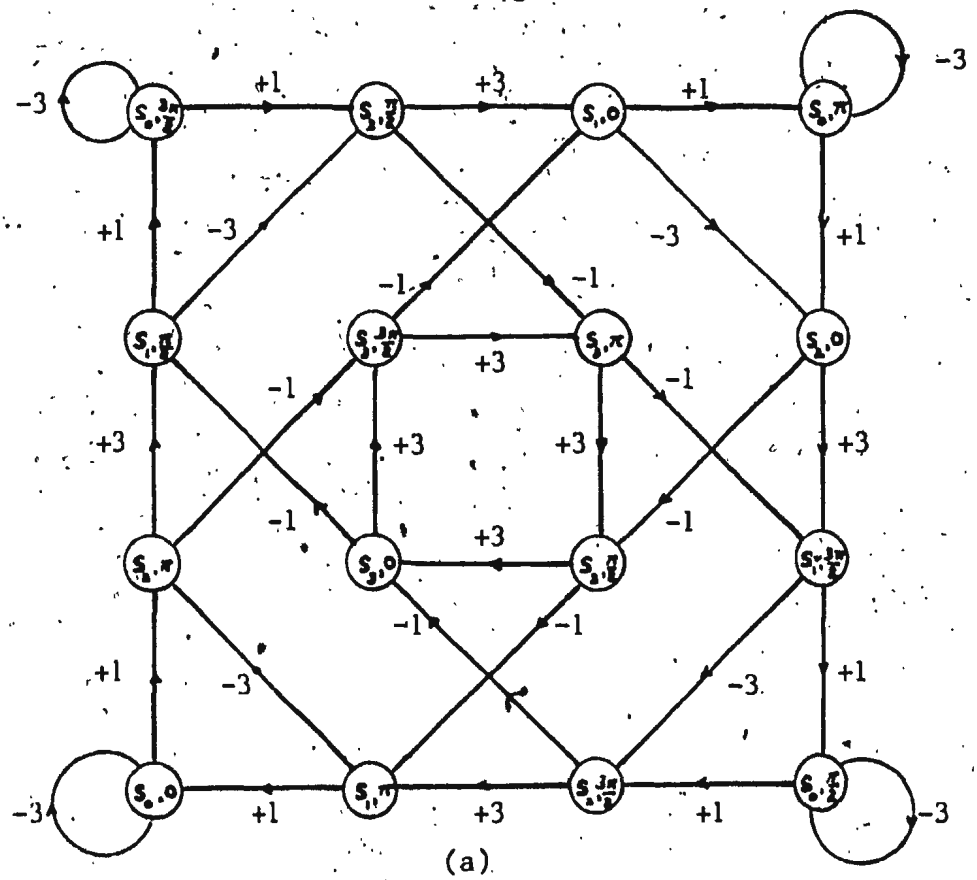

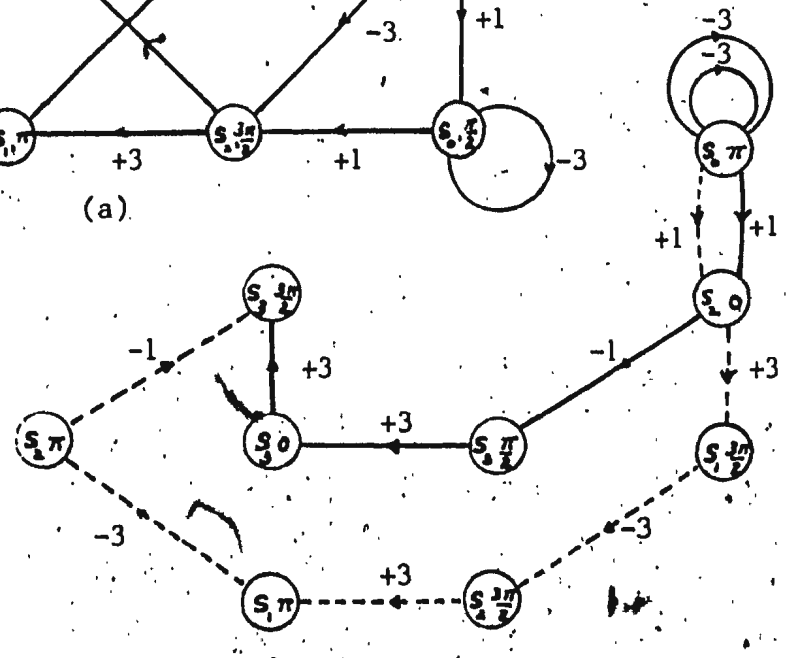

Figure 3.10: State diagram of quaternary CPFSK for h=1/4 with the trellis code of Fig.3.9.

$$d^2_{min} = 6 - \cos\left[\frac{\pi}{8}(4)\right] \operatorname{sinc}(1/2) - \cos\left[\frac{\pi}{8}(6) + \pi\right] \operatorname{sinc}(3/4)$$
$$- \cos\left[\frac{\pi}{8}(-4) + 5\pi/2\right] \operatorname{sinc}(1/2) - \cos\left[\frac{\pi}{8}(4) + 3\pi/2\right] \operatorname{sinc}(1/2)$$
$$- \cos\left[\frac{\pi}{8}(-6) + 5\pi/2\right] \operatorname{sinc}(3/4) - \cos\left[\frac{\pi}{8}(-4) + \pi\right] \operatorname{sinc}(1/2)$$
$$= 6 - 4\pi/3 - 4/\pi$$
$$= 4.302$$

For phase detection also, the same path yields the minimum distance. d^2_{min} for phase detection is calculated using (2.42).

$$d^2_{min} = 6 - \cos(\pi - 0) - \cos(3\pi/2 - \pi)$$
$$- \cos(3\pi/2 - 0) - \cos(\pi - \pi/2) - \cos(\pi - 0) - \cos(0)$$
$$= 5.000$$

All other split-merge events will have larger minimum distances than 4.302 for correlation detection and 5.000 for phase detection. Clearly the minimum distance path can start at any of the four states $(S_0, 0)$, $(S_0, \pi/2)$, (S_0, π), $(S_0, 3\pi/2)$ ending at $(S_3, \pi/2)$, (S_3, π), $(S_3, 3\pi/2)$, $(S_3, 0)$ respectively. Because of the rotational symmetry of the state diagram it is sufficient to consider path-pairs starting at four states only, namely $(S_0, 0)$, $(S_1, 0)$, $(S_2, 0)$, and $(S_3, 0)$.

Sign complementing the transition labellings of the trellis leaves the distance properties unchanged [20]. For instance, the trellis of Fig. 3.11 obtained by sign complementing the transition labellings of the trellis of Fig. 3.9 , gives rise to the combined state diagram of Fig. 3.10 . Except for a rotational shift of the states S_0 to S_4, S_1 to S_2, S_2 to S_3, and S_4 to S_0, the minimum distance path is unchanged and the minimum Euclidean distance is preserved.

A second equivalent type of trellis occurs when two trellises are labelled so that complementary states and complementary branches are identically labelled [20]. For example the trellises shown in Fig. 3.12a and Fig. 3.12b are equivalent. This fact too is useful in reducing the number of trellises, when searching for optimal codes.

An exhaustive search for optimal codes involves an impractical number of trellises. In general for codes of memory m, the trellis has 2^{m+1} branches and the number of possible trellis labellings with M-ary symbols becomes M^2. Thus for combination of memory 1 codes with octal CPFSK there are $(8^2)^2 = 4096$ codes for consideration. This difficulty has been overcome to a certain extent by using the following heuristic rules to reduce the number of trellises searched:

- All channel symbols should occur with equal frequency and with a fair amount of regularity and symmetry [24].
- Sign complementing the trellis labellings as well as inverting the trellis does not change the distance properties. Therefore such equivalent trellises are considered only once [20].
- The channel symbol corresponding to the lowest tone is always assigned to one of the two self loops of the state diagram of the code.

A computer program was written to find the minimum distance of quaternary and octal CPFSK signals with different trellis codes. The trellis search algorithm found in [17] was used in the program. An exhaustive search was not done in this study, instead, the trellis codes for the search were chosen using the heuristic rules listed above. The code trellis structure was assumed to be of a linear binary code similar to that shown in Fig. 3.9. The trellis searched with octal CPFSK signals is given in Sec.3.3.2. The channel symbols of each

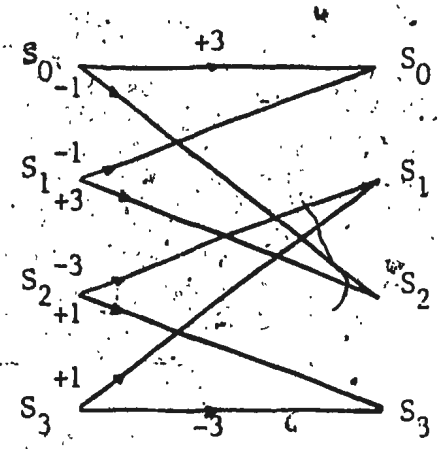

Figure 3.11: Equivalent trellis to the code of Fig. 3.9.

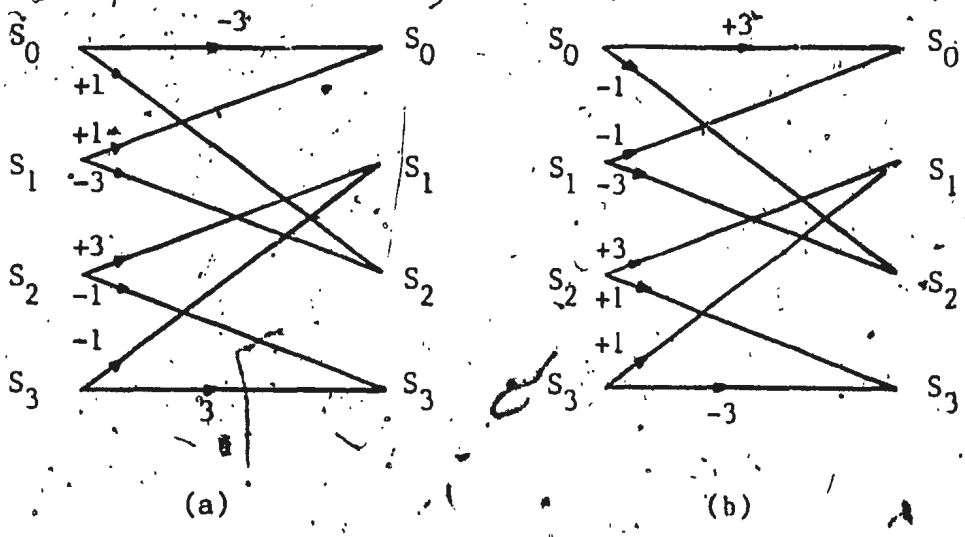

Figure 3.12: Equivalent trellis diagrams of (2, 1, 2) codes.

branch of the trellis were input to the program. The concept of a pair-state trellis [17] was used and this reduced the computer execution time considerably.

The minimum Euclidean distance (MED) and the receiver delay (N_d) were found for the optimal codes. Receiver delay is the trellis depth for a given code, which the algorithm should search, to ensure that all unmerged path-pairs have a larger distance than the minimum distance path-pair [20]. The flow chart outline of the program is shown in Fig. 3.13 .

3.3. Trellis codes combined with quaternary CPFSK signals

This section contains the numerical results as well as a discussion of $r = 1/2$, $m = 1$, 2, 3, 4, and 5 trellis coding of quaternary CPFSK signals. The distances reported are normalized with respect to the minimum distance of binary PSK. That means $d^2_{min} = 2.000$ is considered as the reference point and all distances are divided by $2E_b$ to arrive at the normalized distances.

The minimum Euclidean distances for $r = 1/2, m = 1$, 2, 3 trellis codes combined with quaternary CPFSK have been obtained previously, when the receiver consists of a correlation detector followed by a trellis decoder [14, 16, 20]. These results are extended to longer memory codes of $m = 4, 5$. More importantly, optimal trellis codes are evaluated for a phase detector followed by a trellis decoder. Optimal codes of memory up to 5 are searched for, in conjunction with the latter receiver and the MED compared with those of correlation receiver in the small h region. 'Small h' means those values of modulation index $h \leq 1/M$, where M is the order of the signaling scheme. For quaternary CPFSK

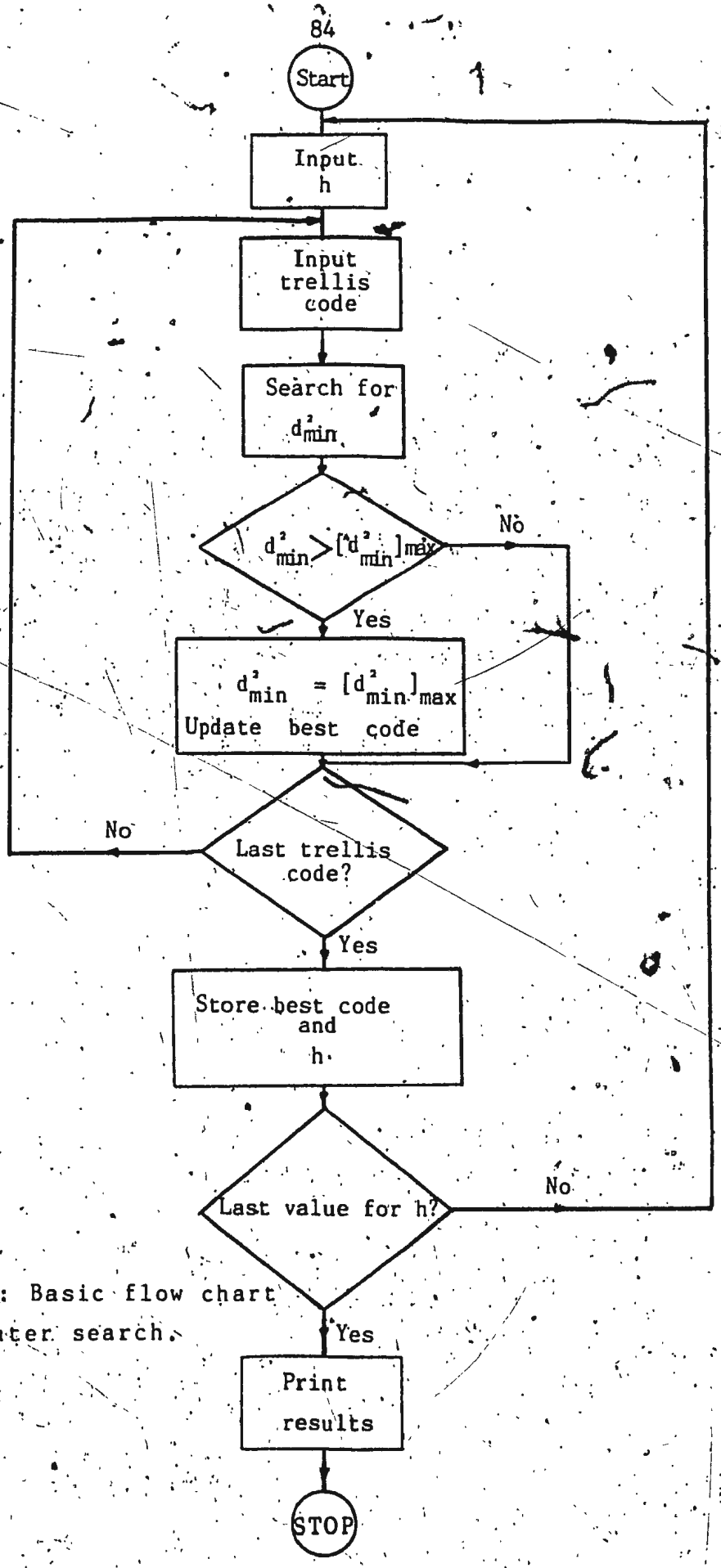

Figure 3.13: Basic flow chart of the computer search.

signals our region of interest is $0 < h \leq 1/4$. This limitation of h is justified by the fact that only for small h, CPFSK signaling becomes attractive from the point of view of signal bandwidth [20].

3.3.1. (2, 1, 1) coding of quaternary CPFSK signals

(2, 1, 1) codes form simple state diagrams when combined with quaternary CPFSK signals. These codes were discussed in some detail in the previous section while explaining the combined state diagram. Due to the simplicity of $m = 1$ codes, an exhaustive search for finding those codes producing the largest minimum distance is possible. However, this is not required when considering the equivalent trellises referred before. The results for correlation detection presented below are in exact agreement with previous investigations [14, 16, 20].

Table 3.2 shows the minimum distances obtained with optimal (2, 1, 1) codes, for some modulation indices. The largest MED monotonically increases for small h. The optimal code for $h \leq 1/4$ with correlation detection is shown in Fig. 3.14a , along with the implementation using a binary mapping rule. Note that the same code may have been implemented differently with other mapping rules. Also due to the presence of equivalent trellis labellings, there can be other equally good codes. For example the code shown in Fig. 3.14b produces the same minimum distance values for small h, but the decoder delay N_d' required is larger than that for the optimal code.

For small h the optimal trellis for phase detection and trellis decoding is as shown in Fig. 3.15 . This code requires a decoder delay of three, while other

Table 3.2: Largest minimum distances of (2, 1, 1) coded quaternary CPFSK for small h.

Modulation Index h	$d^2_{min}/2E_b$	
	Correlation detection	Phase detection
1/40	0.049	0.061
1/16	0.299	0.369
1/10	0.730*	0.882
1/8	1:090	1.293
1/7	1.371	1.599
1/6	1.760	2.000
3/16	2.100	2.324
1/5	2.298*	2.500
2/9	2.633	2.766
1/4	3.000*	3.000
2/7	3.363	3.123
33/100	3.611	3.018
1/3	2.793	3.000
17/50	3.503	2.962
3/8	3.188	2.707
1/2	3.000*	2.000

* Lindell et. al. [16]

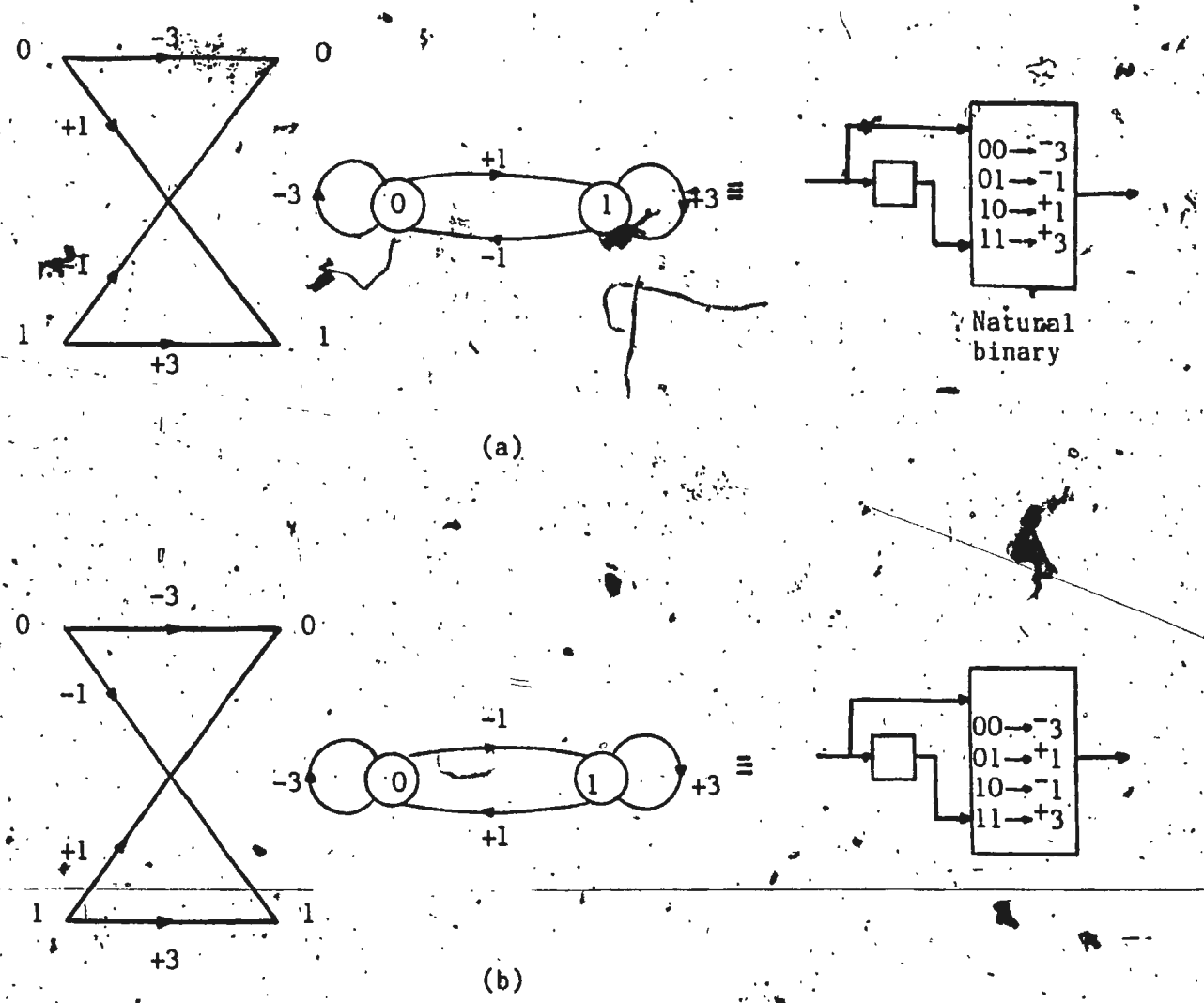

Figure 3.14: Optimal (2, 1, 1) code for correlation detection of coded quaternary CPFSK for small h. (a) Optimal code and its implementation. (b) Equivalent code to (a).

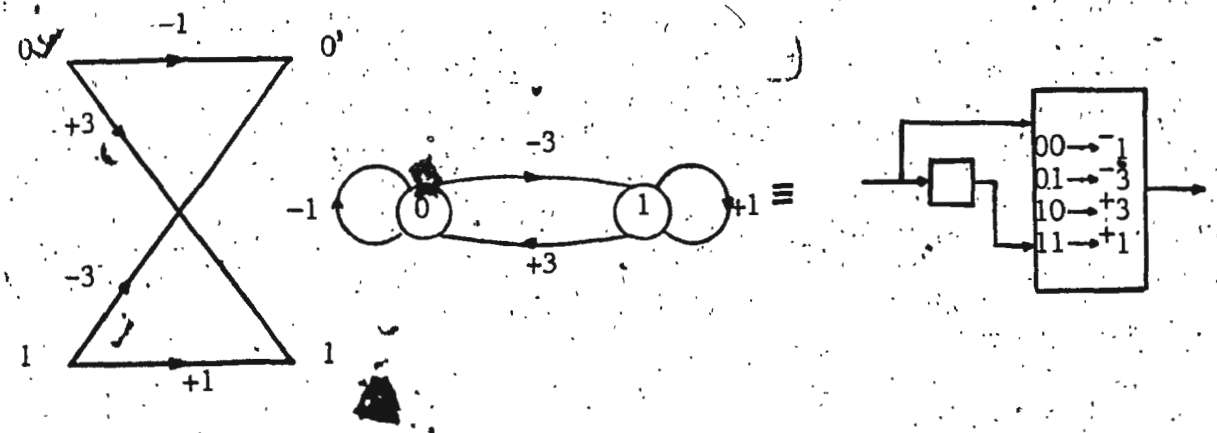

Figure 3.15: Optimal (2, 1, 1) code for phase detection of coded quaternary CPFSK for small h.

equally good codes such as those shown in Figs. 3.14a and 3.14b produce the same minimum distance values, but need larger decoder delays. The optimal trellis above can be implemented using the same (2, 1, 1) linear convolutional code of Fig. 3.14a by changing the mapping rule as shown in Fig. 3.15 .

The variation of minimum distance with modulation index h for the code of Fig. 3.14a [that is the optimal (2, 1, 1) code for correlation detection] is shown in Fig. 3.16 . The two curves give the minimum distance for the same code shown in Fig. 3.14a , for the two receivers considered. Different merger events dominate the minimum distance over different ranges of h [20]. At points such as $h = 1/3$, referred to as 'weak modulation indices' in [20], MED reflects a dip for both receivers. With the help of the state diagram this can be explained as follows.

Recall that for uncoded M-ary CPFSK signals, when $q < M$, the number of branches for each state exceeds the total number of states at each level of the trellis and parallel branches are generated between the adjacent levels. Thus for quaternary CPFSK for $h = 1/3\,(q < M = 4)$ the combined state diagram is affected by the parallel branches of the uncoded CPFSK. This is shown in Fig. 3.17 . For convenience the trellis of the uncoded CPFSK with $h = 1/3$ is reproduced in Fig. 3.17b . The combined state diagram for $h = 1/3$ degenerates into three seperate state diagrams and the length of the minimum distance merging event is only 2. The minimum distance for correlation detection is reduced to 1.793 and for phase detection to 1.500.

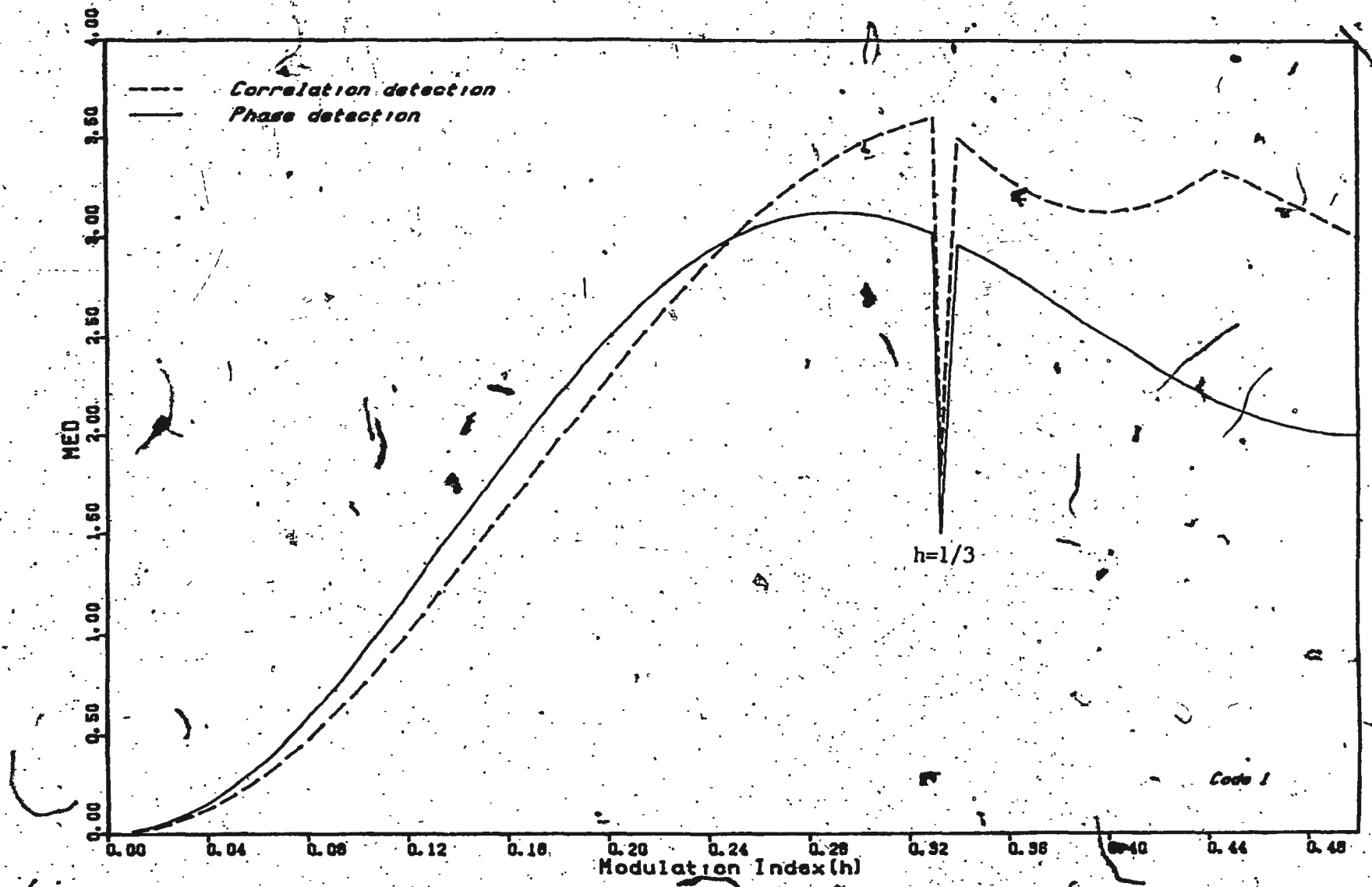

Figure 3.16: Minimum distance versus modulation index for (2, 1, 1) coded quaternary CPFSK with optimal code for correlation detection.

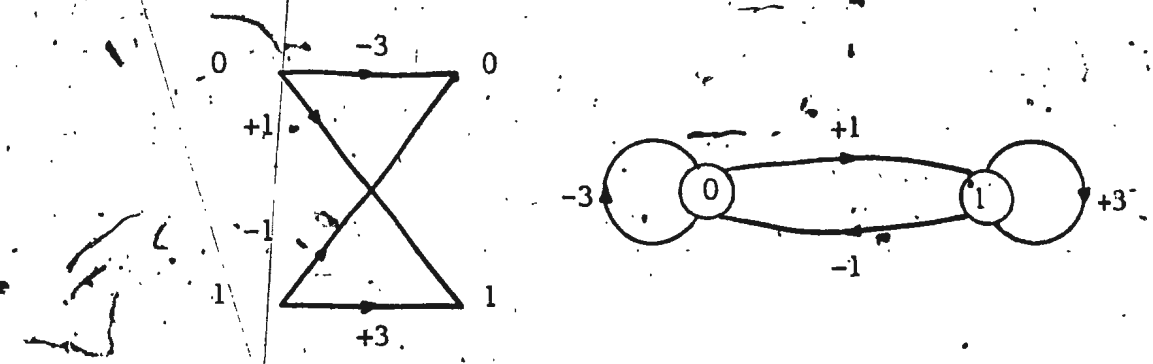

(a) Optimal (2, 1,1) code for correlation detection.

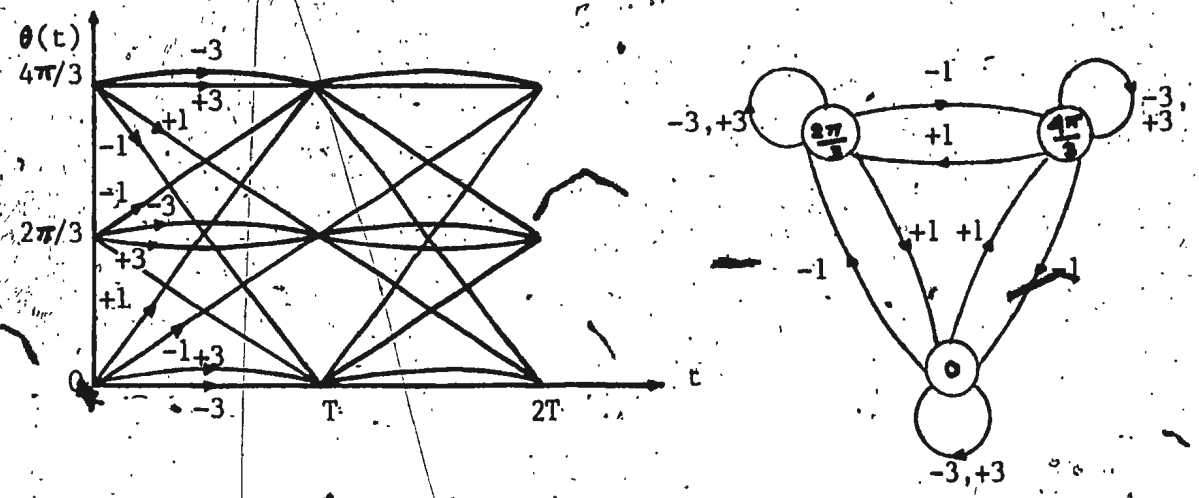

(b) Trellis and the state diagram of uncoded quaternary CPFSK with h=1/3.

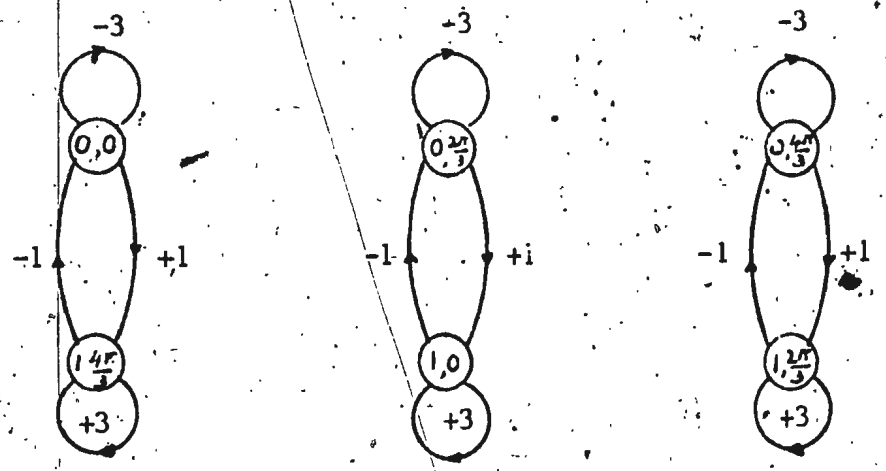

(c) Combined state diagram.

Figure 3.17: (2, 1, 1) coding of quaternary CPFSK with h=1/3.

In Fig. 3.18 , MED is plotted against h for the optimal trellis code with phase detection. This does not reflect any discontinuities. The combined state diagram for this code at $h = 1/3$ is shown in Fig. 3.19 . The trellis does not degenerate, and the minimum distance is preserved at 3.00. However, the decoder memory required around $h = 1/3$ is increased rapidly. When h equals 8/25, N_d equals 92 and when h equals 7/20, N_d equals 66.

For the codes considered above, phase detection yields larger minimum distances than correlation detection for small h values. Table 3.3 shows the coding gains achieved in each case, for some modulation indices, when compared with the uncoded quaternary CPFSK.

3.3.2. (2, 1, 2) coding of quaternary CPFSK signals

Results for (2, 1, 2) codes are presented in this section. Table 3.4 gives the largest minimum distances obtained at some h values, for both phase detection and correlation detection. For small h values the same (2, 1, 2) code is optimum for both receivers. This code is given in Fig. 3.20a , and its implementation using a convolutional encoder with a natural binary mapping function in Fig. 3.20b . In Fig. 3.21 minimum distance is plotted against h for the above optimal code for correlation detection and phase detection.

When considering the curves in detail, it is found that for phase detection, at $h = 1/7, 2/7$ and $3/7$ the minimum distance merging takes place only after three levels, but at neighbouring h the merging occurs at intervals of 4 or 5. Therefore we may suspect degeneracy of the combined trellis at these points. The

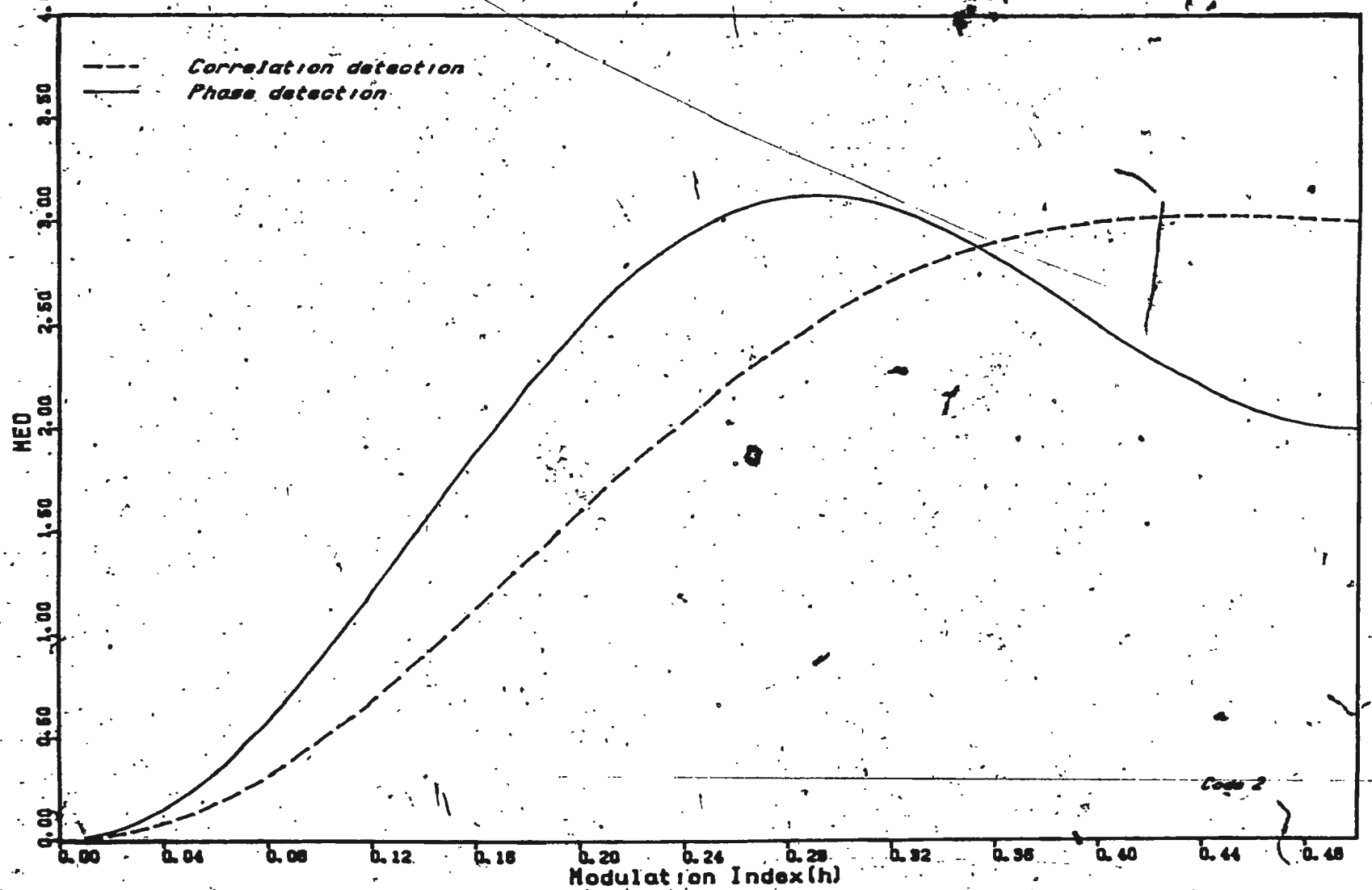

Figure 3.18: Minimum distance versus modulation index for (2, 1, 1) coded quaternary CPFSK with optimal code for phase detection.

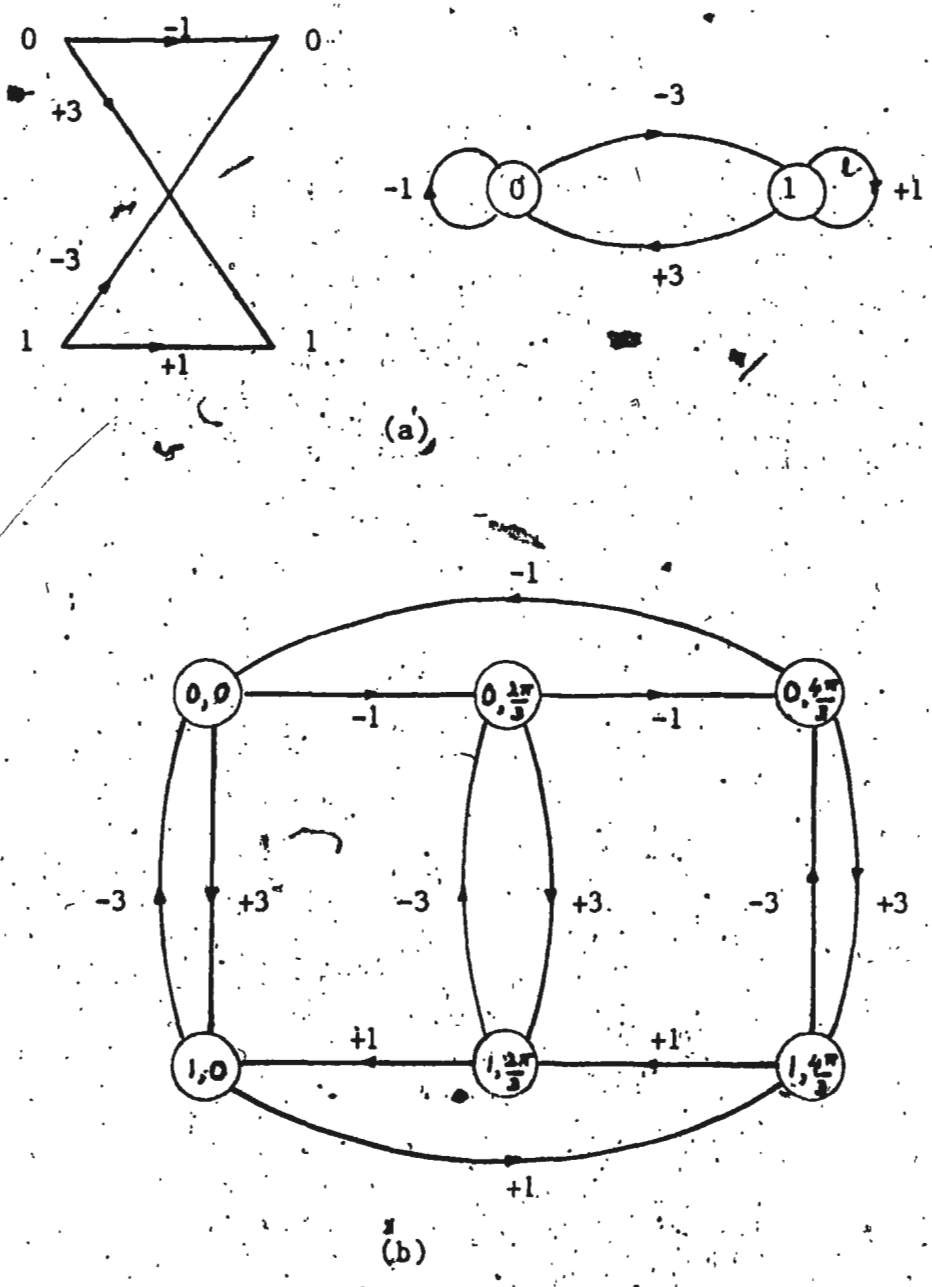

Figure 3.19: Optimal (2, 1, 1) code for phase detection and the combined state diagram with quaternary CPFSK for h=1/3.

Table 3.3: Coding gain of (2, 1, 1) coded quaternary CPFSK over uncoded quaternary CPFSK at same h.

Modulation Index h	$d^2_{min}/2E_b$ (uncoded)	$d^2_{min}/2E_b$ (dB) (coded)	
		Correlation detection	Phase detection
1/40	0.016	4.86	5.81
1/16	0.102	4.67	5.58
1/10	0.258	4.52	5.34
1/8	0.399	4.36*	5.11
1/7	0.516	4.24	4.91
1/6	0.692	4.05	4.61
3/16	0.863	3.86	4.30
1/5	0.973	3.73	4.09
2/9	1.179	3.49	3.70
1/4	1.454	3.15*	3.15

* Pizzi and Wilson [20].

Table 3.4: Largest minimum distances of (2, 1, 2) coded quaternary CPFSK for small h.

Modulation Index h	$d^2_{min}/2E_b$	
	Correlation detection	Phase detection
1/40	0.066	0.110
1/16	0.400	0.662
1/10	0.983*	1.573
1/8	1.477	2.293
1/7	1.867	2.445
1/6	2.416	3.500
3/16	2.908	3.566
1/5	3.202*	3.618
2/9	3.711	4.347
1/4	4.302*	5.000
2/7	3.081	3.802
33/100	3.653	3.074
1/3	3.413	3.000
17/50	3.459	2.859
3/8	2.975	2.293
1/2	4.000*	2.000

* Lindell et. al. [16].

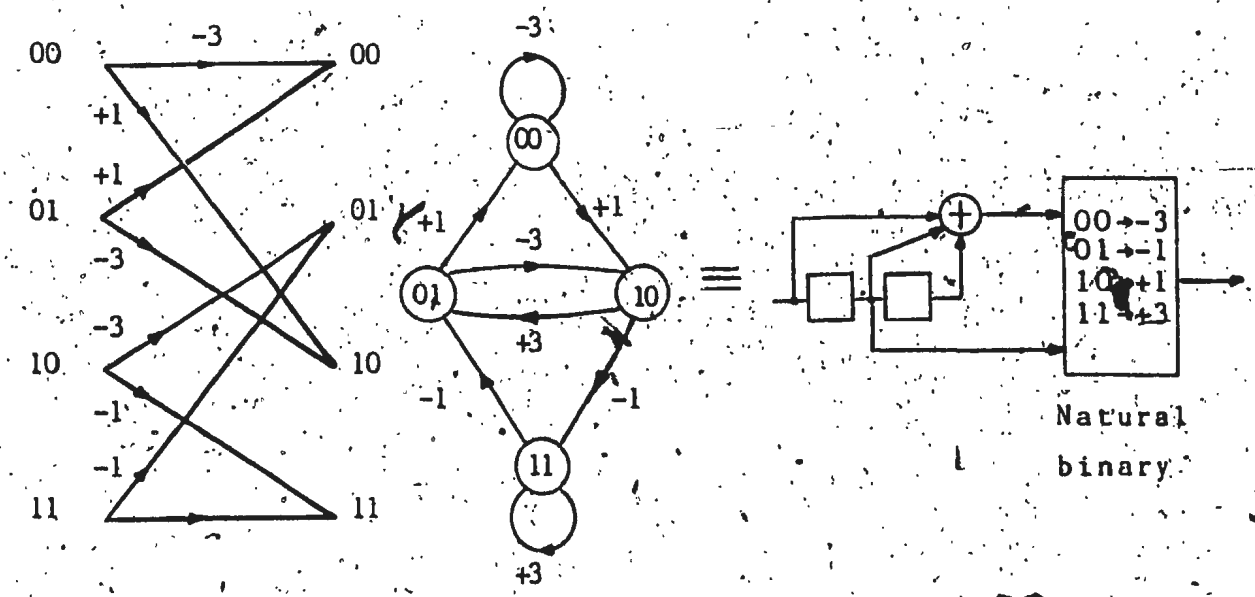

Figure 3.20: Optimal (2, 1, 2) code with quaternary CPFSK for small h.

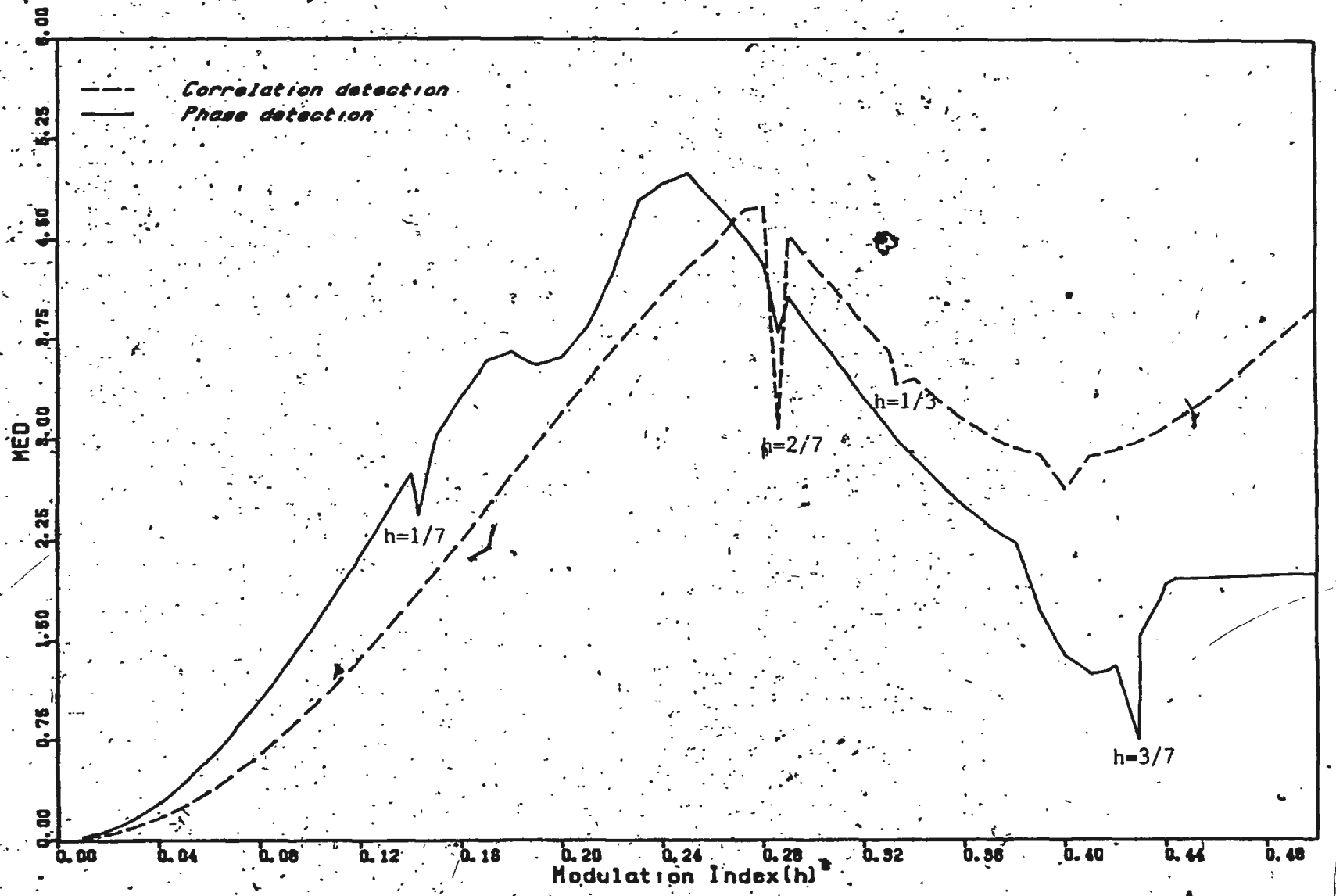

Figure 3.21: Comparison of minimum distance for (2, 1, 2) coded quaternary CPFSK signals.

state diagram at $h = 1/7$ and $2/7$ are shown in Fig. 3.22 and Fig. 3.23 respectively. From the above figures, clearly there is no degeneracy at these two modulation indices, but the minimum distance at these points is reduced. This is due to the short merging events shown in Fig. 3.22b and Fig. 3.23b , and the minimum distance merging paths are identical in this case for phase detection and correlation detection. There are other points such as $h = 1/5, 2/5$ where merging level is again three; but, unlike at $h = 1/7$ and $2/7$ the reduction in minimum distance is gradual. Presumably the trellis does not degenerate at these points either.

For correlation detection, when the optimal small h code is used, shorter merging is observed at three levels when $h = 2/7, 1/3$, and $2/5$. At all other points ($h < 1/2$),the minimum distance merge event length is either 4 or 6 and these merging events can be obtained by drawing the combined state diagram. In Fig. 3.24 , the combined state diagram and the corresponding minimum distance merge event for $h = 1/3$ are drawn. However, the optimal code at $h = 1/3$ is different from the optimal code for small h. This optimal code is shown in Fig. 3.25a with the corresponding combined state diagram in Fig. 3.25b .

Referring to Fig. 3.21 , where the two receivers with the optimal code for small h were compared, it is found that below $h = 4/15$, phase detection gives larger minimum distances than correlation detection. Above $h = 4/15$, the latter receiver yields larger minimum distances, though the coding gains achieved beyond $h = 1/4$ are unattractive when considering the expansion in the bandwidth [20]. In Table 3.5 the coding gain achieved in each case is tabulated, for some modulation indices, when compared to the uncoded quaternary CPFSK.

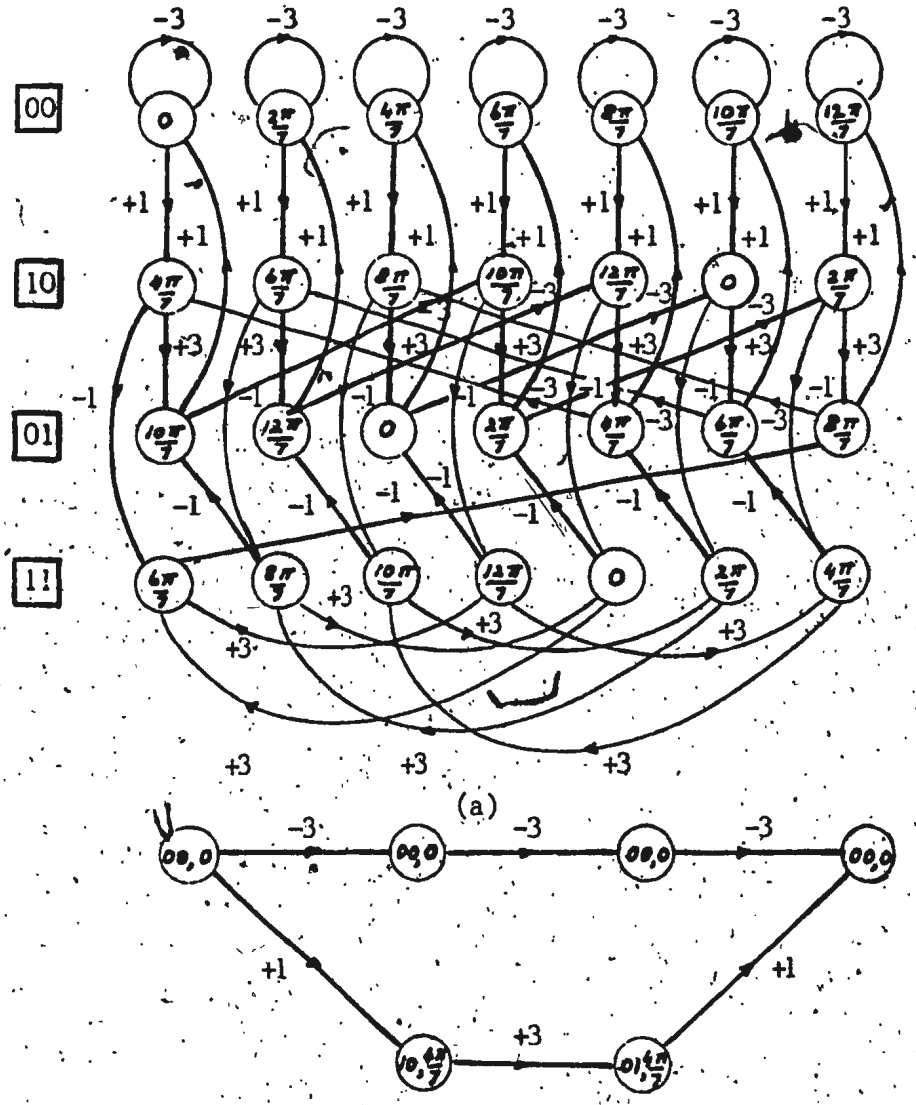

$$d^2_{min}/2\mathcal{E}_b = 3 - \cos(-4\pi/7) - \cos(-10\pi/7) - \cos(0)$$
$$= 2.445$$

Figure 3.22: (2, 1, 2) coding of quaternary CPFSK for h=1/7, (a) Combined state diagram. (b) Minimum distance merging event.

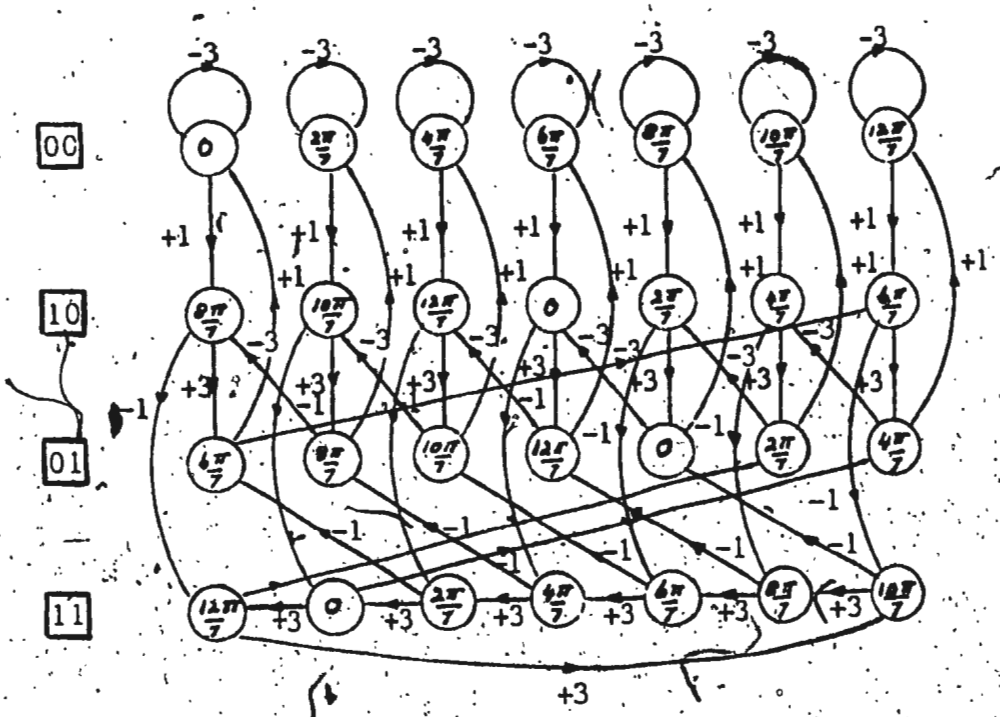

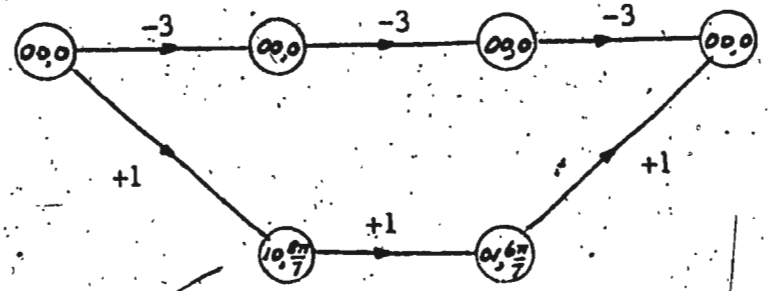

$$d^2_{min}/2E_b = 3 - \cos(8\pi/7) - \cos(6\pi/7) - \cos(0)$$

$$= 3.802$$

Figure 3.23: (2, 1, 2) coding of quaternary CPFSK for h=2/7. (a) Combined state diagram. (b) Minimum distance merging event.

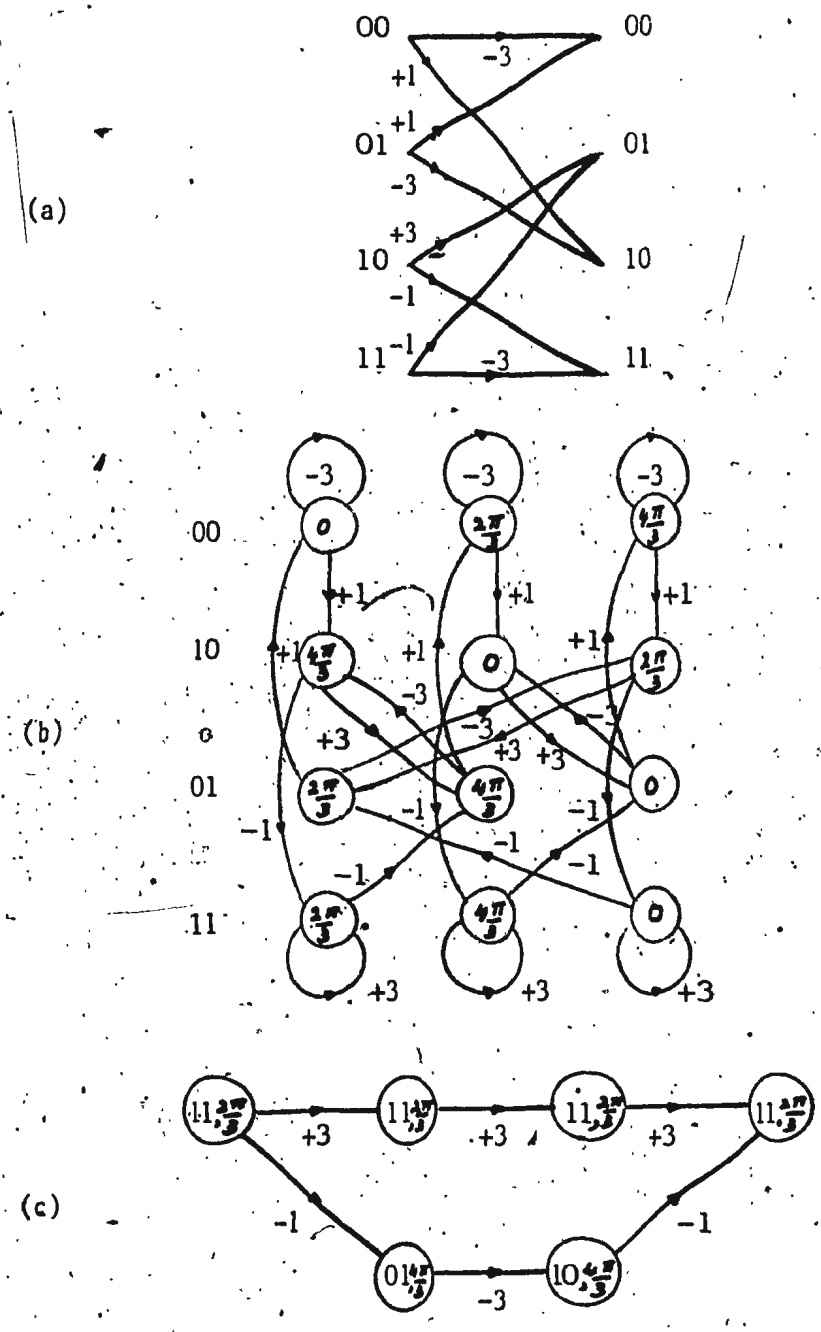

$$d^2_{min} = 3 - \cos(2\pi/3) - \cos(2\pi/3) - \cos(0) = 3.000.$$

Figure 3.24: (2, 1, 2) coding of quaternary CPFSK for h=1/3. (a) Optimal trellis code for small h. (b) Combined state diagram. (c) Minimum distance path.

(a)

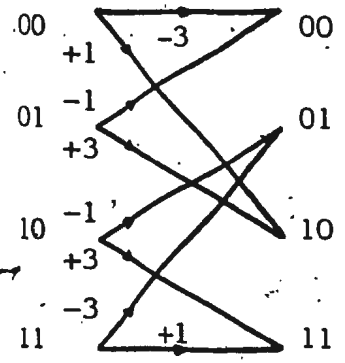

(b)

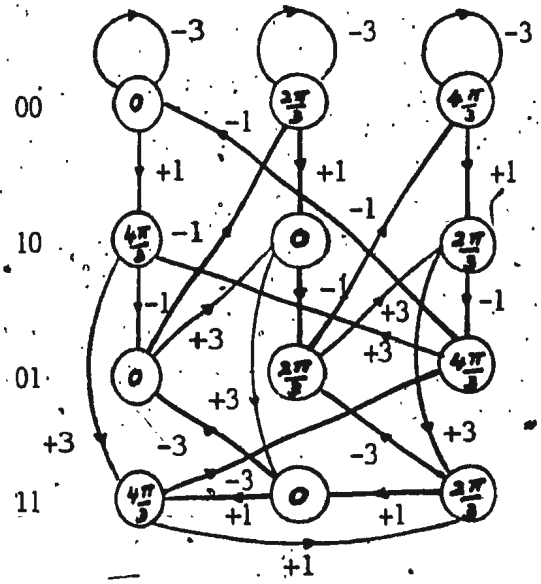

(c)

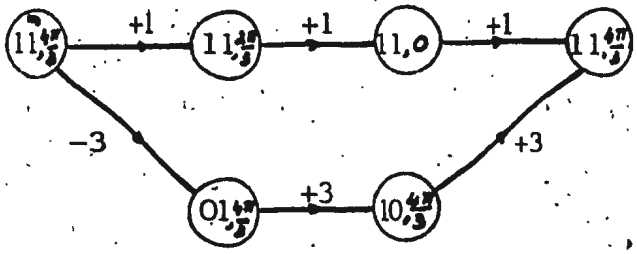

$$d^2_{min} = 3 - \cos(2\pi/3) - \cos(4\pi/3) - \cos(0) = 3.000.$$

Figure 3.25: (2, 1, 2) coding of quaternary CPFSK for h=1/3. (a) Optimal trellis code for h=1/3. (b) Combined state diagram. (c) Minimum distance path.

Table 3.5: Coding gain of (2, 1, 2) coded quaternary CPFSK over uncoded quaternary CPFSK at same h.

Modulation Index h	$d^2_{min}/2E_b$ (uncoded)	$d^2_{min}/2E_b$ (dB) (coded)	
		Correlation detection	Phase detection
1/40	0.016	6.15	8.37
1/16	0.102	5.93	8.12
1/10	0.258	5.81	7.85
1/8	0.399	5.68*	7.59
1/7	0.516	5.58	6.76
1/6	0.692	5.43	7.04
3/16	0.863	5.28	6.16
1/5	0.973	5.17	5.70
2/9	1.179	4.98	5.67
1/4	1.454	4.71*	5.36

* Pizzi and Wilson [20].

3.3.3. (2, 1, 3) coding of quaternary CPFSK signals

Table 3.6 shows the largest minimum distances obtained for (2, 1, 3) coded quaternary CPFSK signals. In Fig. 3.27 , minimum distance is plotted against modulation index, h, for phase detection and correlation detection for the optimal (2, 1, 3) code of Fig. 3.26 .

Optimal codes for correlation detection are considered first. At $h = 1/16$, both the trellises shown in Fig. 3.26 give a distance of 0.476 and the decoder delay required are 19 and 20 respectively. Thus they are equally good codes. At $h = 1/8$ and $h = 1/6$ the same two trellis labellings produced optimal distances of 1.764 and 2.900 respectively. At $h = 1/6$ both codes required a delay of 18 while at $h = 1/8$, the decoder delays were 19 and 20 respectively. For all other small h values, these two codes resulted in the same distance, but the decoder delay required for the code of Fig. 3.26a was less than that for the other code. Therefore the trellis of Fig. 3.26a is optimal for correlation detection. It is possible to obtain equivalent optimal codes by time-reversing the register-adder connections [14, 20].

For small h, the trellis of Fig. 3.26a was optimal for phase detection too. Thus for small h we have the same optimal code for both types of detection. Here too there are other trellis labellings, obtainable by changing the mapping rule and time-reversal of the generator connections [20], which prove to be of equal performance; same minimum Euclidean distance, decoder delay, and merging level.

Table 3.6: Largest minimum distances of (2, 1, 3) coded quaternary CPFSK for small h.

Modulation Index h	$d'_{min}/2E_b$	
	Correlation detection	Phase detection
1/40	0.078	0.123
1/16	0.476	0.738
1/10	1.171*	1.764
1/8	1.764	2.586
1/7	2.234	3.198
1/6	2.900	4.000
3/16	3.501	4.649
1/5	3.863*	4.309
2/9	4.495	5.049
1/4	5.241*	6.000

* Lindell et. al. [16].

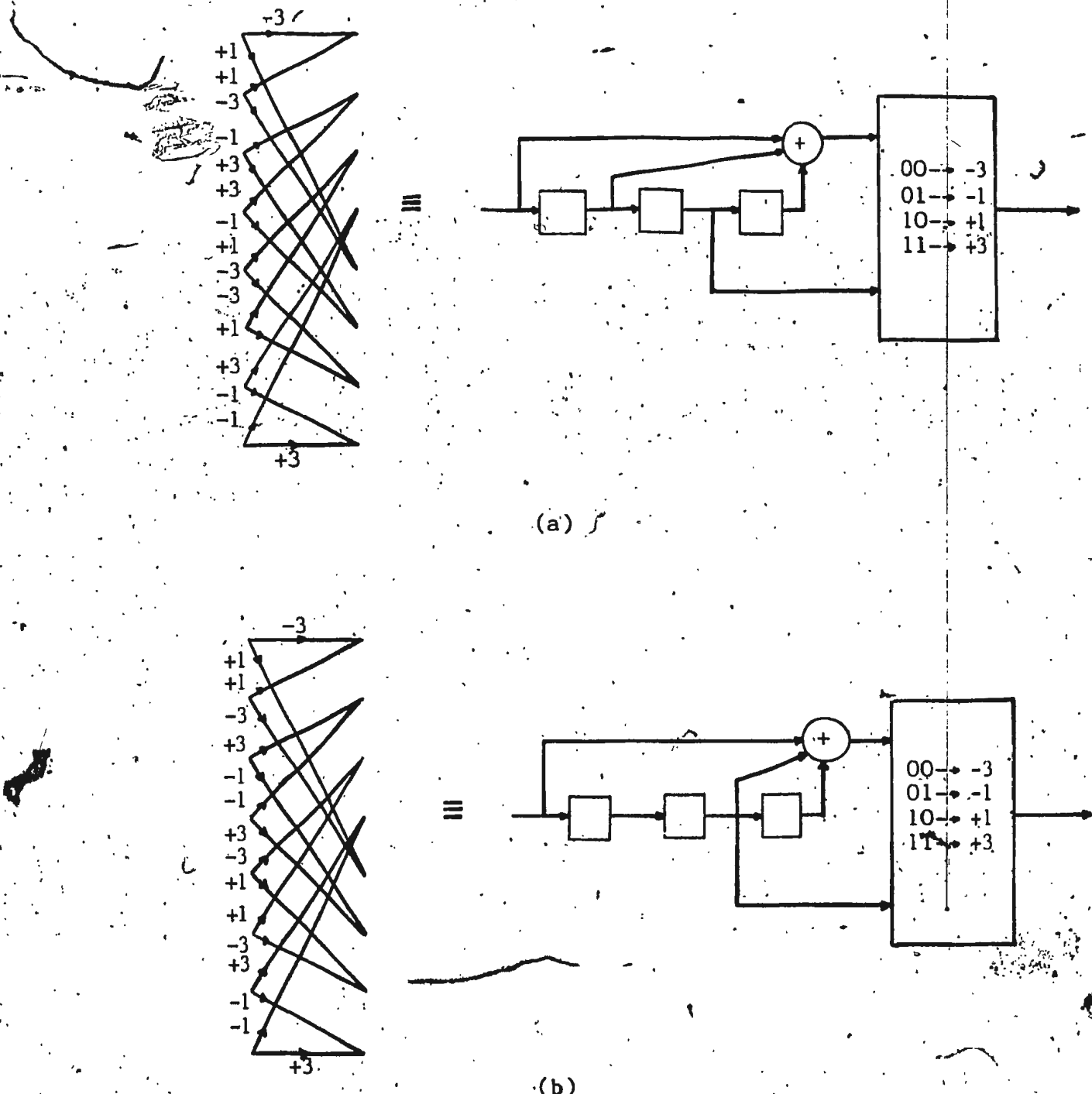

Figure 3.26: Optimal codes for (2, 1, 3) trellis coded quaternary CPFSK with small h.

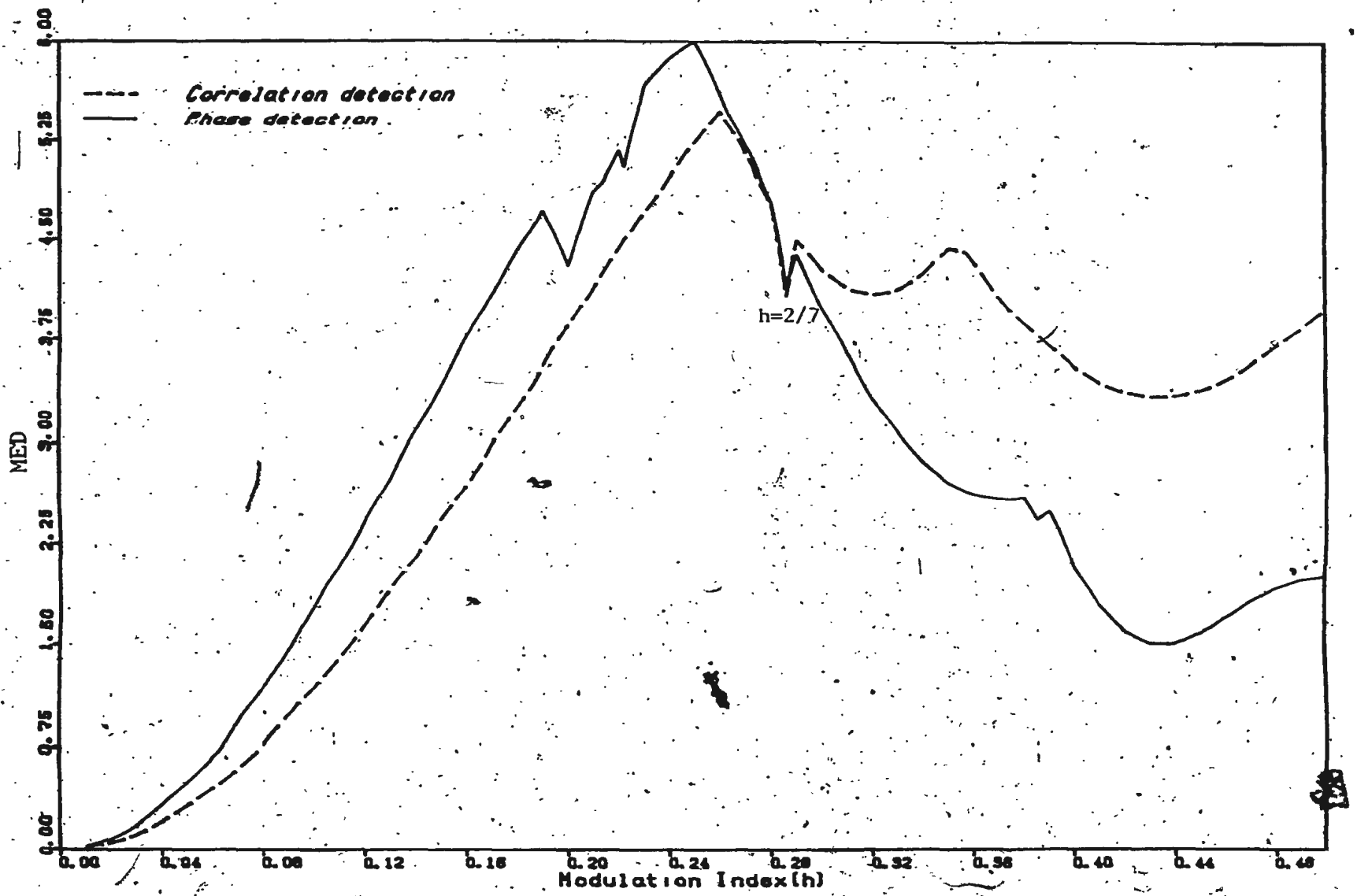

Figure 3.27: Comparison of minimum distance for (2, 1, 3) coded quaternary CPFSK signals.

Referring to Fig. 3.27 , for correlation detection of (2, 1, 3) trellis coded quaternary CPFSK signals, the minimum Euclidean distance is a monotone increasing function of h, up to $h \approx 13/50$ and at $h = 2/7$ it reduces to 4.097, corresponding to a minimum distance merging event of length four. For phase detection, the minimum Euclidean distance monotonically increases until $h \approx 19/100$, and at $h = 1/5$ the distance reduces to 4.309. The minimum distance merging level at $h = 1/5$ is four. Reductions in the minimum distance similar to these occur at $h = 2/7$ and $1/3$, again with a shorter merging event of length four. Neighbouring points of all these modulation indices result in minimum distance merging events of length five or six.

For the optimal (2, 1, 3) code, short minimum distance merging events occur only at $h = 1/5, 2/7$ and $1/3$ ($h < 1/2$). By drawing the state diagram of the coded CPFSK scheme it could have been possible to identify these merging paths. But the state diagram for $m = 3$ and $q = 7$ consists of 56 different states, which makes it impracticable for drawing.

Both types of detection results in monotone increasing distances up to $h \approx 19/100$. This monotone nature implies that the same merging path-pair gives the minimum distance for small h [20]. More importantly, for $h \leq 2/7$, phase detection yields larger minimum distances than correlation detection. Coding gains achieved in each case for some modulation indices is given in Table 3.7 . As before, the dB values are computed with respect to the uncoded quaternary CPFSK.

Table 3.7: Coding gain of (2, 1, 3) coded quaternary CPFSK over uncoded quaternary CPFSK at same h.

Modulation Index h	$d^2_{min}/2E_b$ (uncoded)	$d^2_{min}/2E_b$ (dB) (coded)	
		Correlation detection	Phase detection
1/40	0.016	6.88	8.86
1/16	0.102	6.69	8.59
1/10	0.259	6.55	8.33
1/8	0.399	6.45*	8.12
1/7	0.516	6.36	7.92
1/6	0.692	6.22	7.62
3/16	0.863	6.08	7.31
1/5	0.973	5.99	6.46
2/9	1.179	5.81	6.32
1/4	1.454	5.57*	6.16

* Pizzi and Wilson [20].

3.3.4. (2, 1, 4) coding of quaternary CPFSK signals

A search for good codes resulted in the trellis of Fig. 3.28 as the best for small h with phase detection. The same code was earlier found to be optimal with correlation detection [14]. The largest minimum distance for some h values of (2, 1, 4) coding of quaternary CPFSK signals is tabulated in Table 3.8 .

In Fig. 3.29 , the minimum distance against modulation index h is plotted for correlation detection and phase detection. The minimum Euclidean distance for correlation detection increases monotonically up to $h \approx 13/50$; however, around $h = 1/5$ there is a slight reduction in the minimum distance due to a shorter merging event of length nine. Beyond $h = 13/50$ the minimum distance is less than 6.305, which is the maximum for this code. At $h = 2/7$ and $h = 1/3$, momentary reduction in d^2_{min} is reflected due to shorter merging events of length five, the corresponding distances being 4.473 and 4.207. For phase detection there is a monotone increasing curve when the modulation index $h < 1/5$. At $h = 1/5$, $2/7$, and $1/3$ due to shorter merging events of length five the minimum distance reduces to 5.000, 4.555, and 3.000 respectively. For all $h < 1/4$ the usual minimum distance merging event is of length eight. Furthermore, phase detection gives larger minimum distances than correlation detection for $h \leq 1/4$. Beyond this, the converse is true. The coding gains achieved over the uncoded quaternary CPFSK is given in Table 3.9.

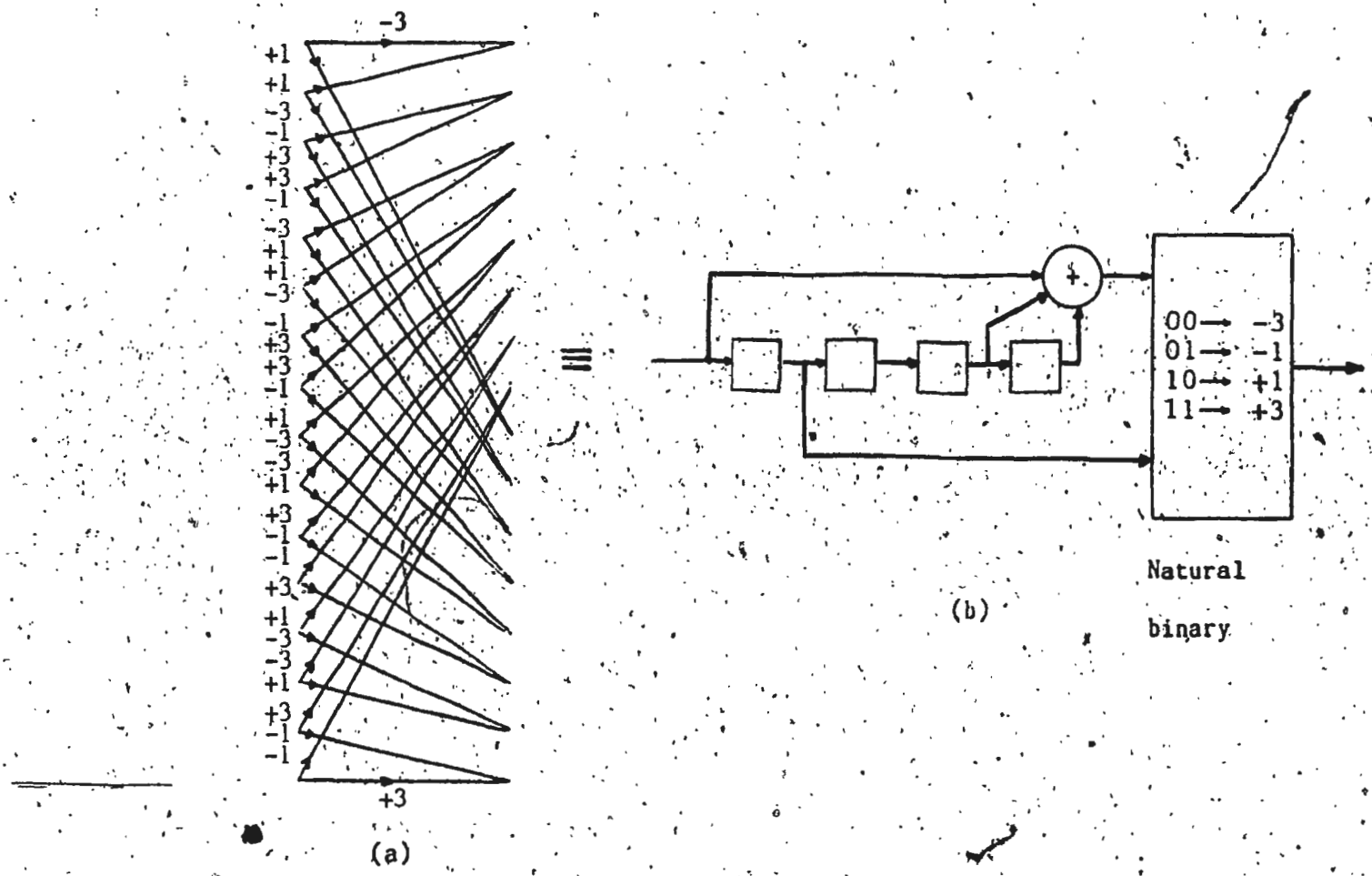

Figure 3.28: Optimal trellis code for (2, 1, 4) coded quaternary CPFSK with small h. (a) Trellis. (b) Implementation using a convolutional code and natural binary mapping rule.

Table 3.8: Largest minimum distances of (2, 1, 4) coded quaternary CPFSK for small h.

Modulation Index h	$d^2_{min}/2E_b$	
	Correlation detection	Phase detection
1/40	0.090	0.135
1/16	0.552	0.814
1/10	1.362*	1.995
1/8	2.057	2.879
1/7	2.611	3.575
1/6	3.400	4.500
3/16	4.119	5.266
1/5	4.427*	5.000
2/9	5.210	5.751
1/4	6.151*	7.000

* Lindell et. al. [16].

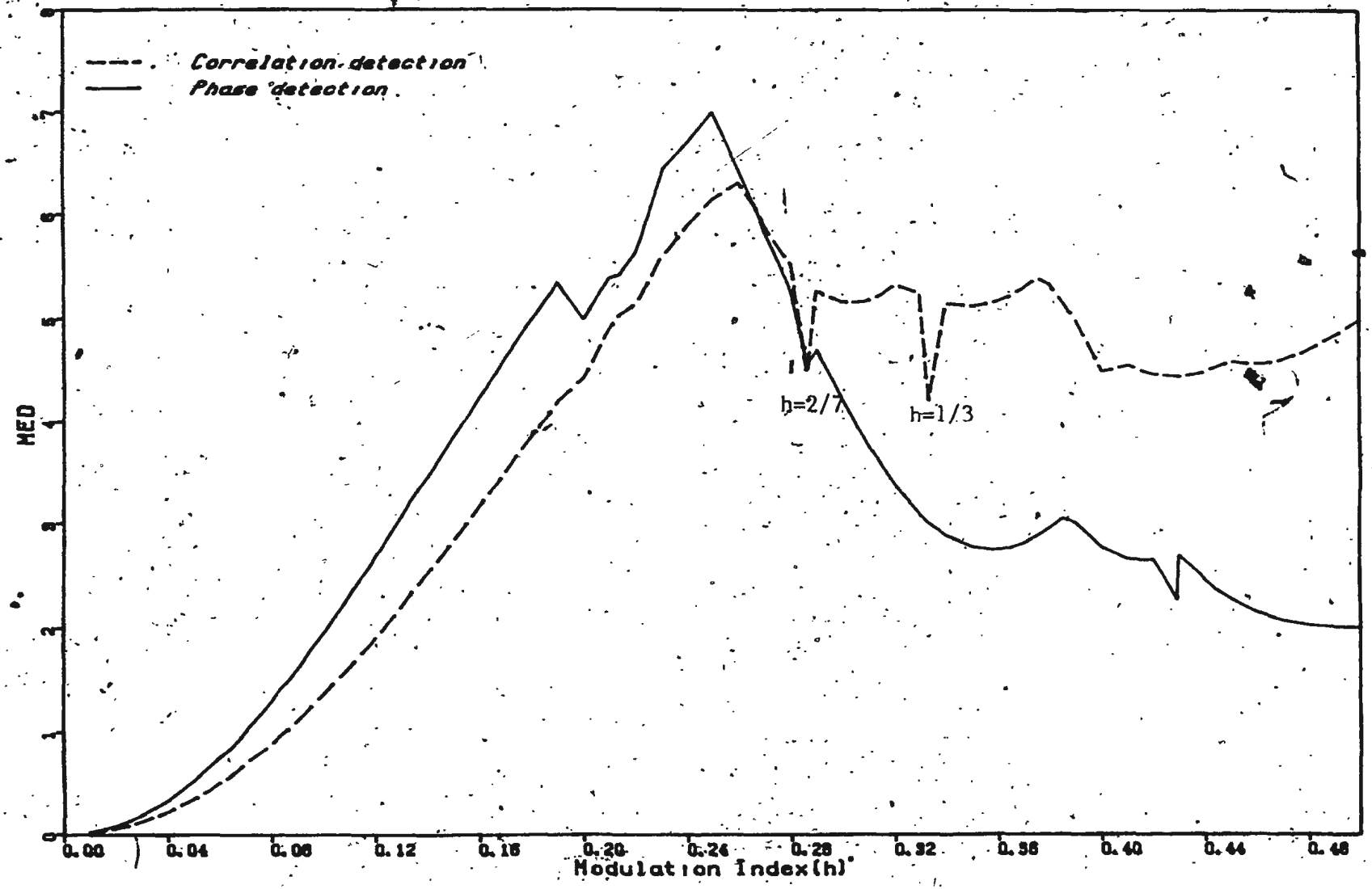

Figure 3.29: Comparison of minimum distance for (2, 1, 4) coded quaternary CPFSK signals.

Table 3.9: Coding gains of (2, 1, 4) coded quaternary CPFSK over uncoded quaternary CPFSK at same h.

Modulation Index h	$d^2_{min}/2E_b$ (uncoded)	$d^2_{min}/2E_b$ (dB), (coded)	
		Correlation detection	Phase detection
1/40	0.016	7.50	9.26
1/16	0.102	7.33	9.02
1/10	0.259	7.21	8.78
1/8	0.399	7.12	8.58
1/7	0.516	7.04	8.41
1/6	0.692	6.91	8.13
3/16	0.863	6.79	7.85
1/5	0.973	6.58	7.11
2/9	1.179	6.45	6.88
1/4	1.454	6.26	6.82

3.3.5. (2, 1, 5) coding of quaternary CPFSK signals

The optimal code for (2, 1, 5) coding of quaternary CPFSK is shown in Fig. 3.30. In this case, a complete search of all the best trellis labellings was not done. Therefore there may be other codes better than this. The above code was found to be the best for correlation detection and phase detection. Nevertheless at a few modulation indices within the small h region, such as $h = 3/16$ and $1/4$ the code shown in Fig. 3.31 was optimum for phase detection. This code can be obtained by changing the mapping rule of Fig. 3.30 to that given in Fig. 3.31 with the binary convolutional code remaining the same.

Table 3.10 gives the largest minimum distances achieved by (2, 1, 5) coding of quaternary CPFSK. The performance of the coded system with the optimal code for small h is compared for correlation detection and phase detection as shown in Fig. 3.32. For $h \leq 1/4$ phase detection yields larger minimum distances than for correlation detection. Table 3.11 is a list of coding gains achieved by the optimal code as shown in Fig. 3.30.

3.3.6. Summary of minimum distances for phase detection of coded quaternary CPFSK signals

Table 3.12 gives a summary of the minimum distances for phase detection of coded quaternary CPFSK signals. Longer memory codes produce larger minimum distances. However, when $h = 1/4$ the minimum distance paths for $m = 4$ and $m = 5$ are identical, resulting in the same minimum distance. Also, the complexity of the trellis decoder is proportional to the number of states in the trellis. Due to the large number of states involved in longer memory length codes,

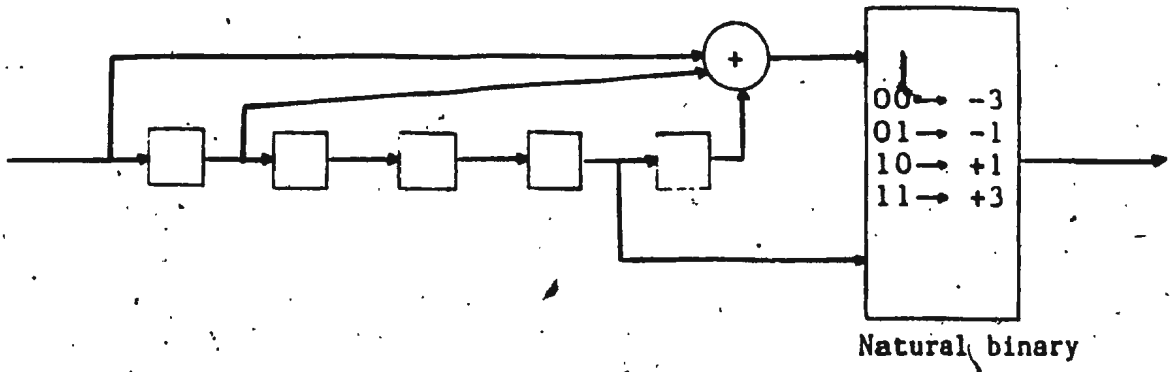

Figure 3.30: Optimal (2, 1, 5) code for trellis coded quaternary CPFSK with small h.

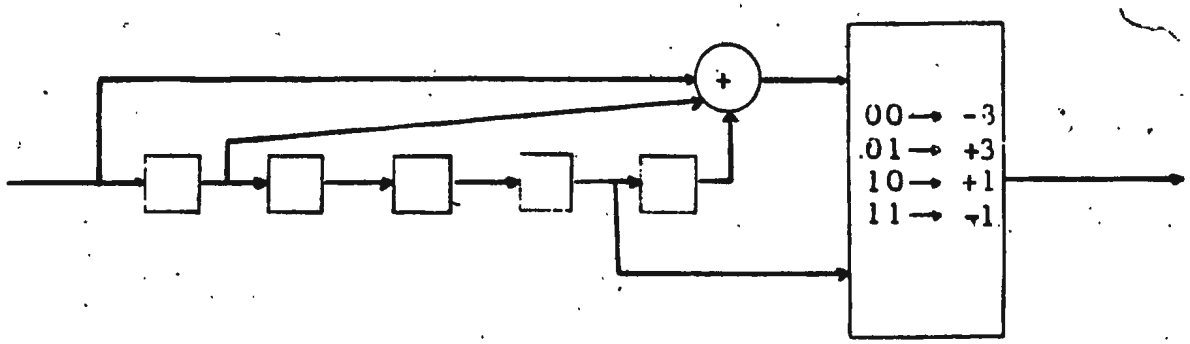

Figure 3.31: Equivalent trellis code to that of Fig. 3.30.

Table 3.10: Largest minimum distances of (2, 1, 5) coded quaternary CPFSK for small h.

Modulation Index h	$d^2_{min}/2E_b$	
	Correlation detection	Phase detection
1/40	0.094	0.147
1/16	0.578	0.890
1/10	1.427	2.146
1/8	2.157	3.172
1/7	2.740	3.952
1/6	3.573	5.000
3/16	4.334	5.739
1/5	4.797	5.691
2/9	5.550	6.453
1/4	6.151	7.000

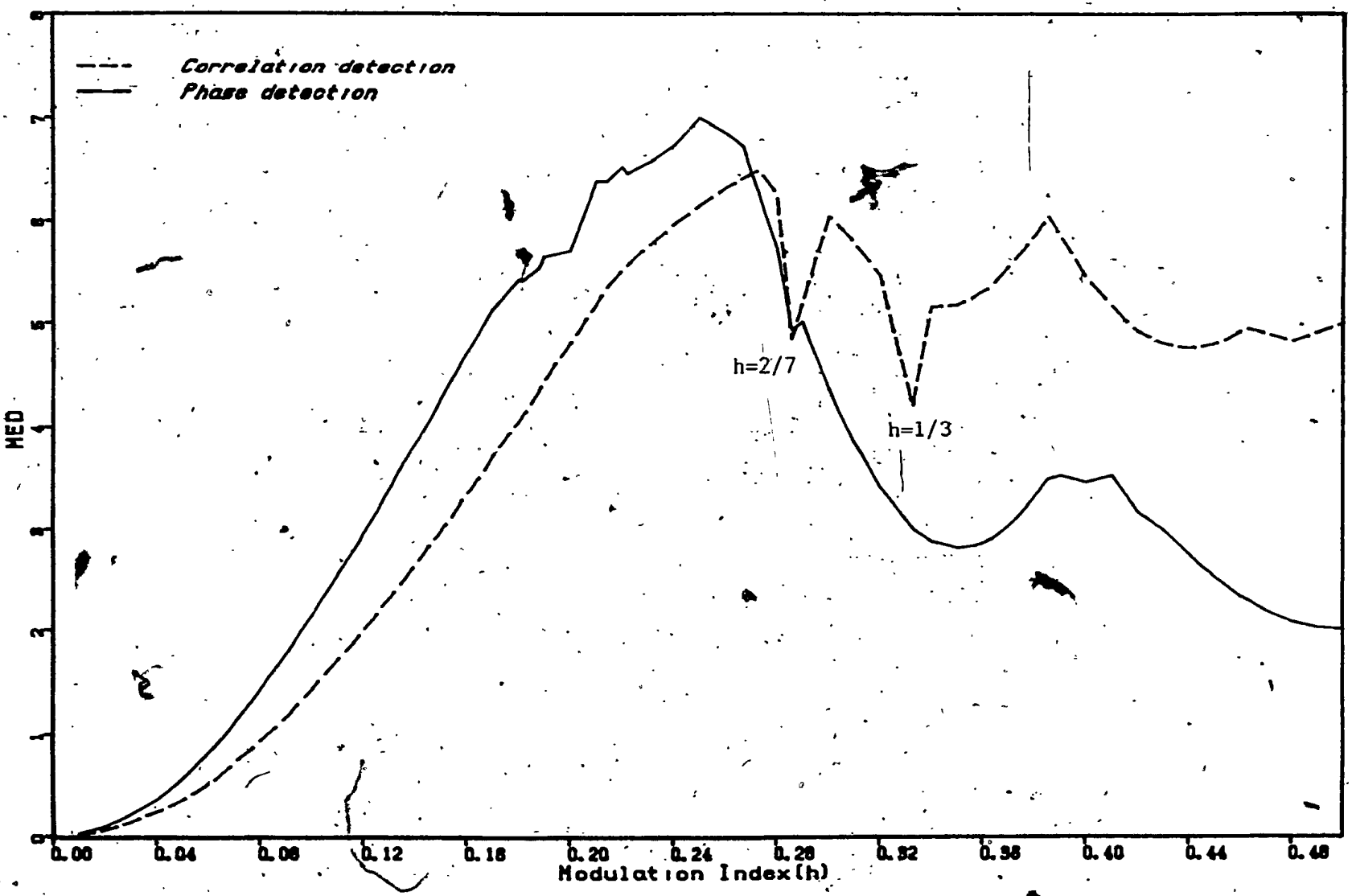

Figure 3.32: Comparison of minimum distance for (2, 1, 5) coded quaternary CPFSK signals.

Table 3.11: Coding gains of (2, 1, 5) coded quaternary-CPFSK over uncoded quaternary CPFSK at same h.

Modulation Index h	$d^2_{min}/2E_b$ (uncoded)	$d^2_{min}/2E_b$ (dB) (coded)	
		Correlation detection	Phase detection
1/40	0.016	7.69	9.63
1/16	0.102	7.53	9.41
1/10	0.259	7.41	9.18
1/8	0.399	7.33	9.00
1/7	0.516	7.25	8.84
1/6	0.692	7.13	8.59
3/16	0.863	7.01	8.23
1/5	0.973	6.93	7.67
2/9	1.179	6.73	7.38
1/4	1.454	6.26	6.82

Table 3.12: Minimum distances for phase detection of coded quaternary CPFSK signals.

Modulation Index h	$d^2_{min}/2E_b$ (coded)				
	(2, 1, 1)	(2, 1, 2)	(2, 1, 3)	(2, 1, 4)	(2, 1, 5)
1/40	0.061	0.110	0.123	0.135	0.147
1/16	0.369	0.662	0.738	0.814	0.890
1/10	0.882	1.573	1.764	1.995	2.146
1/8	1.293	2.293	2.586	2.879	3.172
1/7	1.599	2.445	3,198	3.575	3.952
1/6	2.000	3.500	4.000	4.500	5.000
3/16	2.324	3.566	4.649	5.266	5.739
1/5	2.500	3.618	4.309	5.000	5.691
2/9	2.766	4.347	5.049	5.751	6.453
1/4	3.000	5.000	6.000	7.000	7.000

these codes are practical only when the denominator of the modulation index is small. In the small h region, for quaternary CPFSK, the denominator of the rational valued modulation index ($h = p/q$) is least when $h = 1/4$, making the total number of states for (2, 1, 4) and (2, 1, 5) coding 64 and 128 respectively. This makes the trellis decoder very complex.

3.4. Trellis codes combined with octal CPFSK signals

In this section the distance properties of (3, 2, m) coded octal CPFSK signals are considered. The general model of the communication system was given in Fig. 3.1. When octal CPFSK is used in the modulator, the information sequence has to be encoded by a rate 2/3 trellis encoder. The output of the encoder consists of three-bit coded binary symbols. Blocks of these binary symbols are mapped on to the octal alphabet $\{\pm 1, \pm 3, \pm 5, \pm 7\}$. The channel symbols a_n chosen from the above set are then fed to the CPFSK modulator which produces the transmitted signal. Again an AWGN channel is assumed.

The combined state diagram of trellis coded octal CPFSK signals consists of $q.2^m$ states, where q is the denominator of the modulation index h ($= p/q$) and m is the memory of the trellis code. For rate 2/3 coding, the number of branches per state in the trellis is four. Therefore, as shown in Fig. 3.33, for (3, 2, 1) codes there are parallel branches in the trellis, and only one trellis structure is possible. For (3, 2, 2) codes there can be two possible trellis structures as shown in Fig. 3.34. For higher memory codes, the possible trellis structures increase in number.

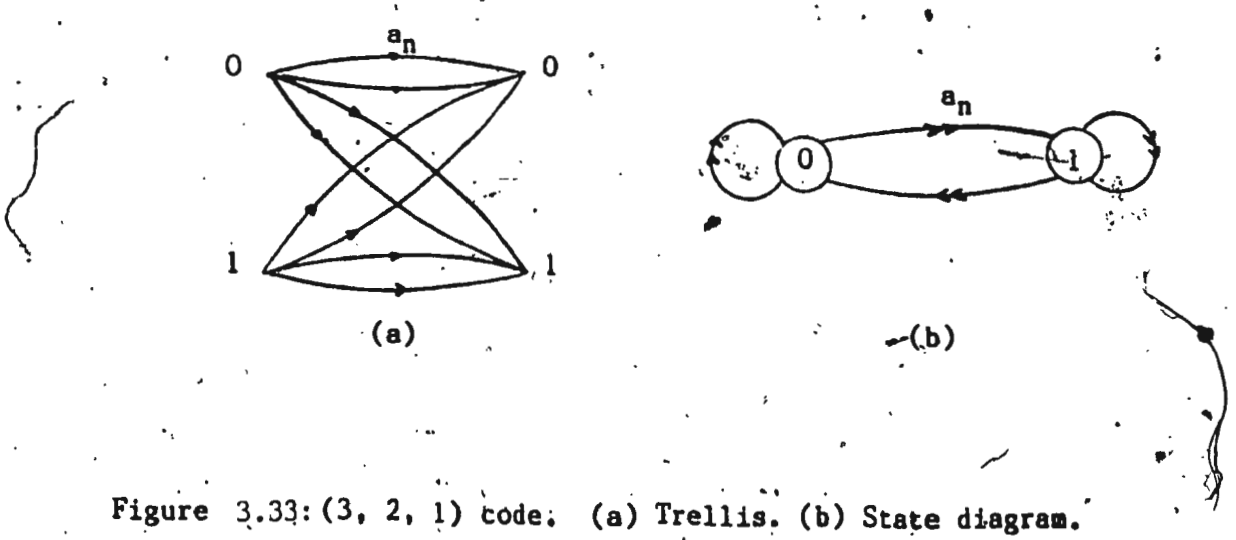

Figure 3.33: (3, 2, 1) code. (a) Trellis. (b) State diagram.

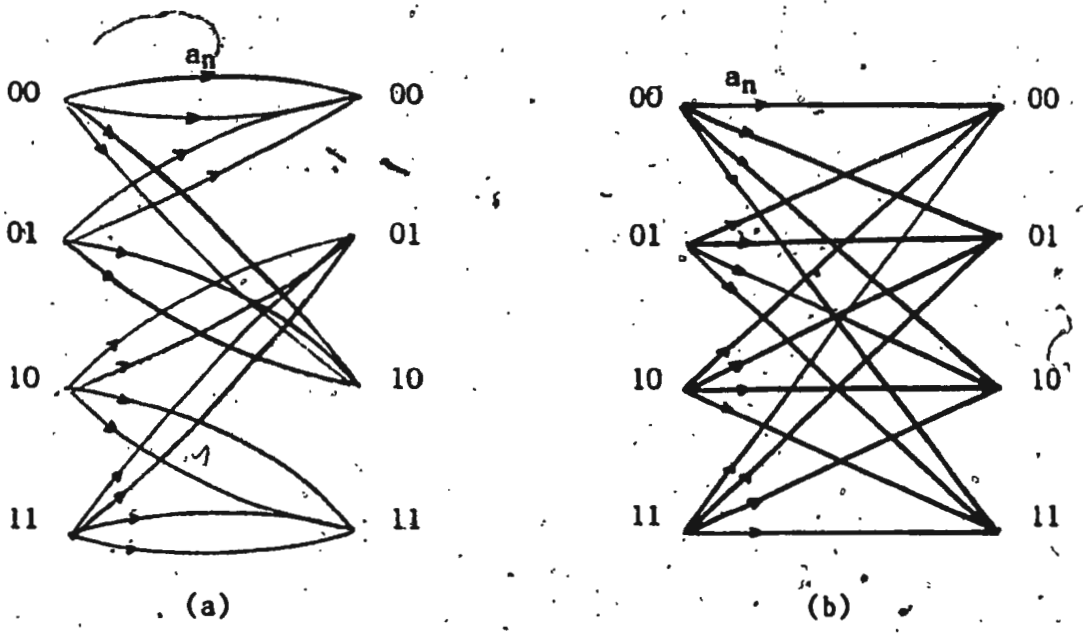

Figure 3.34: Trellis structures for (3, 2, 2) codes.

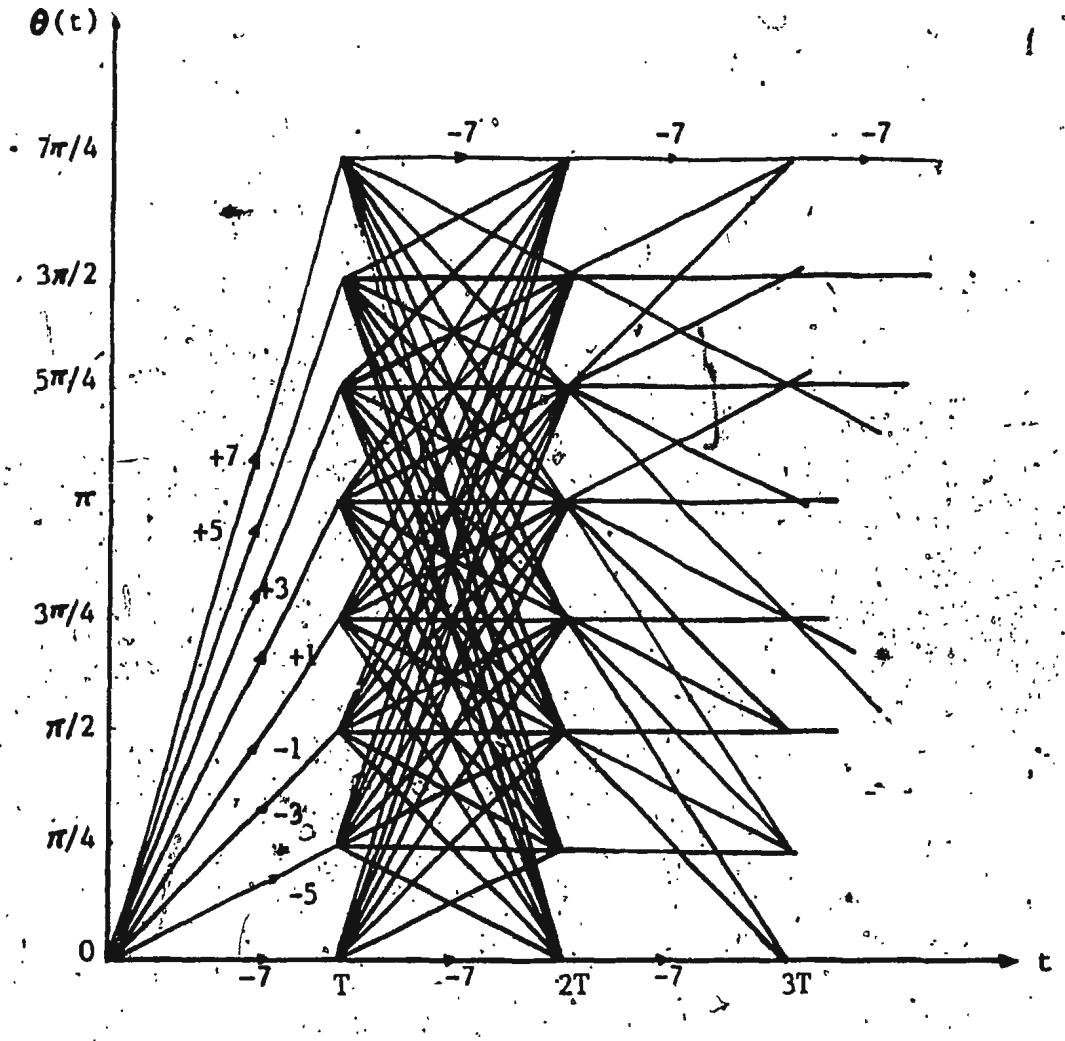

Figure 3.35: Trellis of uncoded octal CPFSK for h=1/8.

The trellis of the uncoded octal CPFSK scheme for a given modulation index h ($= p/q$) has q different states. Fig. 3.35 gives the uncoded trellis of octal CPFSK for $h = 1/8$. There are eight transitions from each state to states of the next level. Each of these transitions corresponds to an octal symbol a_n selected from the set $\{\pm 1, \pm 3, \pm 5, \pm 7\}$.

A computer search for the best trellis labellings with phase detection and trellis decoding was carried out for small h values. For (3, 2, 1) codes, the trellis structure of Fig. 3.33 was used in the search, while the trellis diagrams consisting of pairs of parallel branches between states were used for (3, 2, 2) codes and (3, 2, 3) codes. The numerical results are presented in the following sections.

3.4.1. (3, 2, 1) coding of octal CPFSK signals

The optimal code for phase detection of (3, 2, 1) coded octal CPFSK signals with small modulation indices is given in Fig. 3.36a. This is only one of the equivalent trellis labellings that is possible. In other words, there can be more than one optimal code for a given memory length at each modulation index. The trellis above is found to be optimal for small h in conjunction with a correlation receiver too [14]. With this code, the minimum distance merging occured at level three for all small h values.

Table 3.13 shows the largest minimum distances obtained for (3, 2, 1) coded octal CPFSK for $h \leq 1/8$. Fig. 3.37 shows the variation of minimum distance with h, for correlation detection and phase detection, when the optimal code is used. Comparing the two curves, clearly, up to $h \approx 1/8$, phase detection yields

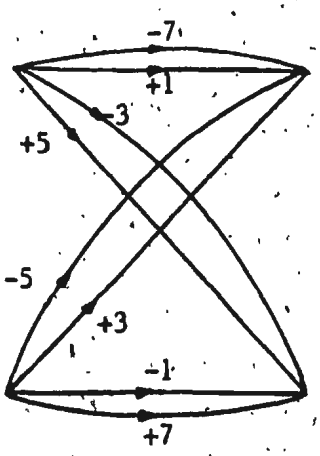

(a)

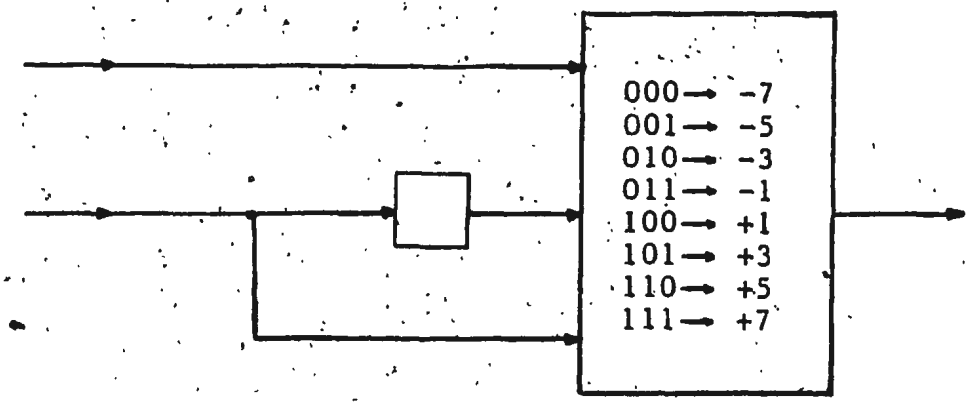

(b)

Figure 3.36: Optimal (3, 2, 1) code for octal CPFSK with small h. (a) Trellis. (b) Implementation using a convolutional code and natural binary mapping [14].

Table 3.13: Largest minimum distances of (3, 2, 1) coded octal CPFSK for small h.

Modulation Index h	$d^2_{min}/2E_b$	
	Correlation detection	Phase detection
1/25	0.167	0.310
1/22	0.214	0.398
1/20	0.259	0.480
1/18	0.318	0.589
1/15	0.454	0.835
2/23	0.756	1.371
1/10	0.983	1.764
2/19	1.081	1.931
1/9	1.194	2.121
1/8	1.477	2.586

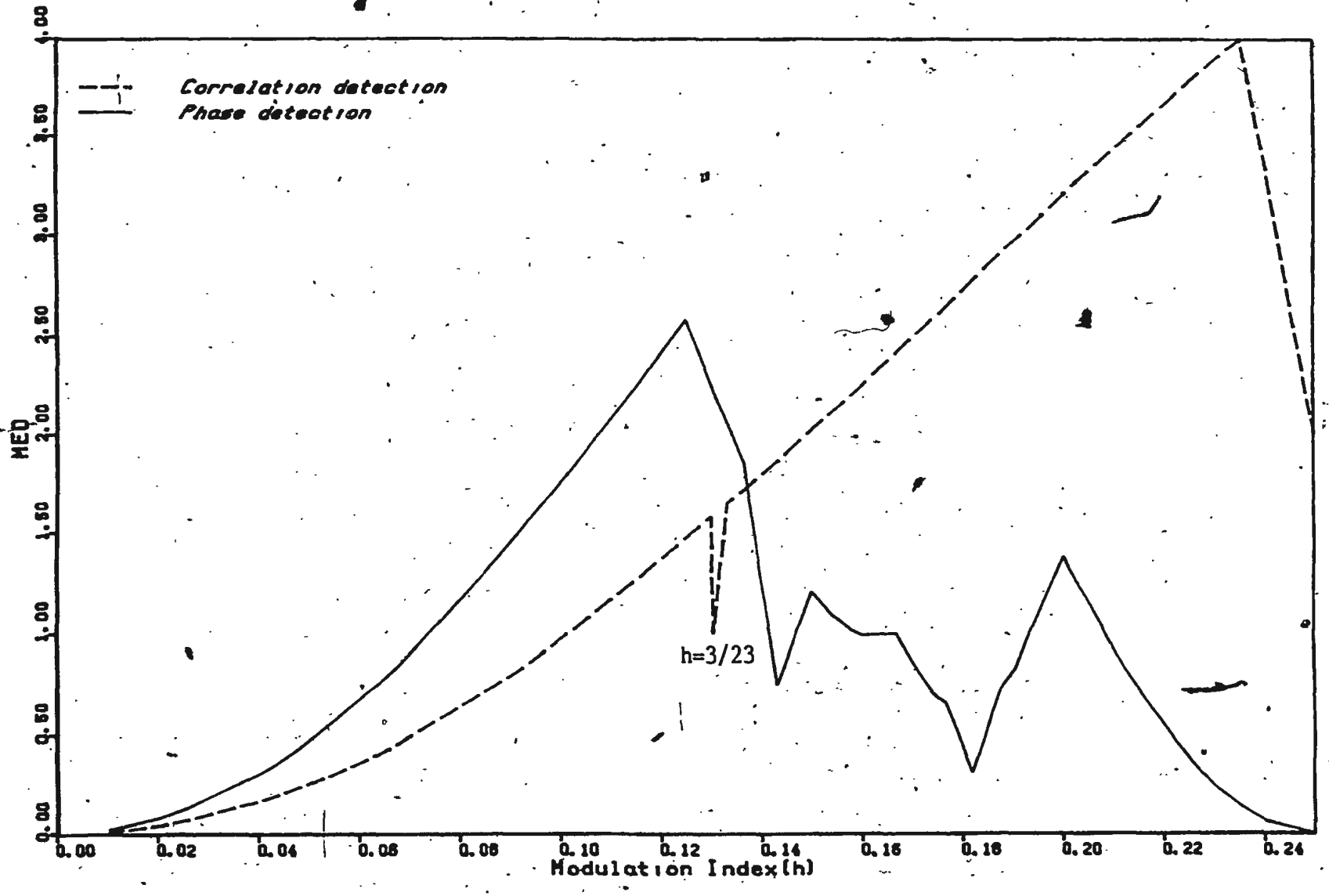

Figure 3.37: Comparison of minimum distance for (3, 2, 1) coded octal CPFSK signals.

Table 3.14:Coding gain of (3, 2, 1) coded octal CPFSK over uncoded octal CPFSK at same h.

Modulation Index h	$d^2_{min}/2E_b$ (uncoded)	$d^2_{min}/2E_b$ (dB) (coded)	
		Correlation detection	Phase detection
1/25	0.094	2.50	5.18
1/22	0.122	2.44	5.13
1/20	0.147	2.46	5.14
1/18	0.181	2.45	5.12
1/15	0.259	2.44	5.08
2/23	0.437	2.38	4.97
1/10	0.573	2.34	4.88
2/19	0.633	2.32	4.84
1/9	0.702	2.31	4.80
1/8	0.879	2.25	4.69

larger minimum distances than correlation detection. The coding gains achieved by the optimal code, when compared with the uncoded octal CPFSK, is given in Table 3.14.

3.4.2. (3, 2, 2) coding of octal CPFSK signals

Fig. 3.38a shows the optimal trellis for phase detection of (3, 2, 2) coded octal CPFSK signals in the small h region. This trellis is optimal for correlation detection as well [14]. The implementation of the optimal code using a convolutional encoder and the natural binary mapping rule are given in Fig. 3.38b. With the (3, 2, 2) code of Fig. 3.38, the minimum distance merging occurs at level four for all $h \leq 1/8$.

Table 3.15 gives the exact values of minimum distances obtained with the best (3, 2, 2) code. Fig. 3.39 shows the variation of minimum distance with modulation index h, for correlation detection and phase detection. Again it is evident that for $h \leq 1/8$ phase detection yields larger minimum distances than correlation detection. The coding gain of (3, 2, 2) coded octal CPFSK calculated with respect to the uncoded octal CPFSK is tabulated in Table 3.16.

3.4.3. (3, 2, 3) coding of octal CPFSK signals

Results for (3, 2, 3) coding of octal CPFSK signals are given in Table 3.17, Fig. 3.40, and Fig. 3.41. As before, phase detection yields larger minimum distances in the small h region and the optimal trellis code is the same for correlation detection. The coding gains for some h values are given in Table 3.18.

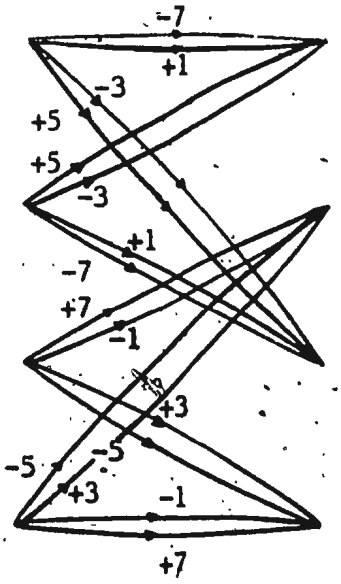

(a)

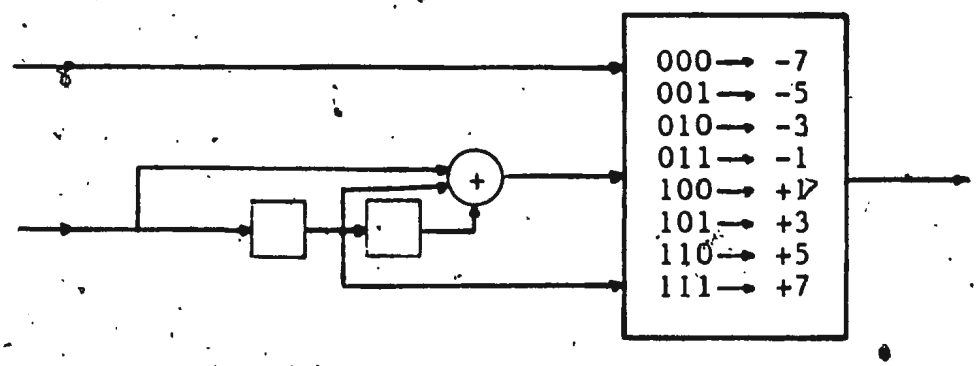

(b) Natural binary

Figure 3.38: Optimal (3, 2, 2) code for octal CPFSK with small h. (a) Trellis. (b) Implementation using a convolutional code and natural binary mapping [14].

Table 3.15: Largest minimum distances of (3, 2, 2) coded octal CPFSK for small h.

Modulation Index h	$d^2_{min}/2E_b$	
	Correlation detection	Phase detection
1/25	0.291	0.558
1/22	0.375	0.716
1/20	0.452	0.862
1/18	0.555	1.056
1/15	0.792	1.496
2/23	1.315	2.451
1/10	1.707	3.146
2/19	1.876	3.235
1/9	2.070	3.305
1/8	2.555	4.000

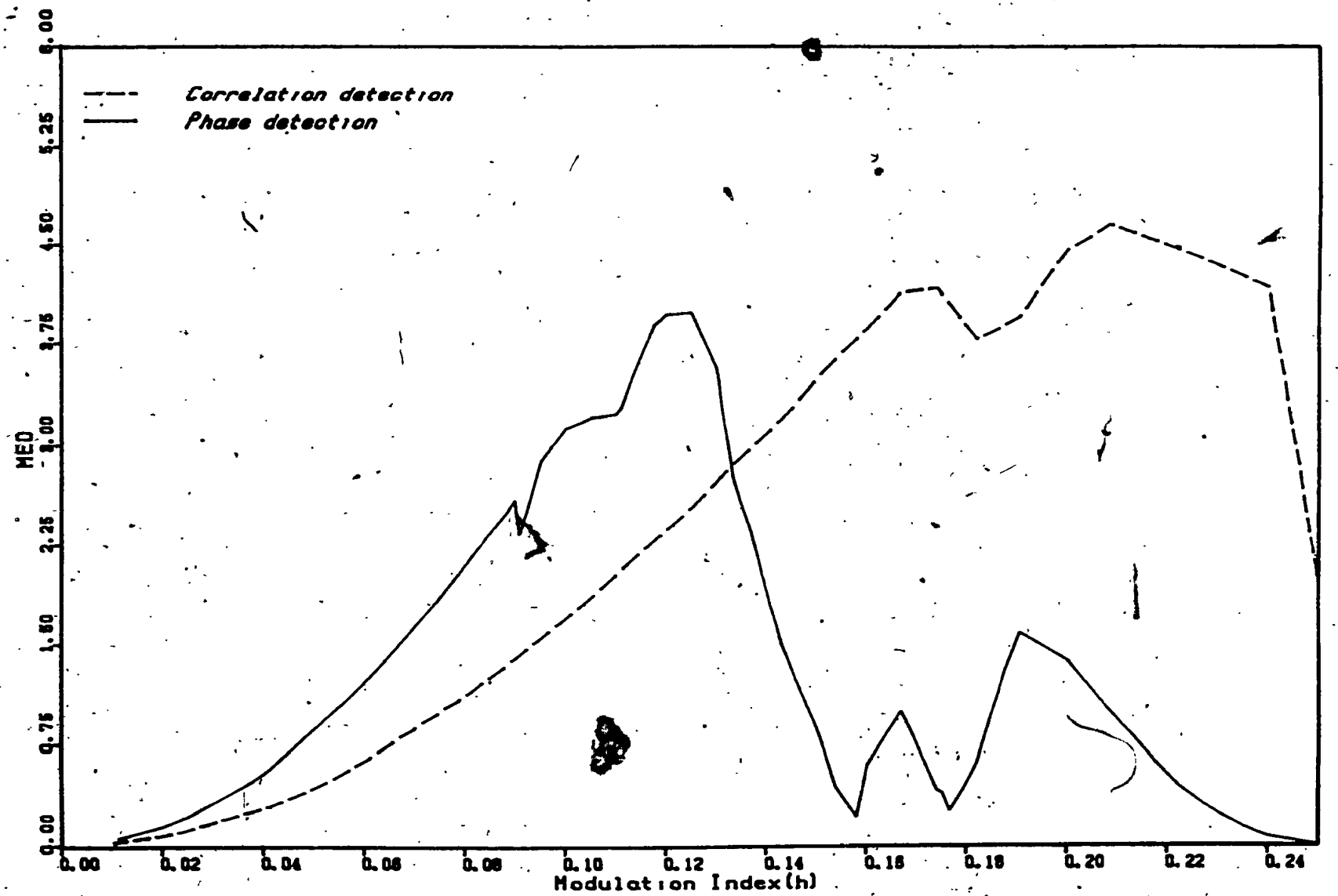

Figure 3.39: Minimum distance versus modulation index for (3, 2, 2) coded octal CPFSK signals.

Table 3.16: Coding gain of (3, 2, 2) coded octal CPFSK over uncoded octal CPFSK at same h.

Modulation Index h	$d^2_{min}/2E_b$ (uncoded)	$d^2_{min}/2E_b$ (dB) (coded)	
		Correlation detection	Phase detection
1/25	0.094	4.90	7.74
1/22	0.122	4.88	7.69
1/20	0.147	4.88	7.68
1/18	0.181	4.87	7.66
1/15	0.259	4.85	7.62
2/23	0.437	4.78	7.49
1/10	0.573	4.74	7.40
2/19	0.633	4.72	7.08
1/9	0.702	4.70	6.73
1/8	0.879	4.63	6.58

Table 3.17: Largest minimum distances of (3, 2, 3) coded octal CPFSK for small h.

Modulation Index h	$d^2_{min}/2E_b$	
	Correlation detection	Phase detection
1/25	0.374	0.620
1/22	0.482	0.797
1/20	0.581	0.960
1/18	0.714	1.177
1/15	1.017	1.669
2/23	1.690	2.742
1/10	2.194	3.528
2/19	2.410	3.759
1/9	2.660	3.773
1/8	3.282	4.000

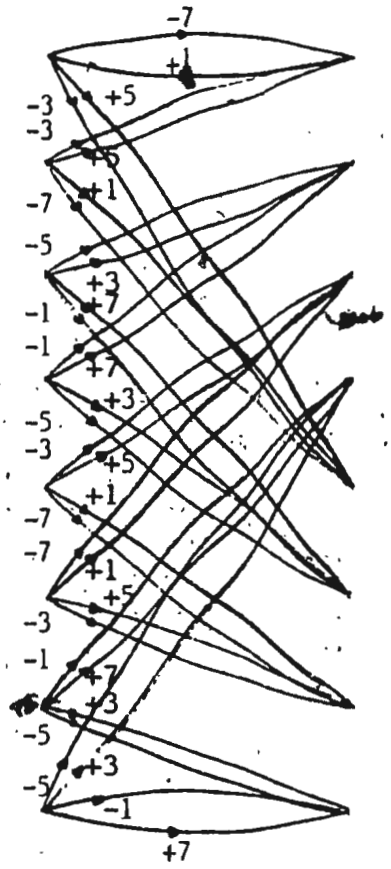

(a)

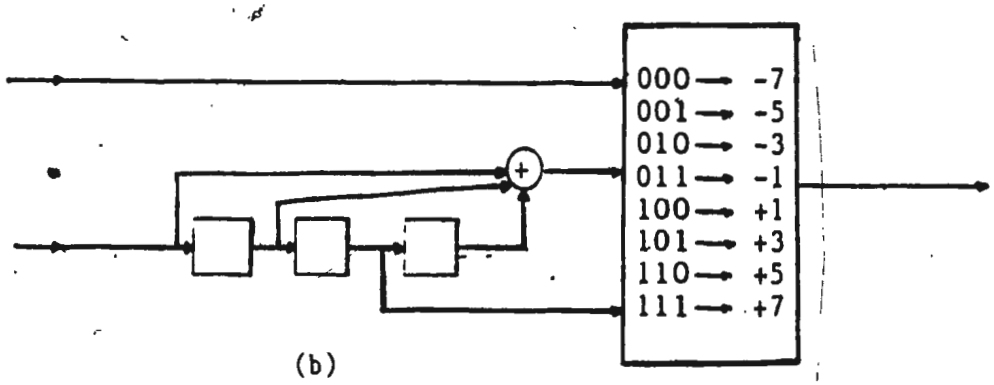

(b)

Figure 3.40: Optimal (3, 2, 3) code for octal CPFSK with small h. (a) Trellis. (b) Implementation using a convolutional code and natural binary mapping [14].

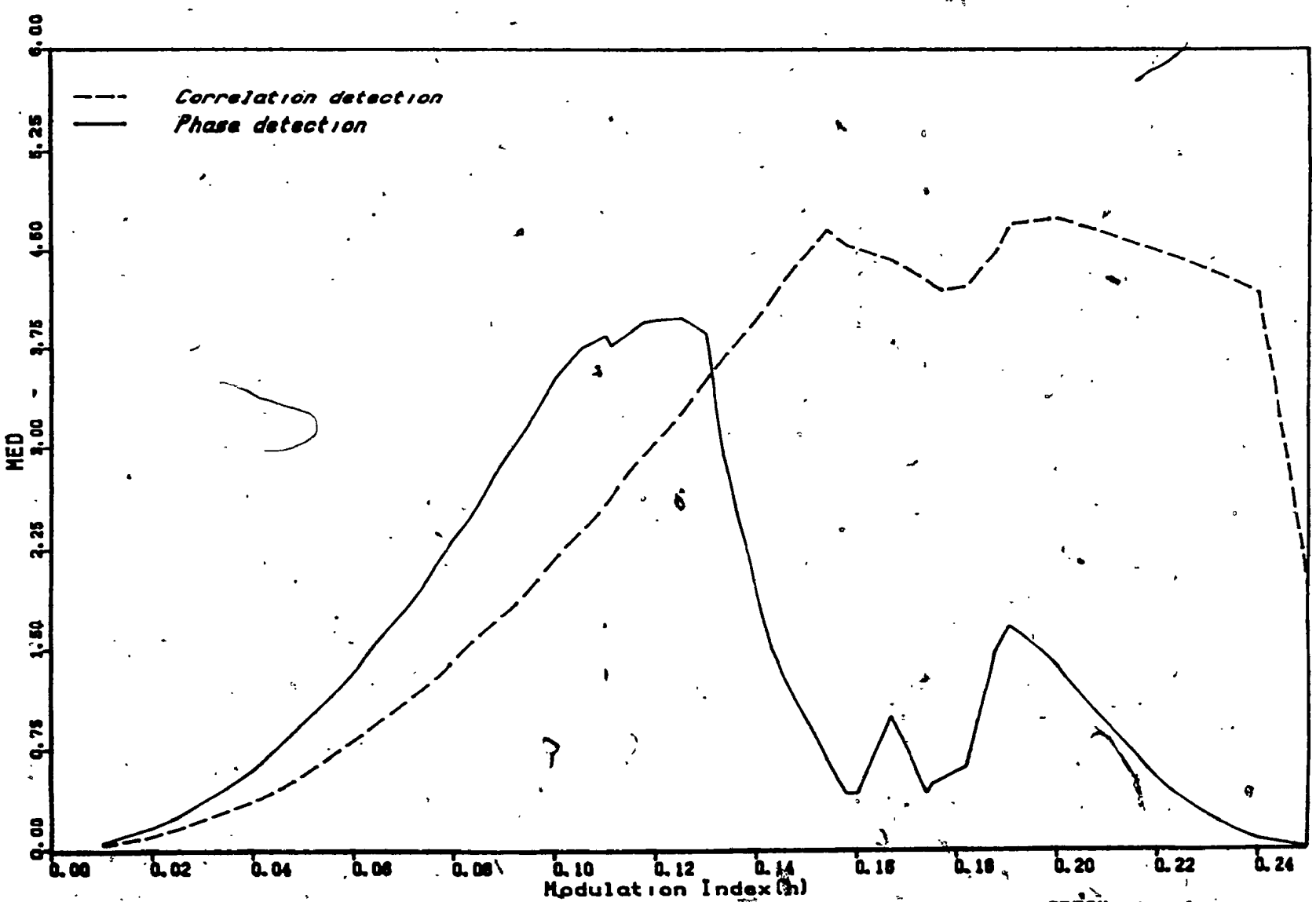

Figure 3.41: Minimum distance versus modulation index for (3, 2, 3) coded octal CPFSK signals.

Table 3.18: Coding gain of (3, 2, 3) coded octal CPFSK over uncoded octal CPFSK at same h.

Modulation Index h	$d^2_{min}/2E_b$ (uncoded)	$d^2_{min}/2E_b$ (dB) (coded)	
		Correlation detection	Phase detection
1/25	0.094	6.00	8.19
1/22	0.122	5.97	8.15
1/20	0.147	5.97	8.15
1/18	0.181	5.96	8.13
1/15	0.259	5.94	8.09
2/23	0.437	5.87	7.98
1/10	0.573	5.83	7.89
2/19	0.633	5.81	7.74
1/9	0.702	5.79	7.30
1/8	0.879	5.72	6.58

3.4.4. Summary of minimum distances for phase detection of coded octal CPFSK signals

A summary of minimum distances for phase detection of coded octal CPFSK signals is shown in Table 3.19. Here too, longer memory codes produce larger minimum distances. Again when $h = 1/8$ the minimum distance paths for $m = 2$ and $m = 3$ are identical, resulting in the same minimum distance. In the small h region, for octal CPFSK the denominator of the rational valued modulation index ($h = p/q$) is least when $h = 1/8$, making the total number of states for (3, 2, 1), (3, 2, 2), and (3, 2, 3) coding 16, 32, and 64 respectively. Therefore increasing the memory length also increases the complexity of the trellis decoder.

3.5. Carrier phase ambiguity and trellis coded CPFSK signals

In Section 2.3 it was shown that trellis decoding of uncoded CPFSK signals is transparent to phase ambiguities of the locally generated reference tones of the coherent demodulator. In what follows we show that this is true for trellis coded CPFSK signals as well.

For the purpose of illustration the simple example of (2, 1, 1) coding of quaternary CPFSK signals with modulation index 1/2 (i.e. MSK) is considered. The trellises and the state diagrams of the (2, 1, 1) code and the uncoded quaternary MSK are shown in Fig. 3.42. The combined state diagram consisting of four states is given in Fig. 3.43. In the discussion which follows, it is assumed that a correlation receiver is used to detect the coded CPFSK signals.

Table 3.19: Minimum distances for phase detection of coded octal CPFSK signals.

Modulation Index h	$d^2_{min}/2E_b$ (coded)		
	(3, 2, 1)	(3, 2, 2)	(3, 2, 3)
1/25	0.310	0.558	0.620
1/22	0.398	0.716	0.797
1/20	0.480	0.862	0.960
1/18	0.589	1.056	1.177
1/15	0.835	1.496	1.669
2/23	1.371	2.451	2.742
1/10	1.764	3.146	3.528
2/19	1.931	3.235	3.759
1/9	2.121	3.305	3.773
1/8	2.586	4.000	4.000

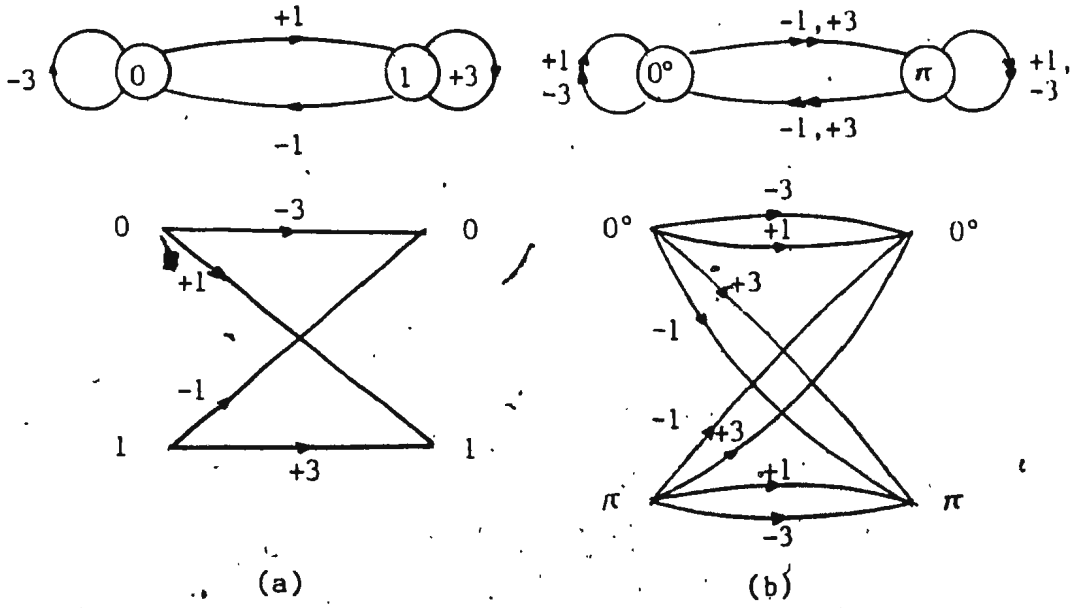

Figure 3.42: State diagram and trellis of (2, 1, 1) trellis code and uncoded quaternary CPFSK with h=½.

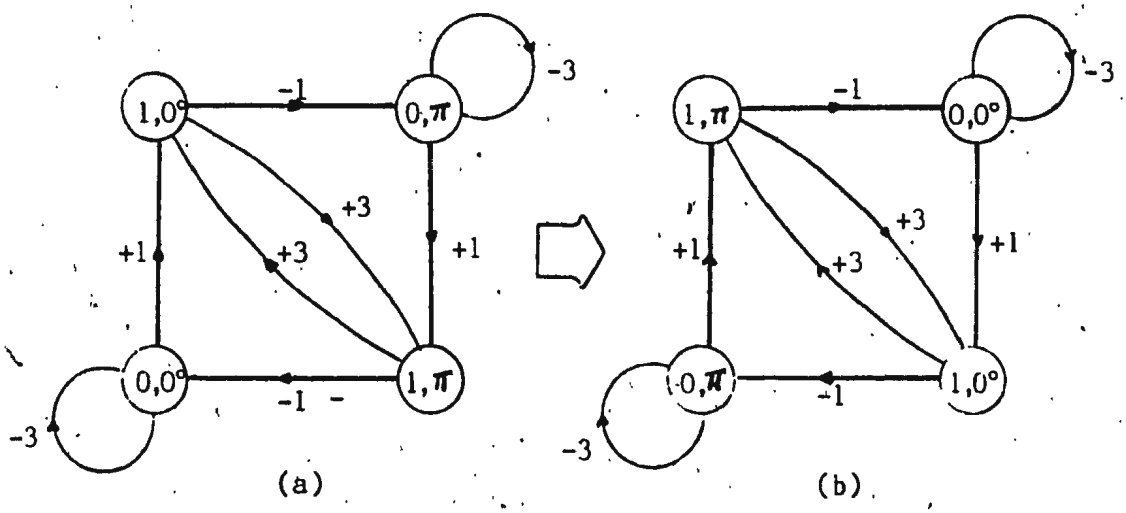

Figure 3.43: Effect of carrier phase ambiguity of 180° on the combined state diagram of (2,1,1) coded quaternary CPFSK with h=½.

If there is a 180° phase error in the regenerated reference tones, the receiver correlates with the incorrect signal. In other words, the correlator corresponding to the state $(0, \pi)$, now appears as the correlator corresponding to the state $(0, 0°)$ and vice versa. This follows from the fact that the phase of the CPFSK signal has a one-to-one relationship with the phase states of the state diagram. Thus a 180° phase error in the reference tones can be considered as a 180° phase shift in the phase states. That means the phase state 0 has to be changed to π and π to 0, in the combined state diagram. The resulting state diagram is shown in Fig. 3.43b. Clearly the two state diagrams are identical. Therefore a 180° phase error has no effect on the trellis decoder.

This can further be clarified by considering the combined trellis of the above coded CPFSK scheme shown in Fig. 3.44. Consider an arbitrary data sequence 3, −1, −3, 1, 3. The path of this data sequence through the trellis, when the reference tones are in exact synchronization with the incoming signals, is shown by the solid line. It is assumed that the demodulator starts at state (1, 0). If the receiver were unable to resolve the phase ambiguity, so that the reference tones are 180° out of phase with the incoming signal, the decoded path will be as shown by the dotted line. The new path also decodes the data sequence correctly. Therefore it can be concluded that trellis decoding of (2, 1, 1) coded quaternary CPFSK signals with $h = 1/2$ is transparent to phase ambiguities of 180°.

For M-ary CPFSK signals with modulation index h, the combined trellis is invariant to rotational shifts of integer multiples of $2\pi h$. This is the result of rotational symmetry of the uncoded M-ary CPFSK trellis discussed in detail in

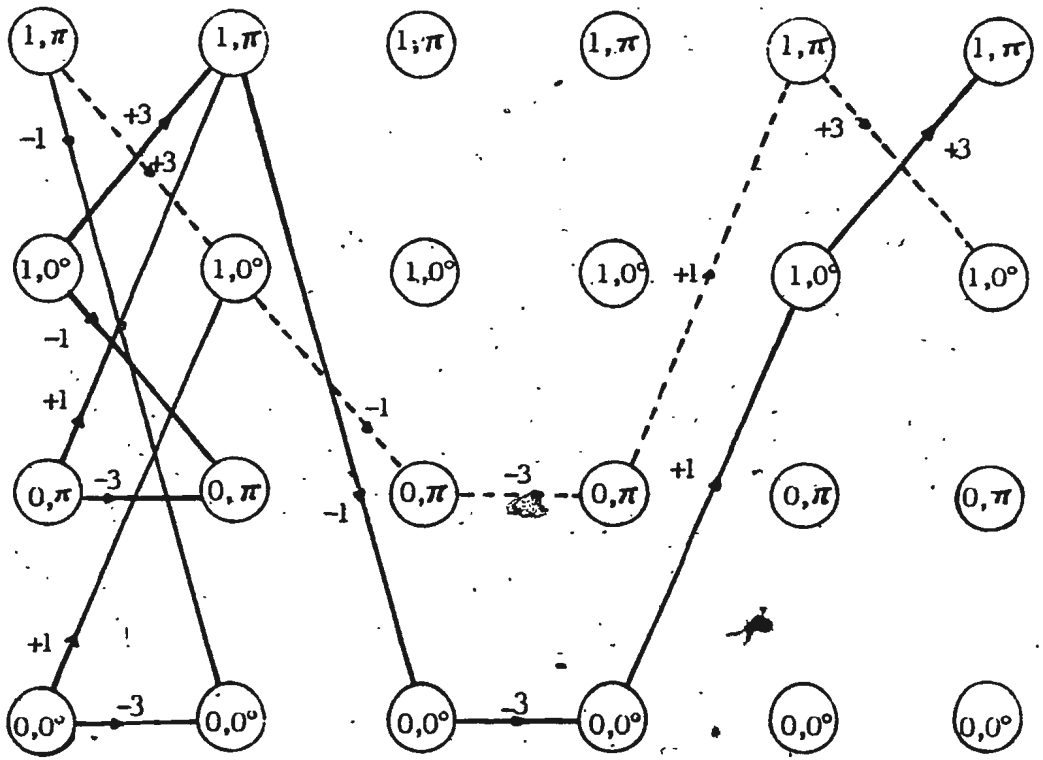

Figure 3.44 Effect of carrier phase ambiguity of 180° on trellis decoding of (2, 1, 1) coded quaternary CPFSK with modulation index 1/2.

Section 2.3. Thus, it can be concluded that trellis decoding of coded M-ary CPFSK signals is transparent to phase ambiguities of the regenerated reference tones. In general, a trellis decoder can successfully resolve phase ambiguities of $2\pi h, 4\pi h, \ldots, 2(q-1)\pi h$.

3.6. Conclusion

In this chapter minimum Euclidean distances were calculated for trellis coded quaternary and octal CPFSK signals when the receiver consists of a phase detector followed by a trellis decoder. Optimal codes were found for a wide range of memory lengths for quaternary and octal CPFSK signals for small h ($h \leq 1/M$). The minimum Euclidean distances obtained with this receiver were shown to exceed those of correlation detection and trellis decoding. The modulation indices considered were $h \leq 1/4$ for quaternary CPFSK signals and $h \leq 1/8$ for octal CPFSK signals. Also it was observed that trellis decoding of coded CPFSK signals is transparent to phase ambiguities of the regenerated reference tones at the coherent demodulator.

Chapter 4

CONCLUSION

In this thesis the distance properties of uncoded CPFSK signals and trellis coded CPFSK signals were examined. For reception of CPFSK signals a coherent phase detector followed by a trellis decoder has been considered, instead of the well known correlation receiver.

Closed-form expressions were derived for the minimum Euclidean distance of uncoded M-ary CPFSK signals. Numerical values of the minimum Euclidean distance were computed for $M = 2$, 4, 8, and 16. Our results were in exact agreement with those obtained using various algorithms. Regardless of the number of states, the minimum distance paths of any CPFSK trellis merge in at most two symbol intervals. This implies that the decisions on symbols can be made after a delay of only a few signaling intervals as in Viterbi decoding of convolutional codes. For phase detection of M-ary CPFSK signals in the small h region ($h \leq 1/M$) it was found that the largest minimum Euclidean distance occurs at $h = 1/M$. It was also shown that the optimum modulation index for correlation detection of M-ary CPFSK signals can be approximated by $(M-1)/M$, without an appreciable reduction in the largest minimum distance that is achieved.

Results for uncoded CPFSK signals show that phase detection and trellis decoding yields larger minimum Euclidean distances than correlation type detection for modulation index $h \leq 1/M$. The investigation was extended to combined trellis coding and CPFSK modulation. In particular quaternary and octal CPFSK signals were considered. For a given code and a modulation index it was found that phase detection always yields a larger minimum distance than in correlation detection. A computer search was carried out to find the optimal codes for phase detection which give the largest minimum distances when combined with quaternary and octal CPFSK signals. It was evident for small modulation indices the codes that were optimal for phase detection were also optimal for correlation detection. Whenever the modulation index exceeded $1/M$, the optimal code for phase detection was different from the optimal code for correlation detection. Also it was observed that the minimum Euclidean distance increases with the memory length of the code. Coding gain, which is interpreted as the increase in minimum Euclidean distance with respect to uncoded MSK, was tabulated for small h values.

Another important outcome of this research was the observation that trellis decoding of both uncoded and coded CPFSK signals is transparent to the phase ambiguities of the locally generated reference tones of the coherent demodulator. The implications of this observation are two-fold:

1. The realization of the coherent demodulator can be simplified by avoiding ambiguity resolving circuitry.

2. The techniques that overcome the necessity for resolving phase ambiguity such as differential encoding of data and differential decoding of data, which almost always degrade the detector performance, can be done away with.

From an implementation point of view the correlation receiver is attractive for the reception of CPFSK signals only for small M and q values. The correlation receiver becomes more complex with increasing M. In contrast, the realization of the phase detector is significantly simpler and the complexity does not grow with M. Nevertheless for both receivers, the complexity of the trellis decoder is proportional to the number of states in the CPFSK trellis; that is to $q\,2^m$, where m is the memory of the code and q is the denominator of the rational value modulation index. In this latter receiver, for all M-ary CPFSK schemes, only two coherent carrier components in quadrature are required. Moreover, it yields larger minimum distances than in correlation detection for small modulation indices ($h \leq 1/M$). CPFSK signals have good spectral properties only in this range of h and hence is the region of interest for implementation. Therefore it can be concluded that for both uncoded and coded M-ary CPFSK signals with $h \leq 1/M$, phase detection and trellis decoding is superior to correlation detection and trellis decoding. The receiver can further be simplified by avoiding the ambiguity resolving circuitry; however, this is true for the correlation receiver as well.

In this study an additive white Gaussian noise channel with inter-symbol interference-free signaling has been considered. In other words, essentially, a wideband channel has been considered. One way of extending this research would be to study the effects of implementing this receiver in bandlimited channels. A computer simulation which would give a fair idea of the extent of degradations that occur under ISI conditions, and an error-event analysis of the phase detector are also suggested.

References

1. Anderson, John B. and James R. Lesh, "Guest editor's prologue", *IEEE Transactions on Communications*,Vol. COM-29, No. 3, Mar. 1981, pp. 185, 186.

2. Anderson, John B. and D. P. Taylor, "A bandwidth efficient class of signal space codes", *IEEE Transactions on Information Theory*,Vol. IT-24, No. 6, Nov. 1978, pp. 703-712.

3. Aulin, Tor, "Symol error probability bounds for coherently Viterbi decoded continuous phase modulated signals", *IEEE Transactions on Communications*,Vol. COM-29, No. 11, Nov. 1981, pp. 1707-1714.

4. Aulin, Tor and Carl-Erik W. Sundberg, "Continuous phase modulation-Part I: Full response signaling", *IEEE Transactions on Communications*,Vol. COM-29, No. 3, Mar. 1981, pp. 196-209.

5. Aulin, Tor and Carl-Erik Sundberg, "CPM-An efficient constant amplitude modulation scheme", *International Journal of Satellite Communications*,Vol. 2, 1984, pp. 161-186.

6. Bhargava, V.K., D. Haccoun, R. Matyas, and P.P. Nuspl, *Digital Communications by Satellite*, Wiley, 1981.

7. Carlson, A. B., *Communication systems*, McGraw-Hill, New York, 1975.

8. de Buda, R., "Coherent demodulation of frequency-shift keying with low deviation ratio", *IEEE Transactions on Communications*,Vol. COM-20, No. 3, June 1972, pp. 429-436.

9. Ekanayake, N, "M-ary continuous phase frequency shift keying with modulation index 1/M", *IEE Proceedings*,Vol. 131, Part F, No. 2, Apr. 1984, pp. 173-178.

10. ----- , "Un-resolved carrier phase ambiguity and trellis decoding of CPFSK signals", *Electronics Letters*,Vol. 21, No. 24, Nov. 1985, pp. 1165, 1166.

11. Forney Jr., G. David, "The Viterbi algorithm", *Proceedings of the IEEE*,Vol. 61, No. 3, Mar. 1973, pp. 268-278.

12. Forney Jr., G. David, Robert G. Gallager, Gordon R. Lang, Fred M. Longstaff and Shahid U. Qureshi, "Efficient modulation for band-limited channels", *IEEE Journal on Selected Areas in Communications*,Vol. SAC-2, No. 5, Sep. 1984, pp. 632-647.

13. Lin, Shu and Daniel J. Costello Jr., *Error control coding: Fundamentals and applications*, Prentice-Hall, Englewood Cliffs, N.J., 1983.

14. Lindell, Goran, *On Coded continuous phase modulation*, PhD dissertation, Telecommunication Theory, University of Lund, Sweden, May 1985.

15. Lindell, Goran and Carl-Erik Sundberg, "Multilevel continuous phase modulation

with high rate convolutional codes", *IEEE Global Telecommunications Conference*,San Diego, USA, Nov. 29-Dec. 1 1983.

16. Lindell, Goran, Carl-Erik Sundberg and Tor Aulin, "Minimum Euclidean distance for combinations of short rate 1/2 convolutional codes and CPFSK modulation", *IEEE Transactions on Information Theory*,Vol. IT-30, No. 3, May 1984, pp. 509-519.

17. Mulligan, Michael G. and Stephen G. Wilson, "An improved algorithm for evaluating trellis phase codes", *IEEE Transactions on Information Theory*,Vol. IT-30, No. 6, Nov. 1984, pp. 846-851.

18. Osborne, W. P. and M. B. Luntz, "Coherent and noncoherent detection of CPFSK", *IEEE Transactions on Communications*,Vol. COM-22, No. 8, Aug. 1974, pp. 1023-1036.

19. Pelchat, M. G., R. C. Davis and M. B. Luntz, "Coherent demodulation of continuous phase binary FSK signals", *Proceedings of International Telemetering Conference, Washington, D.C.*, 1971, pp. 181-190.

20. Pizzi, Steven V. and Stephen G. Wilson, "Convolutional coding combined with continuous phase modulation", *IEEE Transactions on Communications*,Vol. COM-33, No. 1, Jan. 1985, pp. 20-29.

21. Schonhoff, Thomas A., "Symbol error probabilities for M-ary CPFSK: Coherent and noncoherent detection", *IEEE Transactions on Communications*,Vol. COM-24, No. 6, June 1976, pp. 644-652.

22. Sundberg, Carl-Erik, "Continuous phase modulation", *IEEE Communications Magazine*,Vol. 24, No. 4, Apr. 1986, pp. 25-38.

23. Svennson, Arne and Carl-Erik Sundberg, "On error probability for several types of noncoherent detection of CPM", *IEEE Global Telecommunications Conference, Atlanta, Georgia*, 1984, pp. 22.5.1-22.5.7.

24. Ungerboeck, Gotfried, "Channel coding with multilevel/phase signals", *IEEE Transactions on Information Theory*,Vol. IT-18, No. 1, Jan. 1982, pp. 55-67.

25. Viterbi, Andrew J. and Jim K. Omura, *Principles of digital communication and coding*, McGraw-Hill, New York, 1979.

26. Wozencraft, J. M. and I. M. Jacobs, *Principles of communication engineering*, John Wiley, 1965.

27. Ekanayake, N. and R. Liyanapathirana, "Distance properties of trellis coded CPFSK signals", *IEEE International Symposium on Information Theory, Ann Arbor, Michigan*,Oct. 1986.

28. Ekanayake, N. and R. Liyanapathirana, "Closed-form expressions for the minimum Euclidean distance of M-ary CPFSK signals", To be published. □